

Republic of Iraq
Ministry of Higher Education and Scientific Research
University of Bagdad
College of Education for Pure Science / Ibn Al-Haitham
Department of Physics



Simulation of Three Dimensional Images Tomography

A Thesis

*Submitted to The College of Education for Pure Science Ibn Al-Haitham /
University of Bagdad in a Partial Fulfillment of the Requirements for the
Degree of Doctor of sciences in Physics*

By

Hawraa Hadi Chyad

(B.Sc. 2011)

(M.Sc. 2015)

Supervised by

Assist. Prof. Dr. Hameed Majeed Abduljabbar

2019 A.D.

1441 A.H.

بِسْمِ اللَّهِ الرَّحْمَنِ الرَّحِيمِ

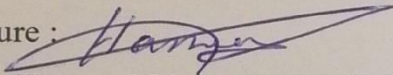
﴿ خِتَامُهُ مِسْكٌَ ۚ وَفِي ذَلِكَ فَلْيَتَنَافَسِ الْمُتَنَافِسُونَ ﴾

صدق الله العظيم

سورة المطففين - الآية 26

Supervisor's Certification

We certify that this dissertation entitled "*Simulation of Three Dimensional Images Tomography*" was prepared by (*Hawraa Hadi Chyad*) under my supervision the University of Bagdad, College of Education for Pure Science Ibn Al- Haitham as a partial fulfillment of the requirement for the degree of PhD of Science in Physics.

Signature : 
Name : **Hameed Majeed Abduljabbar**
Title : Assist. Prof. Dr.
Date : 30/ 7/ 2019

In view of above recommendation, we forward this dissertation for debate by the examining committee.

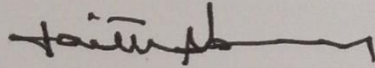
Signature : S. A. MAKI
Name : **Samir Ata Maki**
Title : Prof. Dr. / Head of Department

Head of physics Department, College of Education for Pure Science Ibn Al-Hatham, University of Bagdad.
Date: 30/ 7/ 2019

Certification of the Examining Committee

We certify that we have read this dissertation entitled "*Simulation of Three Dimensional Images Tomography*" submitted by (*Hawraa Hadi Chyad*) and as examining committee examined the student in its content and that in our opinion it is adequate with standard as thesis for the Degree of Ph.D. of Science in Physics.

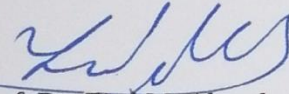
Signature



Name: Prof. Dr. Laith A. Al-Ani
Address: Collage of Sciences, Al-Nahrain,
University

Date: 28 / 11 / 2019
(Chairman)

Signature



Name: Prof. Dr. Ziad M. Abood
Address: Collage of Education, Mustansiriyah
University

Date: 20 / 11 / 2019
(Member)

Signature



Name: Assist. Prof. Dr. Taghreed Abdul
Hameed Naji
Address: Collage of Education for Pure
Science / Ibn Al-Haitham,
University of Baghdad

Date: 20 / 11 / 2019
(Member)

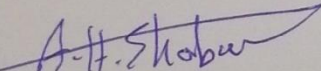
Signature



Name: Assist. Prof. Dr. Amal Jabbar Hatem
Address: Collage of Education for Pure
Science / Ibn Al-Haitham,
University of Baghdad

Date: 20 / 11 / 2019
(Member)

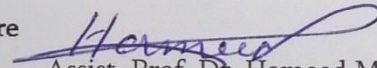
Signature



Name: Assist. Prof. Dr. Auday Hattem
Shaban
Address: Collage of Education for Pure
Science / Ibn Al-Haitham,
University of Baghdad

Date: 20 / 11 / 2019
(Member)

Signature

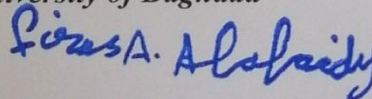


Name: Assist. Prof. Dr. Hameed Majeed
Abduljabbar
Address: Collage of Education for Pure
Science / Ibn Al-Haitham,
University of Baghdad

Date: 20 / 11 / 2019
(Member-Supervisor)

*Approved by the Dean of the College of Education for Pure Science / Ibn Al-Haitham
University of Baghdad*

Signature



Name: Assist. Prof. Dr. Firas Abdulhameed Abdullatif
Address: Behalf / The Dean of College of Education for
Pure Science / Ibn Al-Haitham

Date: 28 / 11 / 2019

Dedication

To my parents...

My lord be merciful to them, as they had Mercy on me when I was young.

Hawraa
2019

Acknowledgments

All praise and thank to Allah, the Lord of the universe. who does not success except by resorting to him.

I will be one day what I want, I repeated it a lot, today I'm achieving it, so I am very proud of myself for my completion the most important part of my life associated with getting the degree of Ph.D..

This dissertation would not have been possible without the guidance, patience, and understanding of whom I'm honored to have had the opportunity to work with him, my supervisor, Dr. Hameed M. Abduljabbar, I would express my respect to you because you the person who learned from him a lot, and your dedication and knowledge of image processing science inspired me to keep reaching for my goals, I am grateful you for bringing me into your group and showing confidence in me and my work that was this enjoyable, challenging and meaningful to me.

My deep thanks to the head of the physics department Dr. Samir Ata Maki for supporting him to us during the period study of Ph.D.

Finally, there are many people that have positively influenced my life, my sisters, brothers and the person who has had the most significant impact is my husband. I am fortunate to have them as part of my life.

Hawraa

2019



Abstract

A new horizon has been opened for researchers using Computed Tomography (CT) technique, due to the possibility of this technique to produce a three dimensional images of the internal structure for the different objects without the need to damage the object.

This work focus on studying models for reconstructing 3D images from its projections for two objects; symmetrical and asymmetrical using three methods.

The first method (Slicing reconstruction) is used the 2D Radon transform to generate a 2D projection for each slice of the 3D object at different heights. The 2D Back-Projection (2D BP) and the Fourier Slice Theorem (FST) methods are used to reconstruct each 2D projection slice of the 3D object. The second method (Direct reconstruction from 3D Projections) has used the 3D Radon Transform to generate a 3D projection for the 3D object. The 3D Back-Projection (3D BP) is performed to reconstruct the 3D object. The third method (Reconstruction from X-ray transform (4D projections)) is used the X-ray projections for a 3D object to generate a 4D projection. The central section theorem FST for the X-ray projection and the 3D Back Projections for X-ray Projection are used to retrieve 3D object from 4D projection. The retrieved object was significantly improved when using the Ramp filter and threshold value.

Three types of interpolation are suggested in this research work, to reduce the dose of radiation to the patient and the time to reconstruct the object, which are; the nearest neighbor, linear, and non-linear interpolation methods. These methods are applied to 2D sinogram that has taken at angular difference greater than one degree. The BP and FST reconstruction methods are adopted to retrieve the object from the interpolated projections. The Slicing reconstruction method showed the capability of the FST to reconstruct the external and the internal object structure. The threshold value is suggested to eliminate the excessive points, due to the blurring artifact then calculate the volume of each retrieved object.

The results of the first method (Slicing reconstruction method) showed the capability of the FST to reconstruct the external and the internal structure of it. Beside that the Fourier Slice Theorem could not remove all blurring artifact, so, the threshold technique is suggested to eliminate the excessive points, due to the blurring artifact, as the FST method could not remove it. The Ramp filter in the frequency domain is suggested to eliminate the blurring artifact and retrieve the object internal structure, as the 2D BP method had the capability to reconstruction the external structure of the object and its inability to reconstruction the internal structure of it because of the blurring artifact.

From the Direct reconstruction from 3D Projections method results, the 3D BP method was capable of reconstruction the external structure of the object and unable to the reconstruction of the internal structure because of the blurring artifact, so the Ramp filter in the frequency domain is proposed to eliminate the blurring artifact but cannot remove the blurring artifact and retrieve the internal structure.

The result of the third method (Reconstruction from X-ray transform (4D projections)) The central section theorem was fielded to retrieve object while the 3D Back Projection is successful to retrieve the external structure but inability to retrieve the internal structure of it because of the blurring artifact, so, this research, suggested the Ramp filter in the frequency domain to eliminate the blurring artifact although it cannot remove the blurring artifact and retrieve the internal structure.

By applying the interpolation methods in this research, the best threshold value to separate the points that belong to the object is ranging between 0.50-0.65. The FST reconstruction method with the interpolation process gave the best results for the internal details than the BP method, while FST failed to retrieve the basic object shape correctly for an angular difference greater than 20° . The basic object shape is maintained by BP reconstruction method even after 15° . In general, the linear interpolation gave the best results.

List of Content

<i>No.</i>	<i>Title</i>	<i>Page</i>
	Abstract	I
	List of content	III
	List of figures	VI
	List of tables	XII
	List of abbreviations	XIII
<i>Chapter One General Introduction to Computed Tomography</i>		
<i>1.1</i>	Introduction	<i>1</i>
<i>1.2</i>	A Brief History of Computed Tomography	<i>2</i>
<i>1.3</i>	Imaging system	<i>5</i>
<i>1.4</i>	Scanning Modes (The Projection System)	<i>8</i>
<i>1.4.1</i>	Parallel ray integral.	<i>9</i>
<i>1.4.2</i>	Fan beam	<i>10</i>
<i>1.4.3</i>	Cone beam	<i>11</i>
<i>1.5</i>	2D Digital Image Representation	<i>11</i>
<i>1.6</i>	3D Digital Image Representation	<i>12</i>
<i>1.7</i>	Quality of CT Images	<i>13</i>
<i>1.7.1</i>	Spatial Resolution	<i>14</i>
<i>1.7.2</i>	Contrast Value	<i>15</i>
<i>1.7.3</i>	Noise	<i>15</i>
<i>1.7.4</i>	Artifacts	<i>16</i>
<i>1.8</i>	Literature Review	<i>18</i>
<i>1.9</i>	Aims of the Study	<i>22</i>
<i>1.10</i>	Layout of the Dissertation	<i>22</i>
<i>Chapter Two Three-Dimensional Reconstructions</i>		
<i>2.1</i>	Introduction	<i>24</i>
<i>2.2</i>	2D Forward projection	<i>25</i>
<i>2.3</i>	2D Tomography	<i>26</i>
<i>2.4</i>	2D Image reconstruction methods	<i>27</i>
<i>2.4.1</i>	Fourier Slice Theorem	<i>29</i>
<i>2.4.2</i>	Simple Back-Projection (BP) (Inverse Radon Transform (IRT))	<i>34</i>
<i>2.4.3</i>	The Filter after the Back-projection (BPF)	<i>36</i>
<i>2.4.4</i>	The Filter before the Back-Projection (FBP)	<i>37</i>
<i>2.5</i>	3D Tomography	<i>38</i>
<i>2.5.1</i>	3D Back-Projections Method	<i>40</i>

2.6	Imaging 3D object by X-ray transform	40
2.7	Methods of Reconstruction 3D Object from X-Ray Projections	42
2.7.1	Three-Dimensional Back Projection for X-Ray Projections	42
2.7.2	The 3D Fourier Slice Theorem for X-Ray Transform	43
2.8	The Relationship between Radon Transform and X-Ray Transform	44
2.9	Ramp Filter In Frequency Domain	45
2.10	Interpolation	45
2.11	Fidelity Criteria	49
2.11.1	Objective Fidelity Criteria	49
2.11.2	Subjective Fidelity Criteria	51
Chapter Three <i>The Methodology of Reconstruction 3D Images</i>		
3.1	Introduction	52
3.2	summarize of methodology	52
3.3	Creating 3D Object	53
3.4	Methods of Forward projections	55
3.4.1	Slicing Method	55
3.4.2	Direct 3D Projections Method	57
3.4.3	X-Ray Transform Method (X-Ray Projections)	57
3.5	3D Object Reconstruction Methods	58
3.5.1	Reconstruction the 3D Object from 2D projection	59
3.5.2	Reconstruction the 3D Object from 3D projection	61
3.5.3	Reconstruction the 3D Object from 4D projection	61
3.6	The Methodology of Interpolation	63
Chapter Four <i>Results and Discussion</i>		
4.1	Introduction	67
4.2	Results of the Forward projections	67
4.2.1	Forward Projection using Slicing Method	67
4.2.2	Forward Projection using Direct 3D Projections Method	70
4.2.3	Forward Projection using X-Ray Transform Method	71
4.3	The Results of Reconstruction Methods	74
4.3.1	Reconstruct 3D Object from the 2D projection	74
4.3.1.1	The Results of Reconstruction Without Filtering	74
4.3.1.2	The Results of Reconstruction With Filtering	78
4.3.2	Reconstruct 3D Object from the 3D projection	84

4.3.2.1	The Results of Reconstruction Without Filtering	84
4.3.2.2	The Results of Reconstruction With Filtering	86
4.3.3	Reconstruct 3D Object from the 4D projection	90
4.3.3.1	The Results of Reconstruction Without Filtering	90
4.3.3.2	The Results of Reconstruction With Filtering	94
4.4	The Results of the Interpolation	99
<i>Chapter Five Conclusions and Future Works</i>		
5.1	Conclusions	110
5.2	Future Works	112
Reference		113

List of Figures

<i>No.</i>	<i>Figure Caption</i>	<i>Page</i>
<i>Figure 1.1</i>	The device of Godfrey N. Hounsfield	4
<i>Figure 1.2</i>	Images of (a) The first CT scanners (b) The CT scanner in 2005	4
<i>Figure 1.3</i>	Apply the CT scanner on the first patient	5
<i>Figure 1.4</i>	The basic devices in CT scanning using X-ray	7
<i>Figure 1.5</i>	A projection and a sinogram	8
<i>Figure 1.6</i>	Three types of projections systems	9
<i>Figure 1.7</i>	Parallel projection	10
<i>Figure 1.8</i>	Fan projection	10
<i>Figure 1.9</i>	Cone beam projection	11
<i>Figure 1.10</i>	2D image representation	12
<i>Figure 1.11</i>	The data that form the CT slice	13
<i>Figure 1.12</i>	(a) Original image (b) decrease spatial resolution, (c) decrease contrast resolution and (d) adding artificial noise	14
<i>Figure 1.13</i>	Numerical of ring artifact	17
<i>Figure 1.14</i>	CT image for heart shows metallic artifacts from the cardiac pacemaker	17
<i>Figure 1.15</i>	Motion causes blurring and double images in a head CT	18
<i>Figure 2.1</i>	The projections at various angles	25
<i>Figure 2.2</i>	The coordinates system of projection and the linear integral	26
<i>Figure 2.3</i>	Steps of Fourier slice theorem	30
<i>Figure 2.4</i>	The FT of a specific projection line from the object	32
<i>Figure 2.5</i>	The reconstruct original object by 2D inverse Fourier transform	34
<i>Figure 2.6</i>	1D projection using parallel beam	36
<i>Figure 2.7</i>	The Projection in 3D	38
<i>Figure 2.8</i>	The Projection geometry in 3D	39
<i>Figure 2.9</i>	Factors of 3D Line of Response (LOR) for the X-ray transform	41

Figure 2.10	The projection taken by X-ray transform	42
Figure 2.11	The 3D Fourier Slice Theorem for X-Ray Transform	44
Figure 2.12	The Radon transform for 3D Object	44
Figure 2.13	A schematic representation of the adopted geometry for the interpolation methods	47
Figure 2.14	The distribution of the summation weights for three interpolation methods (a) Nearest Neighbor (b) Linear (c) Nonlinear	48
Figure 3.1	Summarize of methodology block diagram.	52
Figure 3.2	(a) hollow sphere inside solid sphere (b) Solid sphere	53
Figure 3.3	(a) hollow sphere inside head Mickey Mouse (b) the solid head for Mickey Mouse	54
Figure 3.4	The 2D radon transform for one plane of 3D object	56
Figure 3.5	The forward slicing method block diagram.	56
Figure 3.6	The Forward the Direct 3D Projections block diagram.	57
Figure 3.7	The Forward X-Ray Transform block diagram.	58
Figure 3.8	The Reconstructed 3D Object by back-projection method block diagram.	59
Figure 3.9	The Reconstructed 3D Object by FST method block diagram.	60
Figure 3.10	The 3D BP block diagram.	61
Figure 3.11	The 3D BP for x-ray projections block diagram.	62
Figure 3.12	The central section theorem for the X-ray projection block diagram.	63
Figure 3.13	The interpolation method by using Back projection to reconstruct object block diagram.	65
Figure 3.14	The interpolation method by using FST to reconstruct object block diagram.	66
Figure 4.1	The 2D slices along the Z-axis (a) for hollow sphere inside solid sphere (b) for Mickey Mouse	67
Figure 4.2	(a) 2D slice of sphere at different heights (b) 2D slice of Mickey Mouse at different heights	68

<i>Figure 4.3</i>	A 2D projection for some 2D slice of the 3D object (a) slices of projection for slices of the sphere at different heights (b) slices of projection for slices of the mickey mouse at different heights	69
<i>Figure 4.4</i>	Staking the 2D slices of projections (a) for sphere (b) for Mickey Mouse	69
<i>Figure 4.5</i>	A 3D projections of the 3D object (a) for sphere (b) for Mickey Mouse	70
<i>Figure 4.6</i>	A 2D slices projection from 3D projections (a) the slice of projection for sphere (b) the slice of projection for Mickey Mouse	71
<i>Figure 4.7</i>	A mesh for 3D Projections (a) for sphere (b)for Mickey Mouse	71
<i>Figure 4.8</i>	A 3D X –ray projections of the 3D sphere (a) The 3D projection for all range of Theta and specific Phi (b) The 3D projection for all range of Phi and specific Theta	72
<i>Figure 4.9</i>	A 2D slice projections from 4D x-ray projections for sphere (a) the 2D slice of 4D projection at specific Phi and several degrees of Theta (b) the 2D slice of 4D projection at specific Theta and several degrees of Phi.	72
<i>Figure 4.10</i>	A 3D X –ray projections of the Mickey Mouse (a) The 3D projection for all range of Theta and specific Phi (b) The 3D projection for all range of Phi and specific Theta	73
<i>Figure 4.11</i>	A 2D slice projections from 4D x-ray projections for mickey mouse (a) the slice of 3d projection at specific Phi and several degrees of Theta (b) the slice of 3d projection at specific Theta and several degrees of Phi.	73
<i>Figure 4.12</i>	the 2D reconstructed Slices from the 2D projection of the 3D Sphere for different Z values (a) Sphere reconstruct by BP (b) Sphere reconstruct by FST	75
<i>Figure 4.13</i>	the 2D reconstructed Slices from the 2D projection of the 3D Mickey Mouse for different Z values (a) Mickey Mouse reconstruct by BP (b) Mickey Mouse reconstruct by FST	75
<i>Figure 4.14</i>	The 3D reconstructed sphere from the 2D projection using BP method (a) representing the stacked 2D slices	76

	(b) the 3D representation where there is no internal sphere.	
<i>Figure 4.15</i>	The 3D reconstructed Mickey Mouse from the 2D projection using BP method (a) representing the stacked 2D slices (b) the 3D representation where there is no internal sphere.	76
<i>Figure 4.16</i>	The 3D reconstructed sphere from the 2D projection using FST method (a) representing the stacked 2D slices (b) the 3D representation where there is the internal sphere	77
<i>Figure 4.17</i>	The 3D reconstructed Mikey Mouse from the 2D projection using FST method (a) representing the stacked 2D slices (b) the 3D representation where there is the internal sphere	77
<i>Figure 4.18</i>	The 3D reconstructed sphere from the 2D projection using FST method after applying the threshold value (a) representing the stacked 2D slices after thresholding (b) the 3D representation after thresholding	78
<i>Figure 4.19</i>	The 3D reconstructed Mickey Mouse from the 2D projection using FST method after applying the threshold value (a) representing the stacked 2D slices after thresholding (b) the 3D representation after thresholding	79
<i>Figure 4.20</i>	The slices of reconstructed object from the 2D projection after apply filtering (a) sphere (b) head of mickey mouse	80
<i>Figure 4.21</i>	The 3D reconstructed from the 2D projection after apply filtering (a) sphere (b) head of mickey mouse	81
<i>Figure 4.22</i>	(a)The 3D reconstructed Sphere and head of mickey mouse from the 2D projection after apply threshold on filter object (b)The 3D reconstructed Sphere and head of mickey mouse from the 2D projection after apply threshold on no filter object	83
<i>Figure 4.23</i>	(a) The slices of the 3D reconstructed Sphere and head of mickey mouse from the 2D projection after apply threshold on filter object (b) The slices of the 3D	83

	reconstructed Sphere and head of mickey mouse from the 2D projection after apply threshold on no filter object	
<i>Figure 4.24</i>	The 3D reconstructed object by 3D BP from the 3D Projection (a) Sphere (b) Mickey Mouse	85
<i>Figure 4.25</i>	The 3D reconstructed object using 3D BP method from the 3D Projection (a) Sphere (b) Mickey Mouse	85
<i>Figure 4.26</i>	The 3D reconstructed object by BP after filtering from the 3D Projection (a) Sphere (b) Mickey Mouse	86
<i>Figure 4.27</i>	The 3D reconstructed object using 3D BP method from the 3D Projection after filtering (a) Sphere (b) Mickey Mouse	87
<i>Figure 4.28</i>	(a)The 3D reconstructed Sphere and head of mickey mouse from the 3D Projection after apply threshold on filter object (b)The 3D reconstructed Sphere and head of mickey mouse from the 3D Projection after apply threshold on no filter object	89
<i>Figure 4.29</i>	(a)The slices of the 3D reconstructed Sphere and head of mickey mouse from the 3D Projection after apply threshold on filter object (b)The slices of the 3D reconstructed Sphere and head of mickey mouse from the 3D Projection after apply threshold on no filter object	89
<i>Figure 4.30</i>	The 3D reconstructed Objects by using 3D BP from x-ray projections (a) sphere (b) Mickey Mouse	90
<i>Figure 4.31</i>	The slices of 3D reconstructed objects by using 3D BP from x-ray projections (a) Sphere (b) Mickey Mouse	91
<i>Figure 4.32</i>	The 3D reconstructed Object from x-ray projections by central section theorem at Fai (0°) and Theta (45°) (a) Sphere (b) Mickey Mouse	91
<i>Figure 4.33</i>	The slices of 3D reconstructed 3D Object from x-ray projections by central section theorem at Fai (0°) and Theta (45°) (a) sphere (b)Mickey Mouse	92
<i>Figure 4.34</i>	The Plane Projection at Fai (0°) and Theta (45°)	92
<i>Figure 4.35</i>	The Planes of Projection at Fai (0°) and Theta($45^\circ, 90^\circ$)	93

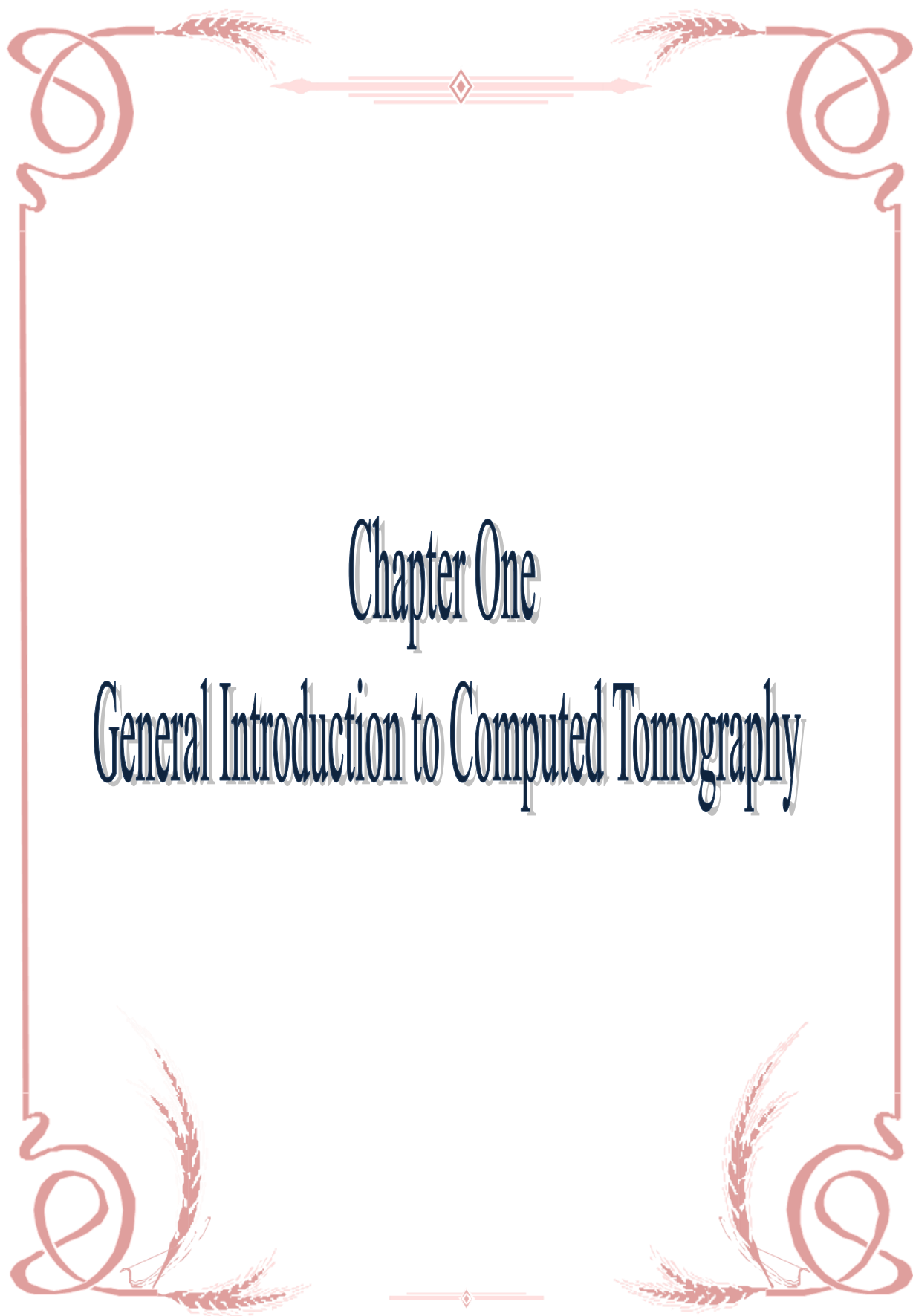
Figure 4.36	The 3D reconstructed Object from x-ray projections by central section theorem at Fai (0°) and Theta ($90^\circ, 45^\circ$) (a)Sphere (b) Mickey Mouse	93
Figure 4.37	The slices of 3D reconstructed 3D Object from x-ray projections by central section theorem at Fai (0°) and Theta ($90^\circ, 45^\circ$) (a) sphere (b)Mickey Mouse	94
Figure 4.38	The slices of 3D Object reconstructed from x-ray projections after filtering (a) sphere (b)Mickey Mouse	95
Figure 4.39	The 3D reconstructed Object from x-ray projections after filtering (a)Sphere(b) Mickey Mouse	95
Figure 4.40	(a)The 3D reconstructed Sphere and head of mickey mouse from x-ray projections after apply threshold on filter object (b)The 3D reconstructed Sphere and head of mickey mouse from x-ray projections after apply threshold on no filter object	98
Figure 4.41	(a)The slices of the 3D reconstructed Sphere and head of mickey mouse from x-ray projections after apply threshold on filter object (b)The slices of the 3D reconstructed Sphere and head of mickey mouse from x-ray projections after apply threshold on no filter object	98
Figure 4.42	(a) A slice of projection at different heights and at $\Delta\theta=2^\circ$ (b) 3D sinogram obtain from stacking the 2D projection and at $\Delta\theta=2^\circ$	99
Figure 4.43	The quality of the interpolated 3D sinogram	101
Figure 4.44	The quality of the reconstructed object before and after the interpolation process (a) Nearest Neighbor interpolation (b)Linear interpolation (c) Non-Linear interpolation	104
Figure 4.45	Number of points that belong to the object (a) Nearest Neighbor interpolation (b)Linear interpolation (c) Non-Linear interpolation	106
Figure 4.46	Number of points that belong to the hollow sphere (a) Nearest Neighbor interpolation (b)Linear interpolation (c) Non-Linear interpolation	109

List of Tables

<i>No.</i>	<i>Table Title</i>	<i>Page</i>
<i>Table 3-1</i>	The location, dimension, and density of the spheres that consist of the object	<i>53</i>
<i>Table 3-2</i>	The location, dimension, and density of the spheres that consist of Mickey Mouse	<i>54</i>
<i>Table 4-1</i>	The SNR, PSNR and RMSE before and after applying the threshold for both reconstructed objects from the 2D projection by FST method	<i>79</i>
<i>Table 4-2</i>	The volume of the reconstruction 3D object from 2D projection	<i>81</i>
<i>Table 4-3</i>	The SNR, PSNR and RMSE before and after apply Filtering for objects reconstructed by back-projections method from the 2D projection	<i>82</i>
<i>Table 4-4</i>	Shown the change in external structure with change the threshold value for filterd Mickey Mouse reconstructed by back-projections method from the 2D projection	<i>84</i>
<i>Table 4-5</i>	The volume of the 3D retrieved object from 3D projection	<i>87</i>
<i>Table 4-6</i>	The SNR and RMSE before and after apply Filtering on the 3D retrieved object from 3D projection	<i>88</i>
<i>Table 4-7</i>	The volume of the 3D retrieved object from X-ray Transform	<i>96</i>
<i>Table 4-8</i>	The SNR and RMSE of reconstruct objects from X-ray Transform before and after apply Filtering	<i>96</i>
<i>Table 4-9</i>	The SNR and RMSE before and after applying the interpolation methods for different dlta	<i>100</i>
<i>Table 4-10</i>	The SNR and RMSE before and after apply the interpolation methods at different dlta	<i>102</i>
<i>Table 4-11</i>	The No. of point Of the Out and internal object before and after apply the interpolation methods at different dlta.	<i>105</i>
<i>Table 4-12</i>	the change of the shape of the retrieved object by the FST method with the increase of the angular interval.	<i>107</i>
<i>Table 4-13</i>	The change of the shape of the retrieved object by the BP method with the increase of the angular interval.	<i>108</i>

List of Abbreviations

<i>Abbreviations</i>	<i>Original</i>
<i>2D</i>	<i>Two Dimensional</i>
<i>3D</i>	<i>Three Dimensional</i>
<i>4D</i>	<i>Four Dimensional</i>
<i>ADC</i>	<i>Analog signal to Digital Converter</i>
<i>BP</i>	<i>Back-Projection</i>
<i>BPF</i>	<i>Filter after the Back-projection</i>
<i>CT</i>	<i>Computed Tomography</i>
<i>dB</i>	<i>Decibel unit</i>
<i>e</i>	<i>error</i>
<i>e_T</i>	<i>Total error</i>
<i>FBP</i>	<i>The Filter before the Back-Projection</i>
<i>FST</i>	<i>Fourier Slice Theorem</i>
<i>IRT</i>	<i>Inverse Radon Transform</i>
<i>LOR</i>	<i>Lines Of Response</i>
<i>MSE</i>	<i>Mean Square Error</i>
<i>PET</i>	<i>Positron Emission Tomography</i>
<i>Pixel</i>	<i>Picture Elements</i>
<i>PSNR</i>	<i>Peaks- Signal to Noise Ratio</i>
<i>RF</i>	<i>Ramp Filter</i>
<i>RMSE</i>	<i>Root Mean Square Error</i>
<i>RT</i>	<i>Radon Transform</i>
<i>SNR</i>	<i>Signal to Noise Ratio</i>
<i>SPECT</i>	<i>Single Photon Emission Computerized Tomography</i>
<i>Voxel</i>	<i>Volume Elements</i>



Chapter One

General Introduction to Computed Tomography

Chapter One

General Introduction to Computed Tomography

1.1 Introduction

Computed Tomography (CT) technology has a significant impact on the medical field to diagnose the disease accurately without the need for surgery. Tomography a method of producing a three-dimensions image of the internal structures of an object in a non-destructive manner [1, 2]. This technique is done using different types of imaging techniques, some of which depend on the exposure of the body to a particular radiation or waves from different angles such electromagnetic (EM) spectrum that consists of visible light, infrared (IR), ultraviolet (UV), X-rays, microwaves, radio waves, or gamma waves or any other signal that can be measured [3] or injecting the body with little quantities of radioactive materials called radiopharmaceuticals, the quantity and type of materials vary depending on the type of organ that wants to be scan [4].

They can be based on one or more physical parameters for the resulting radiations that are emitted, transmitted, or reflected from the object to process by electronic devices and produce computed tomography images for the body [5].

1.2 A Brief History of Computed Tomography

The Austrian scientist Radon explained the main mathematical idea of seeing inside the body where he derived mathematical equations to reconstruct the body from the finite number of projections in his article published in 1917 (the projection system definition in section 1.4) [1] [6].

In the forties of the last century, Gabriel Frank and other scientists explained the first experiments to reconstruct the images from their projections and these experiments were done before the discovery of the computer. In 1940 Gabriel Frank was awarded a patent for his description of the main ideas used in tomography to this day, includes devices used to obtain sinograms and back projection techniques to reconstruct images [7].

In the fifties of the last century, several researches and articles were published in the field of CT based on radon equations one of them in 1956 R. N. Bracewell published a paper titled ‘Stripe Integration in Radio Astronomy’, he was the first scientist applied the main mathematical idea of Radon equations to construct two-dimensional images in his paper mentioned above [6].

In 1961, William H. Oldendorf made in series of experiments based on principles close to the principles used in computed tomography [8], the purpose of his experiments to know the possibility of seeing inside the body through the passage of radiation inside the body and then receive the final signal by a detector. In this experiment, the line required to be reconstructed must pass through the center of the machine, in other words, the process reconstruction here is linear and there were no attempts to reconstruct the two-dimensional because each linear reconstruction process requires a full hour and at that time there was no way to store the data [7].

In 1963, David E. Kuhl and Roy Q. Edwards experiments were done by devices using radioisotopes, these devices are known today as emission computed tomography [9]. They used two detectors in an opposing location and the survey was done in regular steps. At each step, the result was received on the moving film according to the location of the detectors. The film was rotated to summation the back-projected views. In modern equipment, the film has been replaced with a computer [7].

In 1963 and 1964 Allan M. Cormack publishes the results of his experiences where he built the initial CT scanner. Unluckily, his results did not receive significant attention at that time because it requires difficult calculations and a long time to do it [7].

In 1967, Godfrey N. Hounsfield developed the first clinical scanner using X-ray based on algorithms discovered by Allan M. Cormack earlier as shown in figure (1-1), this scan took nine days to produce a picture for specimen because the scan is linear and performed by rotate specimen one degree in each step [10] [7]. Godfrey Hounsfield deduced independent of Cormack that we can see inside the body by taking X-ray measurements on the same body from all directions. In 1979, Godfrey N. Hounsfield won the Nobel Prize for his discovery and shared it's with Allan M. Cormack [7].

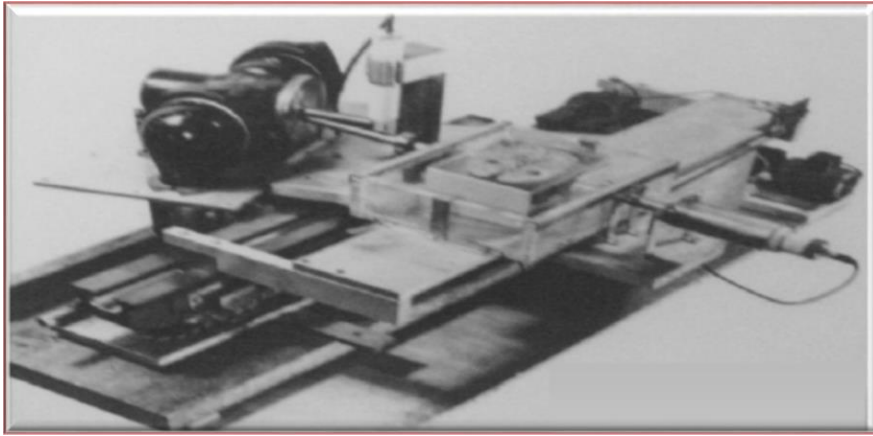


Figure 1-1 The device of Godfrey N. Hounsfield.

Attempts to improve clinical scanner performance continue to this day and after making many modifications to the clinical CT scanner, we can obtain clear and good images in a few minutes compared to the old devices that are not improved as shown in figure (1-2) [7].

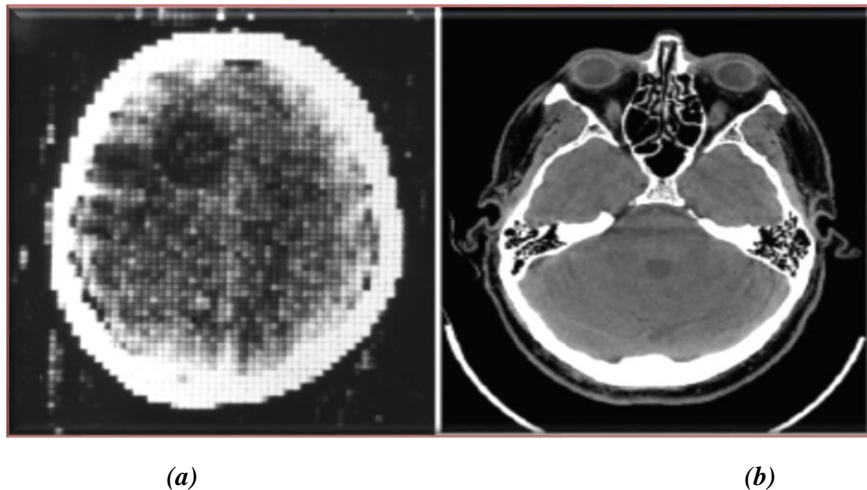


Figure 1-2 Images of (a) The first CT scanners. (b) The CT scanner in 2005 [7].

The improved clinical CT scanner was first installed in a London hospital in September 1971 as shown in figure (1-3) where in October 1971 the technique was applied to the first patient who had a large sac in his head and it clear in the image produced [7].



Figure 1-3 Apply the CT scanner on the first patient [7].

1.3 Imaging System

Digital images are formed when a certain type of energy interacts with the sensor or the detector in the imaging device. The detector or sensor varies from one imaging device to another depending on the type of energy or radiation used in that device. This energy may be an ultrasound or a component of the electromagnetic spectrum, for example, visible light, infrared, microwave, radio waves, gamma waves, or uses radioactive material inside the body that emits a certain type of energy that can be handled by a detector [3].

The energy used for imaging and associated with imaging device is selected depending on the nature of the object or the organ to be photographed or scanning, in terms of the density, the contrast between the organs and the object sensitivity to the energy i.e. its capacity for measuring the weakest possible intensity level, also the type of radiation is chosen depending on its ability to distinguish between different organs of the body and its ability to portray the tiny details [5].

Since the tomography gives us the internal structure of the body so it uses the types of radiation that have the ability to penetrate the tissues to be photographed [11]. In this section, will review some of the devices used in tomography.

In nuclear medicine using (Single Photon Emission Computerized Tomography) (SPECT) and (Positron Emission Tomography) (PET) in these types of the scanner, the patient is injected with a radiopharmaceutical that emits Gamma rays, Gamma rays are detected and measured by detectors then the measured information from this radiation used to create a two- or three-dimensional image for the desired organ [12] [3] [13].

Ultrasonic imaging by sending a series of high-frequency sound waves (higher than 20 KHz) to the organ and then the measured information from reflected waves are used to obtain a 2D or 3D a gray image. The ratio of reflected waves depends on the difference the resistance of the neighboring organs for ultrasonic waves, The proportion of reflected waves increases as the difference in resistance increases between the two neighboring members so the difference in the density and resistance of organs to the waves is the basis for the formation of ultrasound images [3] [14].

In this dissertation, we will focus on X-rays tomography. X-ray is an electromagnetic ray widely used in radiography and in many technical and scientific fields. In 1895, William Rontgen discovered unknown ray has the ability to see the skeleton in a living person. Where he had been working with a device used to generate "cathode rays" in a vacuum glass tube when the high voltage between the cathode and the anode is applied and a phosphoric screen was placed at the end of the tube. When the electron beam (cathode rays) collided with it, this screen began to glow, then Richard

Roentgen put his hand between the tubing that generates X-ray and the phosphoric screen, he saw the skeleton form for his hand on the phosphoric screen. This was the first operation of X-ray imaging [15].

On this day X-rays are much used in the medical field to generate a 2D image (in traditional radiography) or 3D image (in a CT) to the skeleton of the patient to diagnose his illness. This done by passing X-rays through the patient and recorded on the film that responds to X-ray energy in conventional radiography or captured it by the detector in CT scanner [3].

Figure (1-4) shown the basic devices in CT scanning using X-ray. The Filtering used to reduce radiation dose and to get better quality for images. The Collimators used to restrict the X-ray beam on a specific area. The Detector used to measure the X-ray photons and convert it to an analog signal (electric), the ADC (Analog to Digital Convert) is to convert the analog signal to a digital format and sent to the computer [16].

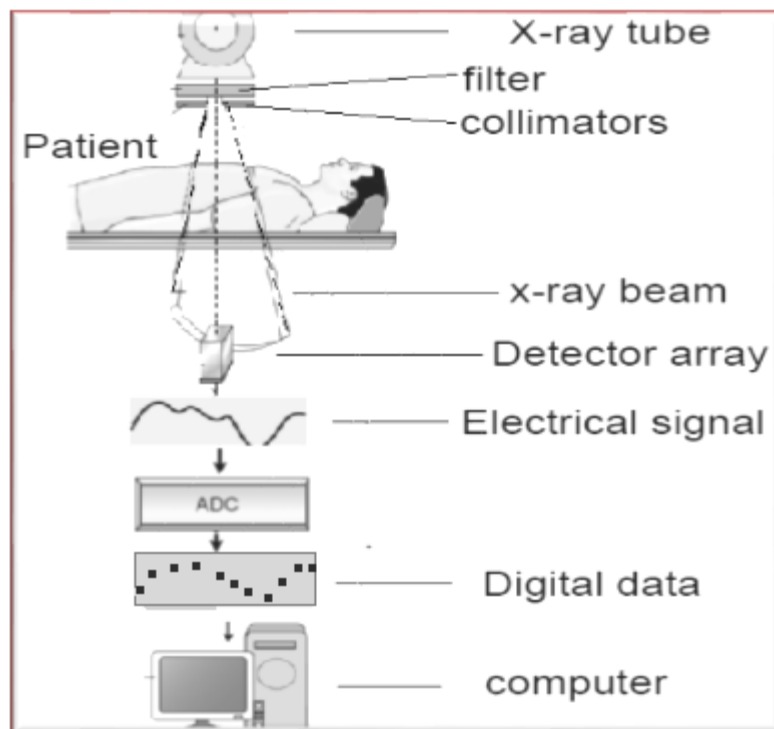


Figure 1-4 The basic devices in CT scanning using X-ray [16].

1.4 Scanning Modes (The Projection System)

The combining of a set of linear integrals along all parallel lines of response (LOR) forms the projection $p(t, \theta)$ for a certain angle (θ) to the object $f(x, y)$ with x and y the spatial Cartesian coordinates [1]. The combination of all projections for $0 \leq \theta < \pi$ forms a 2D function with t and θ the polar coordinates that is called a sinogram as shown on the right of figure (1-5), in which the horizontal and vertical axis's represents the values of the distance from the center of rotation and the angles respectively [17] [18].

The name of the sinogram comes from the fact that every point in the spatial space (in the body) when converted into the space of Projection, the behave of each point will path of a sinusoidal. So, the sinogram for the whole object would be a superposition of all paths sinusoids corresponding to each point in the object as shown in figure (1-5). Each row in the sinogram has values of the projection at a certain angle [17] [19].

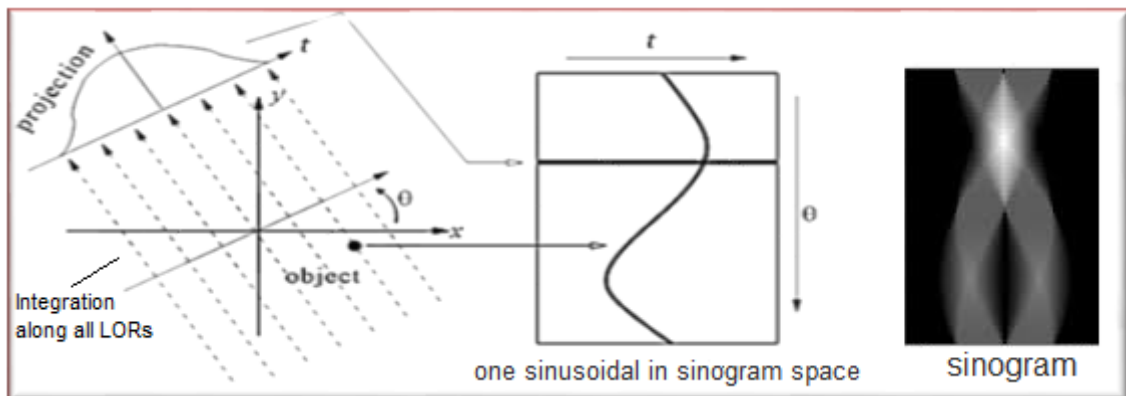


Figure 1-5 A projection and a sinogram [17].

Although there are many types of scanning techniques, some of the advantages and disadvantages of only three major types will discuss in this section, as shown in figure (1-6).

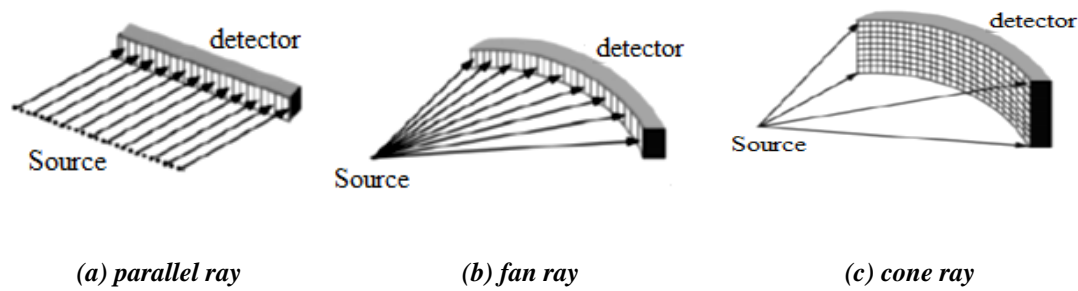


Figure 1-6 Three types of projections systems [7].

- a) The first system uses the ray in the form of parallel (projections on parallel form).
- b) The second system uses the ray in the form of a fan (projections on fan form).
- c) The third system uses the ray in the form of a cone (projections on cone form).

In this dissertation, the parallel ray system will be focus on.

1.4.1 *Parallel Ray Integral.*

The simplest type of the scanner is a collection of the parallel ray as shown in figure (1-7). This method also called parallel projections because of the measurement of linear integrations in the form of parallel lines for a number of different angles. For example, to forms a 2-D sinogram for slices of the object, the sources that generate an X-ray and the detectors that receive the X-ray that located on the opposite side of an object must rotate around object and by using a set of slices sinogram that forms a 3-D sinogram for the 3-D object [1]. This method is slow so it needs a long time [20].

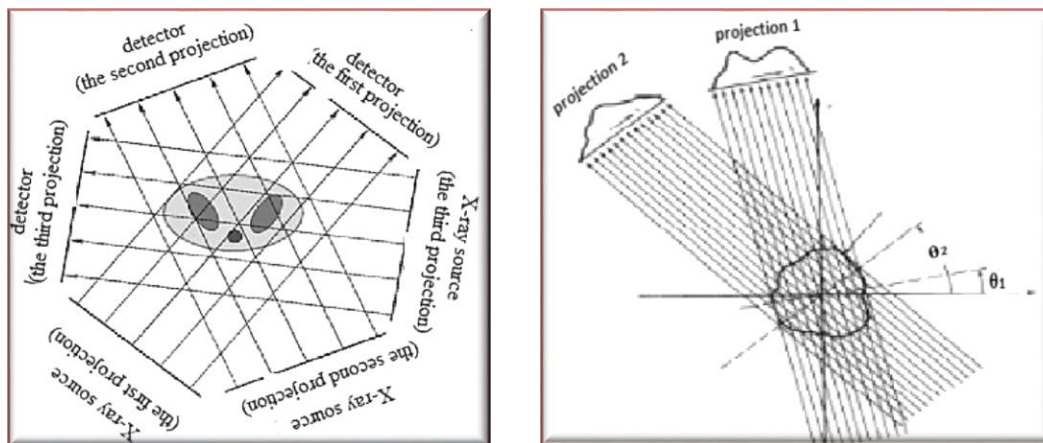


Figure 1-7 Parallel projection [20] [1].

1.4.2 Fan Beam

This technique, a single source and the array of the detectors uses on the opposite side of an object as shown in figure (1-8). This method also called a fan projection because of the measurement of linear integrations in the form of a fan for a number of different angles [1]. Projections in the fan form can cover an extensive area of the object at each moment of scanning, so, in this method can reduced the number of projections that require to retrieve object in high quality and the time required for taking the projections for an object has been reduced compared to the first method [20].

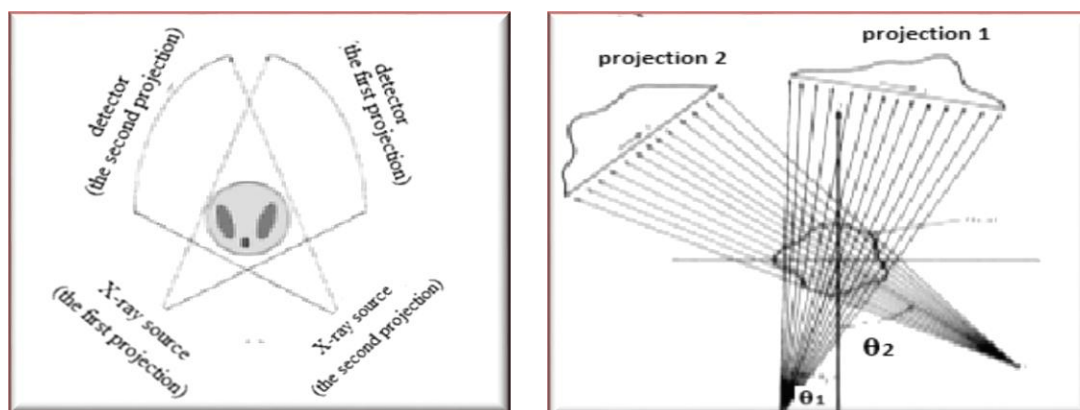


Figure 1-8 fan projection [20] [1].

1.4.3 Cone Beam

A single source and the array of the detectors on the opposite side of an object uses this technique as shown in figure (1-9), Here the whole object is illuminated from source rather than one slice as in the previous two methods. This method called a cone beam reconstruction because the rays form a cone [1].

The main advantage of this technique that it increased scan speed where the time required to take the projections for an object was reduced compared to previous methods [20].

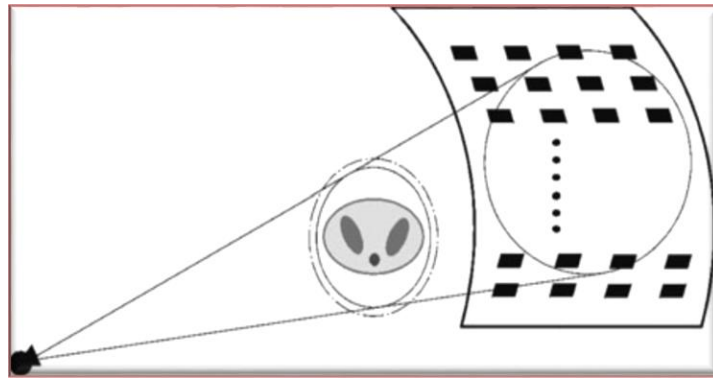


Figure 1-9 Cone beam projection [20].

1.5 2D Digital Image Representation

The digital images are formed when a certain type of energy interacts with the sensor or the detector in the imaging device. When the energy used is visible light, the image formed by a summation of light energy called the optical image and the device used to capture it by the camera [3].

The 2D digital images, $I(r, c)$, can represent it as a 2D matrix of data $I(r, c)$, and one row (or column) is called a vector, it is composed of a finite number of elements as shown in figure (1-10). These elements are referred to as picture elements (pixels). Pixel is the term used most widely, each of

which has a particular location and value, the value of the point (r, c) represents the brightness of the image at that point [3].

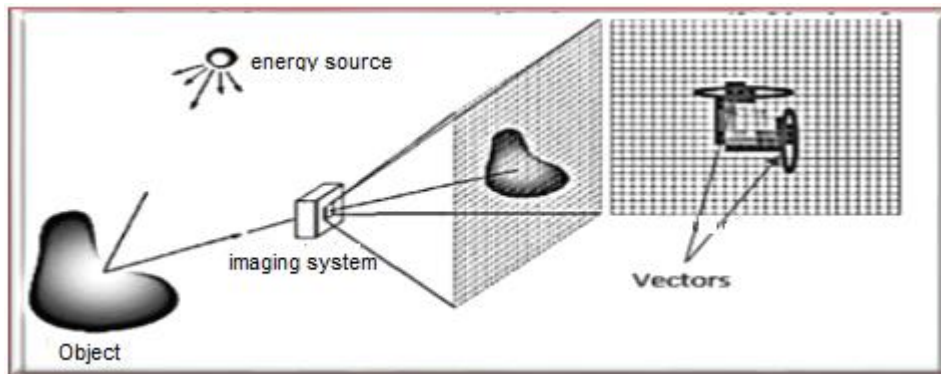


Figure 1-10 2D image representation [21].

1.6 3D Digital Image Representation

Three-dimensional digital images are widely available for the computer representation inclusive computed tomography, medical imaging, and computer vision [22], a Computer Tomography CT images consist of a number of slices, each of these slices corresponds to the part or section that is scanned from the patient's body. Each slice of CT has a specific thickness so it is composed of voxels (volume elements) rather than a typical digital image is composed of pixels [23] [24]. A voxel or volume element is a representation of 3D data of the tissue volume as shown in figure (1-11) whereas X, Y and Z are an indication of the width, length and height (or thickness) of a voxel in sequence. The face of the voxel is the pixel (i.e. X and Y) [16].

The 3D image doesn't reconstruct directly in most the tomography imaging systems but reconstructed in series of steps such as reconstructing multiple 2D slices from its projections in a specific direction and then sticking them in the same direction [25].

In this dissertation, the reconstruction of three-dimensional images will be a focused on.

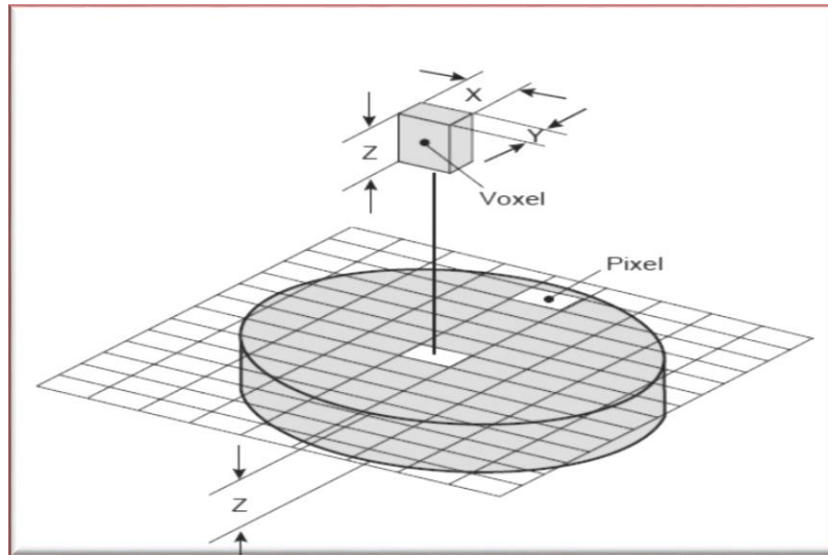
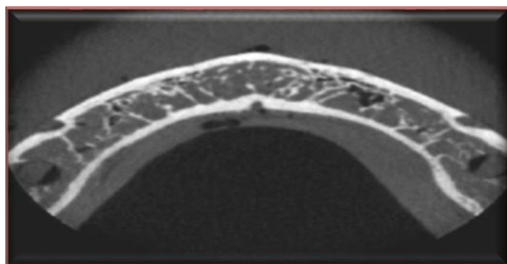


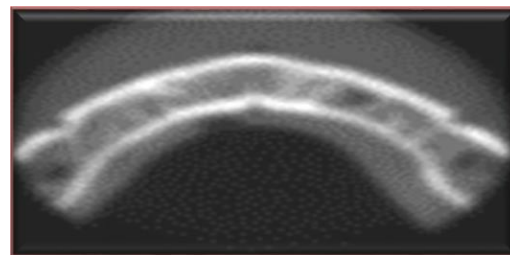
Figure 1-11 The data that form the CT slice [16].

1.7 Quality of CT Images

It is important to estimate the quality of CT images to clarifying its features accurately and to achieve good diagnostic data from the CT images [26]. There are four essential factors that have a significant impact on the image quality they are the spatial resolution, contrast value, noise, and artifacts as shown in figure (1-12). Additionally, there are other minor factors that have an effect on image quality. These factors depend on the geometry of the imaging technique used. This section will present a summarized view of the essential factors that affect image quality [27].



a



b

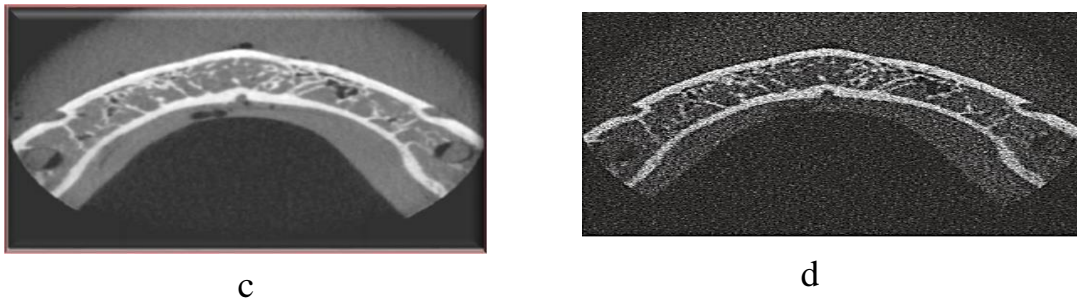


Figure 1-12 (a) Original image (b) decreasing spatial resolution, (c) decreasing contrast value and (d) adding artificial and noise [27].

1.7.1 Spatial Resolution

Spatial resolution (or sharpness) is the capacity to identify small details in the images, or can be expressed as the capacity to differentiate between details and edges of objects or structures that vary in its densities, for example, differentiate between bone and soft tissue. So, for differentiating between converging structures requires high spatial resolution [27]. The estimation of the spatial resolution of CT images is influenced by a huge number of factors. The properties of the computed tomography system have essential effects in spatial resolution, the X-ray scatter and focal spot size of the X-ray source is an operator that should be taken into account when determining the spatial resolution where generality X-ray tubes have two focal spot sizes (small and large focal spots size). Small focal spots made to minimize blurring and best perceivability of details, while large focal spots have greater heat-dissipate capability [29]. The other property of the CT system that has effects on the spatial resolution is detector (pixel size, scattering), also, other factors can effects on a spatial resolution for example projection geometry, patient move, and reconstruction algorithm [28] [27].

1.7.2 Contrast Value

Contrast value in CT images is the capability to distinguish between objects that have variation in density or can define it as attenuation by the body at different parts depending on the density of each part [29] [27]. Where the white color in the image represents bone, the soft tissue represents by various shades of gray levels where the degree of gray color depends on the amount of water in the soft tissue and the black color in CT images represents the space (air) [30].

There are two kinds of contrast resolution in computed tomography images which are high contrast resolution and low contrast resolution, These types are classified depending on the degree of contrast between the body and the background, whether high or low [31].

Contrast value in computed tomography images is influenced by a number of factors such as, the type of ray used, the thickness of the object, object size, reconstruction algorithm, image shows and noise [32].

1.7.3 Noise

The definition of image noise in computed tomography images as the variability (e.g., standard deviation) of gray levels values in a homogenous body [27]. There are different sources of noise of CT images including X-ray dispersion that perform undesirable results in CT images and noise associated with the detector's bad response, the noise can be reduced or removed by the applied filter in reconstruction algorithms [27].

1.7.4 Artifacts

There is no explicit definition of artifacts in CT images, but its theoretical meaning can be explained at a certain point as follows: the

difference between the reconstructed value and the actual value of the object at that point [7]. In other words, any difference between the reconstructed image and the physical reality considered artifacts [27].

The major types of artifact in computed tomography images can be summarized as streaking, shading, rings, bands, aliasing artifact and artifacts due to motion object [7] [27].

Streaking artifacts are formed as straight lines, random or parallel across the image and appear in black, bright or mixed between the two colors depending on the cause of appearance. The streaks are due to an error in the data collection process, a mechanical malfunction, object motion or because of the presence a metal [7].

Shading artifacts often appear near objects of high contrast. such as, in the smooth tissue zone close to the bone. They can be either bright or dark, depending on the kind of causative [7].

Ring and band artifacts as shown in figure (1-13), It is clear to us from the name of the artifacts that they are shaped as perfect rings, partial rings (arcs) or bands in CT images. We can easily identify artifacts if they are whole rings or bundles while the brackets may be described as a disease rather than a defect and this poses a risk in medical diagnosis [7], Depending on the signal given by the detector, these artifacts appear bright or dark [32].

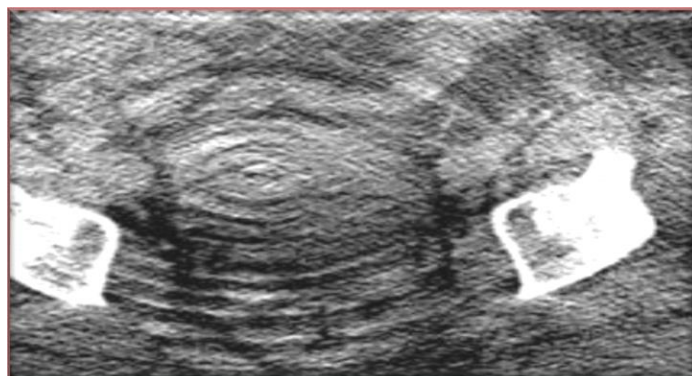


Figure 1-13 Numerical of ring artifact [33].

Metal artifacts appear as star in CT images, they are produced because of the difference in absorption between a material placed in the body and the original body as shown in figure (1-14) [32], It is commonly made from materials that are hard to penetrate by X-rays like titanium or stainless steel compared to the original body such as the knee, the hip, shoulder prosthesis, cardiac pacemakers, dental fillings and metallic screws to fix teeth replacements [34].

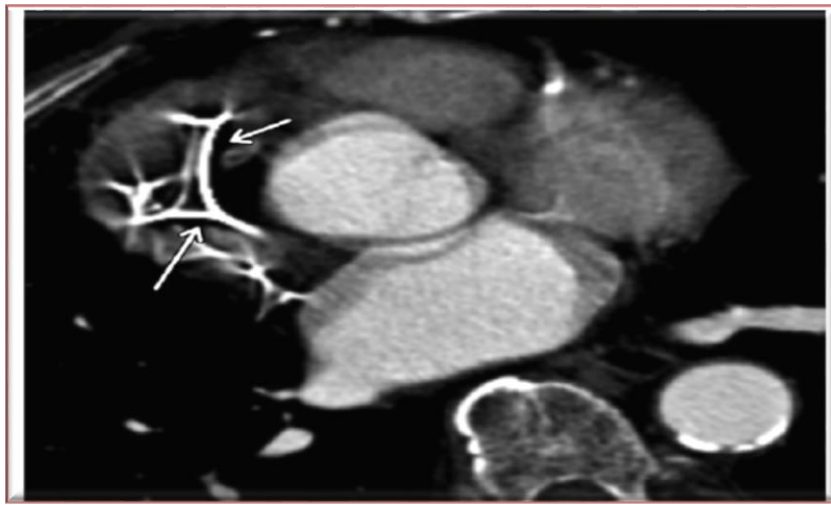


Figure 1-14 CT image for heart shows metallic artifacts from the cardiac pacemaker [35].

There are other types of artifacts, including the happens when the patient moves during taking the CT image called motion artifacts [31] as shown in figure (1-15). When the patient moves a small movement, for example, taking a deep breath during image capture, the artifacts will be in the form of blurring while the artifacts will be in the form of double images when the patient movement is large [32].

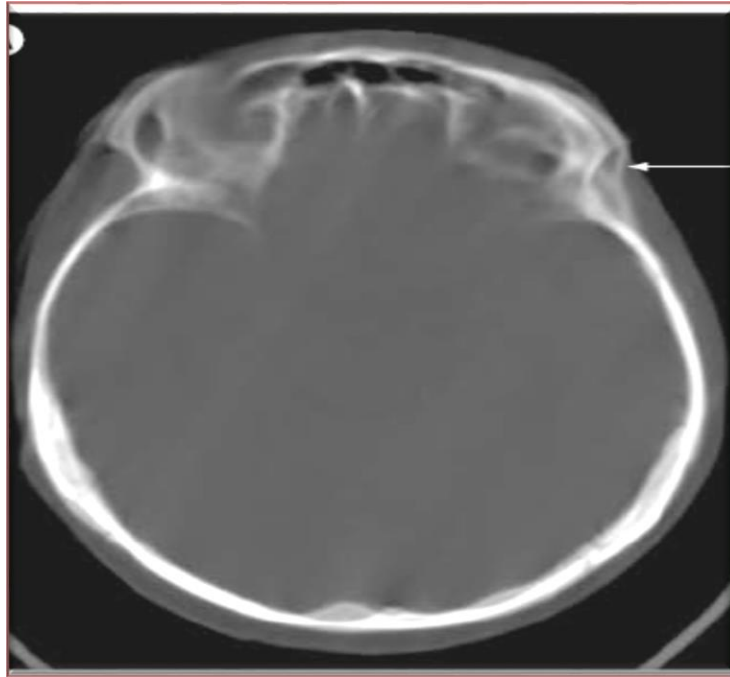


Figure 1-15 Motion causes blurring and double images in a head CT [33].

1.8 Literature Review

Many researchers use tomography as headlines in their work; some of the published works are:

- ❖ In 1999, Lanzavecchia et al., [36] studied a new algorithm to reconstruct 3D object. It recovers the 3D Radon transform from the 2D Radon transforms. They have shown that this algorithm works with accuracy and is faster than commonly used algorithms.
- ❖ In 2000, Zeng [37], studied reconstructing a three-dimensional object by sticking several of two-dimensional images that reconstructed by back-projection process, the author deduced from the results is that the final object is unclear and inaccurate because of the blurring, which is resulting from the participation of points that located outside the body in the reconstruction of the object.

- ❖ In 2002 Abdul Jabar [25], depended on equations proposed by Kak & Slany and Pratt for a two-dimensional projection with modifications on back projections equations to derive the back projections equations in the Polar and Cartesian coordinates. Then compare these two methods based on the time it took to reconstruction images and the quality of the image's reconstruction. Also, he studied the impact of four types of filter on the CT images, and compare the performance of these filters against standard filters.
- ❖ In 2007, Zosso et al., [38] left to the readers an open-source National Library of Medicine Insight Segmentation and Registration Toolkit (ITK) implementation of a direct Fourier method for tomographic reconstruction, by using parallel-beam X-ray images. They had given the framework of direct Fourier reconstruction and the algorithm they developed. They supply results based on the Shepp-Logan phantom image also discuss the various reconstruction parameters and display their particular effect on the reconstruction results. One of the results they have shown that the image reconstructed by the proposed method is of high quality compared to the image reconstructed a standard filtered back-projection method provided by Matlab.
- ❖ In 2012, Rajendran et al., [39] studied Radon transform to obtain local tomography rather than global tomography, one of the aims of that is to reduce the dose of X-ray exposure to the patient. The local tomographic reconstruction is obtained for a defined ROI (A region of interest, samples important inside information set specific for a certain study), the ROI can be either a square or circular region. They used the filtered back-projection technique,

whose length is dependent on ROI size and projection angle. From results, the authors show Cosine filter provides better results vs to Shepp Logan filter.

- ❖ In 2015, Sobani et al., [40] reconstructed an object using multiple-views of 2D images using MATLAB tools, while data is captured by a digital camera. The results showed that 3D reconstruction it's good enough to reconstruct exactly the same shape as the original object.
- ❖ In 2015, Tang, [41] studied the impact of projection angle errors on reconstructing three-dimensional electron tomography by using the Fourier iterative method (FIRM) as a reconstruction method. That thesis focuses on impacts of miss alignment on reconstruction vs noise and missing wedge impacts. He found that the missing wedge has the greatest effect among the studied factors, loss of necessary information for complete reconstruction causes damage to the reconstruction image. Missing alignment and Gaussian noise have the same impacts on the reconstruction image. He concluded when the projection angle error does not change too much, the reconstructed 3D volume has a few changes which were measured both with normalized mean square error (NMSE) and Fourier shell correlation (FSC).
- ❖ In 2016, Xiaoli Yang, [42] proposed the use of a little number of projections to produce accuracy tomography reconstruction. He proved image reconstructed from confined projections using optimized CGTV (Conjugate gradient-based restoration algorithm with Total Variation regularization) with data obtained by X-ray imaging, it preserved resolution to accepted limit and their several

disadvantages in the filtered back-projection (FBP) method overridden by the proposed method. His method decreased the number of projections from about 1000 to about 100 with preserve reconstruction image quality. He suggested that in addition to applying this method in biological and medical fields, it is also applied in industrial fields for example structure analysis of materials.

- ❖ In 2016, Vassholz et al., [43] in their article suggested a new method to the reconstruction of the three-dimensional object. They used anisotropic sources to obtain isotropic 3D imaging, the reconstruction based on three-dimension radon transform. They applied special geometric to avert artifacts that produced by the contribution of the points outside the reconstructed object when using the integral of the projections that pass through and outside the object, as usually consists in a two-dimensional Radon transform.
- ❖ In 2018 Louis Godon, [44] introduced a number of suggestions for the development of computed tomography. Where he gave an empirical description of computed tomography model and implementation of this model in companies, he also gave estimate the oil and water ratio inner a porous rock. He focused on three-dimensional imaging by the use of cone ray geometry in computed tomography and the importance of determining scanner geometry that has an impact on the reconstruction process the geometry was determined based on a set of projections of a calibration phantom. He used FDK (Feldkamp analytic cone beam algorithm) and SART (Simultaneous Algebraic Reconstruction Technique) reconstruction algorithms to reconstruct a phantom.

- ❖ In 2018 Kim et al., [45] applied the interpolation methods to sinogram to reconstruct an image from a little number of projections where they used sparse angular sampling rather than normal dense angular sampling in computed tomography scanning then normalized the sinogram obtained by little (sparse angular) they applied some methods of interpolation on the normalized sinogram. They generated a corrected sinogram using multiplying the interpolated sinogram by the prior sinogram and is used to reconstruct the final CT image by using the FBP algorithm.

1.9 Aims of the Study

The aims of this present work can be abbreviated by the following:

- ❖ Study the algorithms to reconstruct 3D image for any object by parallel beams geometry in computed tomography, using the slicing, direct 3D projections and X-Ray transform methods in spatial and frequency domain by the 2D, 3D and 4D sinogram spaces.
- ❖ A new interpolation method is proposed to recover the short in available projections due to the high angular difference that used in the object scanning phase.

1.10 The Layout of the Dissertation

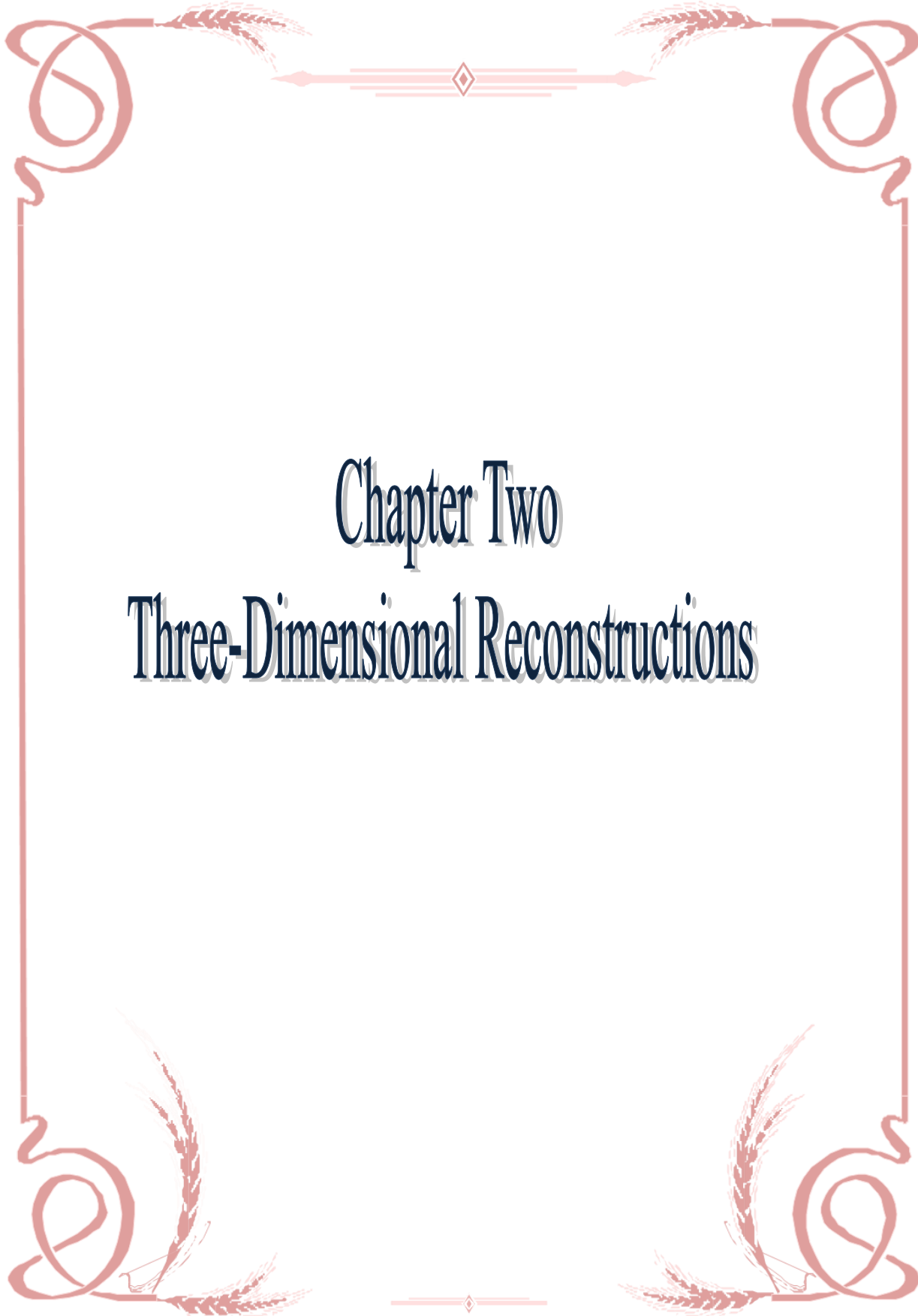
In addition to the current chapter, this work includes another four chapters:

- ❖ **Chapter 2: “*Three-Dimensional Reconstructions*”** supplies some basic definitions in the field of computed tomography and other necessary ideas that have been used in this thesis. Such as the mathematical equations of 2D and 3D projections. The methods of reconstruction of 3D images are shown, also the type’s interpolation used in this work.

- ❖ **Chapter 3: “*Methodology of Reconstructing 3D Images*”** discusses the steps to establish algorithms for the 3D image reconstruction in computed tomography and describes the steps of the algorithms in detail.

- ❖ **Chapter 4: “*Results and discussion*”** included the computed results and schemes are given to illustrate the reconstruction and the improvements in the performance of the suggested method.

- ❖ **Chapter 5: “*Conclusions, Suggestions and Future Works*”** displays the conclusions obtained from the discussion of the test results. In addition to the several suggestions are given for future work.



Chapter Two
Three-Dimensional Reconstructions

Chapter Two

Three-Dimensional Reconstructions

2.1 Introduction

This chapter focused on the reconstruction of a three-dimensional image for a three-dimensional object by tomographic imaging based on linear integration projections and planar integration projections.

Imaging the inside density distribution of a 3D object using a collection of its 2D projections can be considered an extension of computerized tomography, which was originally developed for reconstructing two-dimensional cross-sections (slices) of a three-dimensional object from its one-dimension projections [46] [47]. It was first used in positron emission tomography based on two planar detectors rotating around an object in a static angular interval [48]. While reconstructing the three-dimensional object using the Fourier transform was first proposed in 1977 by Chu and Tarn [48].

As mentioned earlier in the first chapter that one of the purposes of X-ray computed tomography is to acquire images internal structure of the object. This chapter will present several ways of reconstruction it depends on radon transform in two or three dimensional and others depend on X-ray projections.

2.2 2D Forward Projection

To understand the concept of reconstructing 3D images in the first must understand the concept of projection which is called Radon transform according to the name of scientist Austrian mathematician **Johann Radon (1887)** which laid the fundamentals of this transform [49]. Radon transform works to find the amount of density inside the body along a particular line (l) tilted from the X-axis at particular angle and a distance (t) from the point of origin by a linear integral along each line [50], and by combining the set of linear integrals lead to form the projection that has various values at each different angle as shown in figure (2-1) [50], [1].

The line integral means the integral of some parameters inside an object along a straight line. The choice of the type of parameter depends on the type of physical phenomena (e.g. absorption, attenuation, reflection, etc.) that occur for the radiation used for CT imaging, for example when the X-ray passes through the object, it will be attenuated [1]. So, the linear integration value of a single straight line represents the total attenuation of X-ray along that line [1].

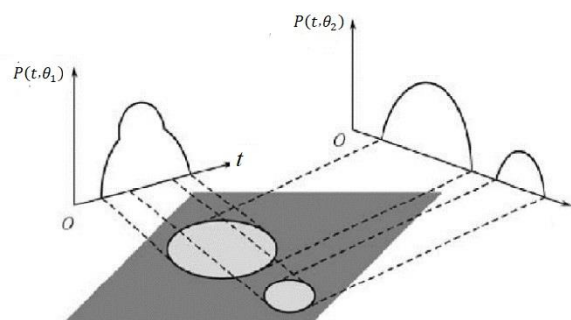


Figure 2-1 The projections at various angles [51].

2.3 2D Tomography

To illustrate the mathematical equations of the projection we assume an object represented by a two-dimensional function $f(x,y)$ and each line integral represented by the $P(t,\theta)$ parameters, the coordinate system will be used to describe the projection and linear integral can be illustrated in figure (2-2).

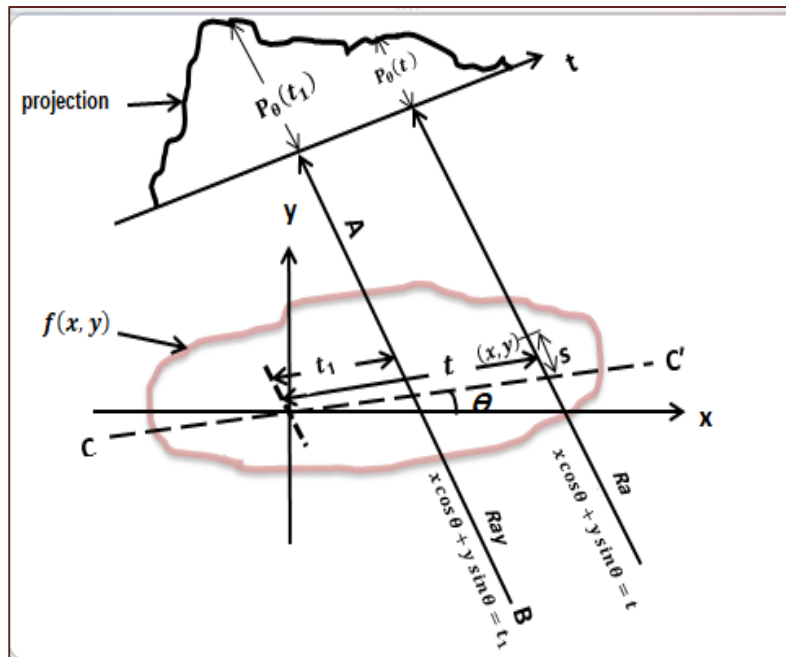


Figure 2-2 The coordinates system of projection and the linear integral [1].

The line AB define by equation (2-1) [1]:

$$x \cos \theta + y \sin \theta = t \quad (2-1)$$

The orientation of projection can define by:

$$\vec{a} \equiv (\cos \theta, \sin \theta)$$

Where (t) represents the length of the line integral distance from the origin and symbol (θ) represents the angle of rotation.

The linear integration $P_{\theta}(\vec{\alpha}, \vec{X})$ can be defined as the following:

$$P_{\theta}(\vec{\alpha}, \vec{X}) = \int_{(t,\theta)\text{line}} f(x,y) ds \quad (2-2)$$

Where $\vec{X} = (x,y)$ and (s) represent the set of (x,y) points that belong to the integral line $P_{\theta}(t)$ that have distance (t) from the origin and making angle equal to (θ) with the positive X-axis [25].

Using a delta-Dirac function to calculate the (x,y) set the point that belongs to the $P_{\theta}(t)$, the equation of forwarding Projections became [1].

$$P_{\theta}(t) = \int_{-\infty}^{\infty} \int_{-\infty}^{\infty} f(x,y) \delta(x \cos \theta + y \sin \theta - t) dx dy \quad (2-3)$$

The equation $P_{\theta}(t)$ is known as the forward projections or the Radon transform of the object $f(x,y)$. Where the projections are produced when collection a series of linear integrals [1], [25].

In addition, we must clarify that the transform from $f(x,y)$ to $P_{\theta}(t)$ by linear integral transform also called X-ray transform, it is completed by the imaging operation, which is similar to Radon transform in two dimensions while in three dimensions does not resemble Radon transform in three-dimensional, which will be explained in sections (2.4).

2.4 2D Image Reconstruction Methods

In computed tomography, the reconstruction algorithms are basically categorized into two groups which are: methods that depend on Transform (analytical method) and on Finite series expansion (iterative methods) each of these methods has its advantages and limitations [17].

The method to reconstruct the image is selected, if it is analytic or iterative, depending on the nature of the projections in terms of their

number and quality of capturing them and also, depending on the type of object that needs to be imaged it (bone or soft tissue), the maximum time allowed to reconstruct the image and the nature of the equipment used in tomography imaging [17] [40].

The transform methods are widely used for image reconstruction, it is used when the time required to reconstruct the image is limited and the resulting image in this method is acceptable quality, although this method is based on fictional models which are somewhat unrealistic [52]. Transform methods are the most widely used methods in many devices that depend on X-ray computed tomography technology which fair highly to Signal to Noise Ratio (SNR), to obtain a high-quality image that reconstructed by any method of transforming methods requires quality and high density of projections. In many statuses, the quality and /or quantity of data is not enough for the transform methods. These statuses notice, for example, when the image is taken with a small dose of radiation in medical imaging, taken an image for an object with widely varying densities or taken an image with a limited number of projections [25].

To form the image in an analytical method requires a direct mathematical solution while in the iterative method requires many iterations based on a complex mathematical solution [17], in addition, while the Series-expansion methods (Iterative method) have advantages than analytic, where an acceptable image can be obtained when the data is incomplete, inconsistent and noisy in data resulting from attenuation, scatter and random in projections beam [53] [48].

Besides these advantages of series-expansion methods, there are two major disadvantages that make these methods undesirable for reconstructing the images, which are [25]:

First, this method is based on the statistical mathematical concept in which it estimates from a given two-dimensional projection the closest image that could produce such projection, so it is an inaccurate method if compare it with the transform methods [25].

Second, this method is based on an estimating the image from the projection based on the iterative process for linear equations for reconstructing an image, and to increase the quality and accuracy of the reconstructed image, we must increase the number of iterations needed to reconstruct the image, so this method needs a long time because the iterations make it very slow, to accelerate this method and make it in a few minutes requires special and expensive devices. So in most imaging devices that rely on tomography use the transform methods to reconstruct the image [25].

For the above reasons, our work in this dissertation will be based on the transform methods, but this does not mean that the series expansion methods are bad and cannot be used in the future. On the contrary, they provide high-resolution reconstructed images from incomplete data and noise data. There are several transform methods to reconstruct the image as shown below.

2.4.1 Fourier Slice Theorem (FST)

The Fourier slice theorem was the first introduced to reconstruct an image from the parallel beam by Bracewell [54]. The Fourier slice theorem

can be defined by other names such as projection slice theorem and Central slice theorem [51].

The Fourier slice theorem gives a relationship between the projection and the Fourier transform of an object [41]. Its method is done by taking the FT of the projections at an angle θ that yields to obtain one cross-section of the original object in frequency domain this cross-section correspond to forward Fourier transform of one cross-section of the original object $F(u_x, v_y)$ [55]. Thus if take the Fourier transform for the projections at all θ that yields to obtain the whole profile of the original object in the frequency domain that corresponds to forward Fourier transform of the whole original object $F(u, v)$ then by take reverse Fourier transform of $F(u, v)$ this produces the full retrieved of object $f(x, y)$ see figure (2-3) [17].

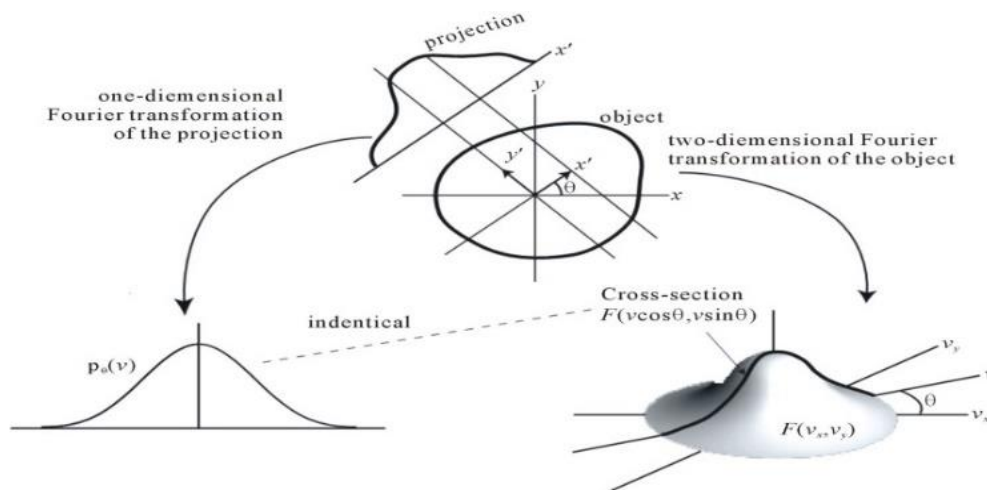


Figure 2-3 Steps of Fourier slice theorem [17].

To explain Fourier slice theorem from the mathematical side, must know in first the two-dimensional forward Fourier transform for an object [1].

$$F(u, v) = \int_{-\infty}^{+\infty} \int_{-\infty}^{+\infty} f(x, y) e^{-i2\pi(ux+vy)} dx dy \quad (2-4)$$

On the other hand, we take a look at the Fourier transform of projection $P_{\theta}(t)$,

$$S_{\theta}(w) = \int_{-\infty}^{\infty} P_{\theta}(t) e^{-i2\pi\omega t} dt \quad (2-5)$$

The simplest case to derive the mathematical equations for Fourier slice theorem is done when suppose the projection at an angle equal to zero ($\theta = 0$), and the Fourier transform along a line of an object get him by considered $v = 0$ thus the forward Fourier transform become [1]:

$$F(u,0) = \int_{-\infty}^{+\infty} \int_{-\infty}^{+\infty} f(x,y) e^{-i2\pi ux} dx dy \quad (2-6)$$

The last equation can split into two sections because the phase doesn't longer dependent on factor y [1] :

$$F(u,0) = \int_{-\infty}^{+\infty} \left[\int_{-\infty}^{+\infty} f(x,y) dy \right] e^{-i2\pi ux} dx \quad (2-7)$$

The section in parentheses in the equation (2-7) represents as an equation to find projections along lines of constant x or can be written as equation (2-8) [1]:

$$P_{\theta=0}(x) = \int_{-\infty}^{\infty} f(x,y) dy \quad (2-8)$$

Replace the section between brackets in equation (2-7) by equation (2-8)

$$F(u,0) = \int_{-\infty}^{+\infty} P_{\theta=0}(x) e^{-i2\pi ux} dx \quad (2-9)$$

The part after the equality process of the last equation represents the 1D-FT for the projections $P_{\theta=0}(x)$; so, we can deduce an equation that links the projections and a two-dimensional transform for any object as equation (2-10):

$$F(u,0) = S_{\theta=0}(u) \quad (2-10)$$

The FST is an easier case which isn't dependent on the angle between the object and the coordinate system [1]. If it has taken into consideration the angle between the object and the coordinates system, the Fourier transform of a parallel projection of the image $f(x, y)$ tilted at the angle θ with the x-axis gives 2D slice in frequency domain also tilted at the angle θ with the u-axis. In another word, when applying the FFT of $P_{\theta}(t)$ leads to giving the values of $F(u,v)$ over the line BB^{-} that shown in figure (2-4) [1].

In deriving of the equations of Fourier slice theorem with a more generalize and solid foundation, assume that the coordinates system (t,s) will be the rotated version of the original coordinates system (x,y) at a certain angle θ instead of zero as shown in figure (2-4), that can be done by the following matrix [1]:

$$\begin{bmatrix} t \\ s \end{bmatrix} = \begin{bmatrix} \cos \theta & \sin \theta \\ -\sin \theta & \cos \theta \end{bmatrix} \begin{bmatrix} x \\ y \end{bmatrix} \quad (2-11)$$

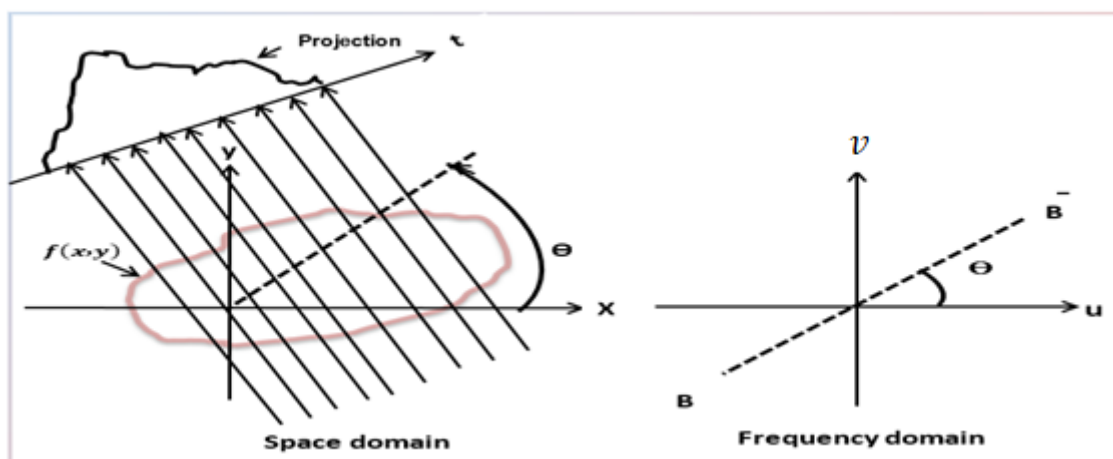


Figure 2-4 The FT of a specific projection line from the object [1].

When the point specified by the coordinate (t,s) the equation of projections for fixed t it became as equation (2-12) [1]:

$$P_{\theta}(t) = \int_{-\infty}^{\infty} f(t,s) \, ds \quad (2-12)$$

Replace the $P_{\theta}(t)$ in equation (2-5) by the right-hand side of equation (2-12) we get [1]:

$$S_{\theta}(w) = \int_{-\infty}^{\infty} [f(t,s) \, ds] e^{-i2\pi\omega t} \, dt \quad (2-13)$$

The equation (2-13) may be converted into the (x, y) coordinates system by applying the matrix in (2-11), we get:

$$S_{\theta}(w) = \int_{-\infty}^{+\infty} \int_{-\infty}^{+\infty} f(x,y) e^{-i2\pi w(x \cos \theta + y \sin \theta)} \, dx \, dy \quad (2-14)$$

The right-hand side of the equation (2-13) represents the 2D forward Fourier transform at a spatial frequency of $(u = w \cos \theta, v = w \sin \theta)$ or:

$$S_{\theta}(w) = F(w, \theta) = F(w \cos \theta, w \sin \theta) \quad (2-15)$$

The summarily of the equations (2-13), (2-14) and (2-15) is when taking the parallel projections of an object at different angles $(\theta_1, \theta_2, \theta_3, \dots, \theta_k)$ and then taking the forward Fourier transform for each of these projections, we get from each transform the values of $F(u, v)$. If we taking an unlimited quantity of projections in this way the $F(u, v)$ will be known at all points in the uv -plane. Finally, we apply the inverse Fourier transform for whole data in the frequency domain we get the reconstructed object as shown in figure (2-5) [1] [41]:

$$f(x,y) = \int_{-\infty}^{+\infty} \int_{-\infty}^{+\infty} F(u,v) e^{i2\pi(ux+vy)} \, du \, dv \quad (2-16)$$

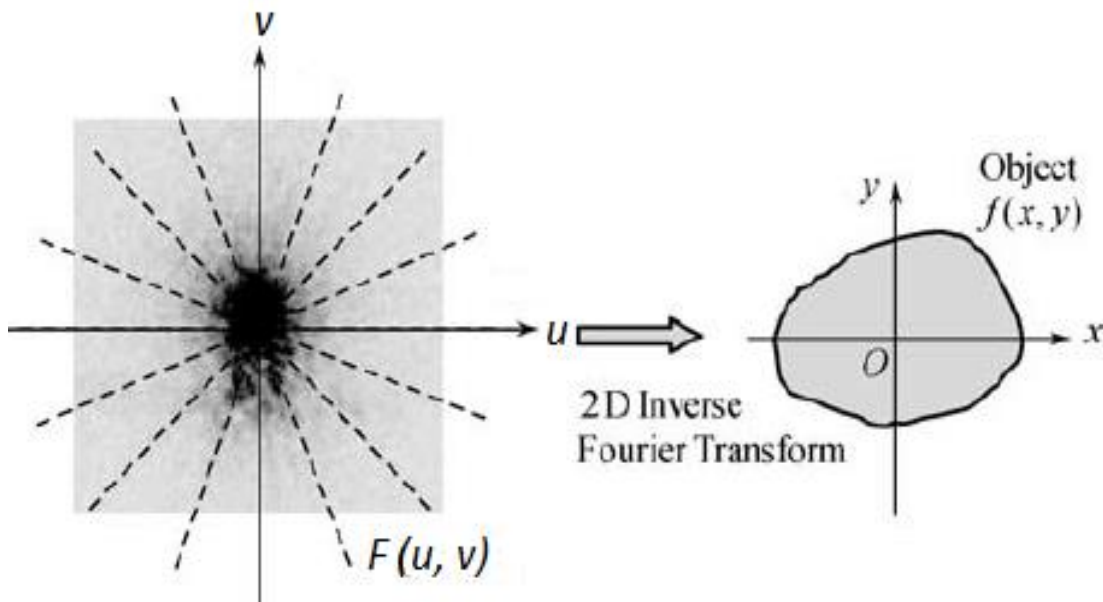


Figure 2-5 The reconstruct original object by 2D inverse Fourier transform [51].

2.4.2 Simple Back-Projection (BP) (Inverse Radon Transform (IRT))

To reconstruct the image from its projections we need an inverse process for the forward projection. This process is called back projection or inverse Radon transform. The Simple Back-Projection was first introduced to reconstruct an image from the series of its projections by Radon [56], and it is the simplest method to reconstruct the original object [23] [25], in which consider, the collecting of all projections $p_{\theta}(t)$ that passing through a point (x,y) for all orientations will obtains the retrieved object, that denoted as $BP(x,y)$. Because these projections are linear integrals through a point $f(x,y)$. Thus $f(x,y)$ is retrieved by this collecting although it containing blurring because of the participation from the other points that the projection passing through it, that does not represent the value of the point to be restored [17].

If assume using the simplest geometric as illustrated in figure (2-6), ones whose source beams are parallel and opposite the detector, the source and detector rotate about the object that fixed in the center of the coordinate system (x,y) , the ray beam passes through the object at each rotation angle (θ) , symbolizes the rotation angle by the symbol (θ) , and a rotating coordinate system represented by (t,s) that has the same point of origin of the coordinate (x,y) , (s) represents the detector position, (t) represents the distance along of a ray, any point on the object can be represented by either (x,y) or (t,s) coordinates system and the coordinates system are rotated by a rotational transformation [25].

$$\begin{bmatrix} t \\ s \end{bmatrix} = \begin{bmatrix} \cos \theta & \sin \theta \\ -\sin \theta & \cos \theta \end{bmatrix} \begin{bmatrix} x \\ y \end{bmatrix} \quad (2-17)$$

Or inversely

$$\begin{bmatrix} x \\ y \end{bmatrix} = \begin{bmatrix} \cos \theta & -\sin \theta \\ \sin \theta & \cos \theta \end{bmatrix} \begin{bmatrix} t \\ s \end{bmatrix} \quad (2-18)$$

As shown in section (2-2) and equation (2-2), we get the projection $p_{\theta}(t)$ by linear integration of all points $f(x,y)$ that pass through the projection line that has a length (t) , figure (2-6) shows the Radon transform $Rf(t,\theta)$ for the function $f(t,s)$ [25].

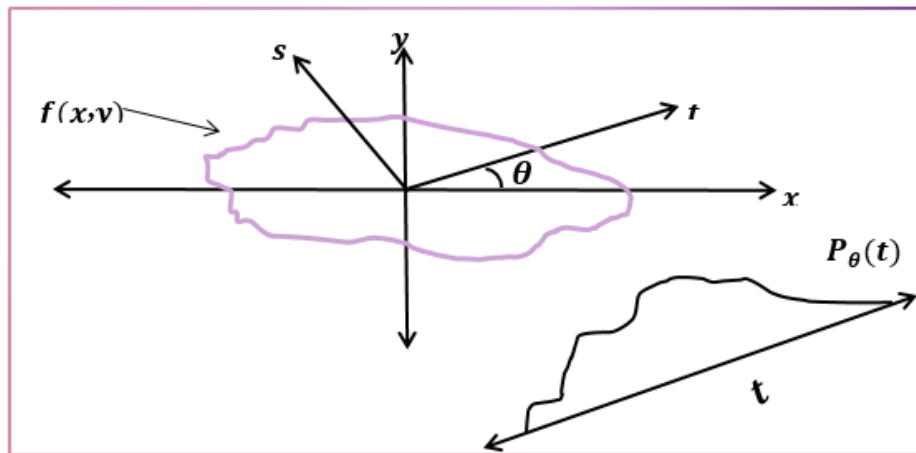


Figure 2-6 1D projection using a parallel beam [25].

Using the above geometry and starting from the idea of back-projection (to reconstruct the point (x,y) must collect all the projection values that pass through this point) i.e. [25].

$$BP(x,y) = f(x,y) = \int_0^\pi Rf(t,\theta)d\theta \quad (2-19)$$

Or

$$BP(x,y) = f(x,y) = \int_0^\pi Rf(x\cos\theta + y\sin\theta, \theta)d\theta \quad (2-20)$$

This equation for back-projection produces an image in the Cartesian coordinate by using the rotation equation (2-18) [25]. There are other equations for back-projection that produce an image in the polar coordinates [23].

2.4.3 The Filter After the Back-Projection (BPF)

The image reconstruction by the previous method (simple back-projection) is blurring, so will using different types of filters to remove the blurring here will explain the method of the filter after back projection. Initially reconstructing the image from the projection by back-projection, apply forward Fourier transform, filtering in the Fourier domain by multiplying the image in the frequency domain by the filter, and then apply

the inverse Fourier transform to reconstruct the filtered image. Instead of that, the filter operation may be performed in the spatial domain through the convolution process of the $BP(x,y)$ and a filter operator. However, this method has two problems [17]:

- 1) The Back-Projection in the frequency domain ($BP(u_x, v_y)$) should be calculated within a matrix much broader than that in $f(x,y)$. As blurring in the retrieved image $BP(x,y)$ makes it take more space than the original image space $f(x,y)$ [17].
- 2) The values of $f(x,y)$ are positive values at each point (x,y) in the original object. While the values of the original object after applied the FT on it be equal to zero ($FT(u_x, v_y) = 0$) when values of coordinates in Fourier space equal to zeros ($u_x = v_y = 0$), so the retrieved image $BP(x,y)$ does not have data in the origin point because of diverges at the origin point ($u_x = v_y = 0$). From the above reasons, the retrieved image $f(x,y)$ have values zeros and negative, this is contrary to values of the original image $f(x,y)$. To avoid this disadvantage must exchange the sequence of operations of the filter and BP, this will be done in the next section [17].

2.4.4 The Filter Before the Back-Projection (FBP)

In this section, first, apply a filter on projection data and then BP, where the FT is applied to the projections domain rather than applying on the blurring object. In one of the steps in this method, we need to convert between the Cartesian coordinates and the polar coordinates. This conversion is almost similar to the Fourier transform in the previous method, but the resulting image in the conversion method between the

coordinates does not have a lot of defects and artifacts as in the previous method. Besides that, this method takes a long time because the filter is applied to each parallel projections at the specific theta independently and applied to the rest of the angles in the sequence for improving the final image [17].

2.5 3D Tomography

The three dimensional Radon Transform is defined in the same way as in equation (2-4), except that (x,y) is now defined as a vector (x,y,z) in three dimensional and the integral is the surface integration whose orientation defined by a pair of angles (θ, φ) , rather than linear integration that done in 2D forward transform, see figure (2-7) [57]

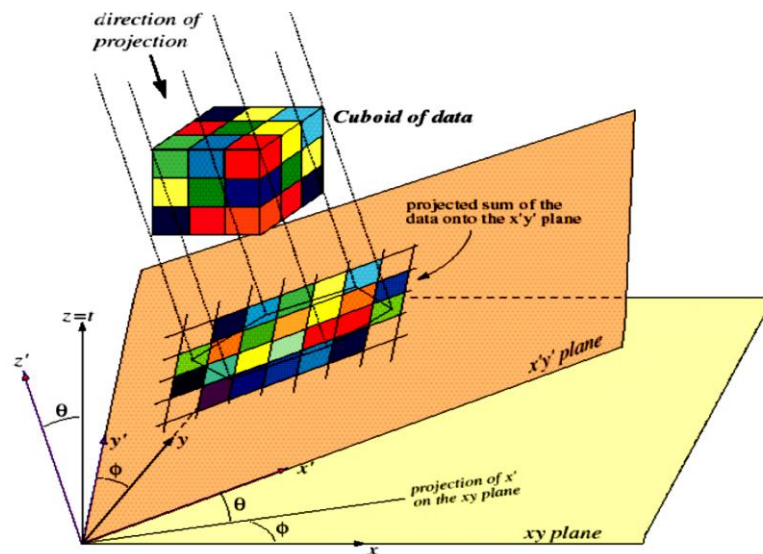


Figure 2-7 The Projection in 3D [57].

The three dimensional forward projections are known by using the 2D-projections of a 3D-function $f(x,y,z)$ where these projections are obtained by integrating $f(x,y,z)$ each a plane surface, where the orientation of this plane can be defined by a vector \vec{a} shown in figure (2-8) [58] [59].

$$\vec{\alpha} \equiv (\sin \theta \cos \varphi, \sin \theta \sin \varphi, \cos \theta)$$

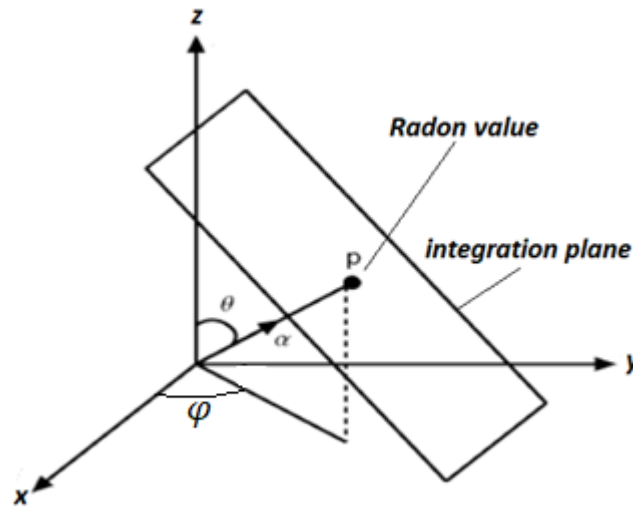


Figure 2-8 The Projection geometry in 3D [58] [59].

To derive mathematical equations of Radon transform in three dimensional, at first suppose a three-dimensional function $f(x,y,z)$ and a plane that can be represented by a unit vector $\vec{\alpha}$ and the distance s of the plane from the point of origin, so the three dimensional forward projections of function $f(x,y,z)$ is given by [58]:

$$P_{\theta,\varphi}(\vec{\alpha}, \vec{X}) = \int_{-\infty}^{+\infty} \int_{-\infty}^{+\infty} \int_{-\infty}^{+\infty} f(x,y,z) dt \quad (2-21)$$

Where $\vec{X} = (x, y, z)$ and the distant defined by:

$$t = x \sin \theta \cos \varphi + y \sin \theta \sin \varphi + z \cos \theta \quad (2-22)$$

From equation (2-21) and Dirac's delta function, we find:

$$P_{\theta,\varphi}(\vec{\alpha}, \vec{X}) = \int_{-\infty}^{+\infty} \int_{-\infty}^{+\infty} \int_{-\infty}^{+\infty} f(x,y,z) \delta(x \sin \theta \cos \varphi + y \sin \theta \sin \varphi + z \cos \theta - t) dx dy dz \quad (2-23)$$

The function $P_{\theta,\varphi}(\vec{\alpha}, \vec{X})$ is known as the Radon transform of three-dimensional object $f(x,y,z)$. The forward projections operate on the

conversion of spatial space (x,y,z) to the $(\vec{\alpha}, \vec{X})$ space. Where every single point in the $(\vec{\alpha}, \vec{X})$ space correspond to the plane in the spatial space (x,y,z) [58]. The 3D back-projection method applies to reconstruction 3D object from 3D Radon transform.

2.5.1 3D Back-Projections Method

Three-dimensional back projection is an extension to the two-dimensional back-projection shown in equation (2-21). To reconstruct the three-dimensional object from its projection, an inverse process for the forward projection is needed. This process is called back projection, which considers, the collecting of $P_{\theta,\varphi}(\vec{\alpha}, \vec{X})$ passing through (x,y,z) for all θ and φ yields, the reconstructed image denoted $BP_{\theta,\varphi}(x,y,z)$. Since these projections are surface integrals through $f(x,y,z)$. Thus $f(x,y,z)$ is retrieved by this collecting although it containing blurring because of the participation from the other points that the projection passing through it, which does not represent the value of the point to be restored [17].

$$BP_{\theta,\varphi}(x,y,z) = f(x,y,z) = \int_0^{2\pi} \int_0^\pi Rf(x \sin \theta \cos \varphi + y \sin \theta \sin \varphi + z \cos \theta, \theta, \varphi) d\theta d\varphi \quad (2-24)$$

2.6 Imaging 3D object by X-ray transform

X-ray transform is applied to a three-dimensional object $f(x,y,z)$ in which the object is stationary and the radiation is revolving around the object. So here four variable parameters are needed to parameterize the LOR (a line of response) that shown in figure (2-9): two of these parameters are angles (θ, φ) to define the unit vector $\hat{z}_r(\varphi, \theta) \equiv (\cos \varphi \cos \theta, \sin \varphi \cos \theta, \sin \theta)$ parallel to the line of response (LOR) and

the two other parameters (x_r, y_r) are used to select the location of the cross point of the Line of response (LOR) with the plane perpendicular to $\hat{z}_r(\varphi, \theta)$ [60].

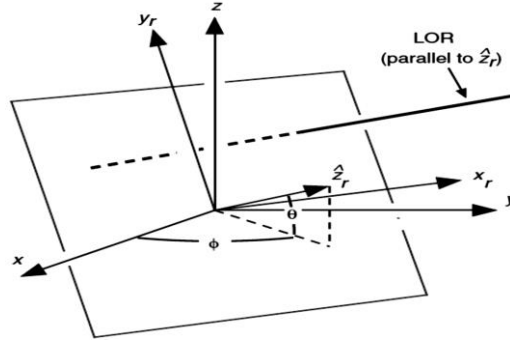


Figure 2-9 Factors of 3D Line of Response (LOR) for the X-ray transform [60].

The derivation of mathematical equations for the X-rays transform is based on two conditions, the first condition is $\hat{x}_r \cdot \hat{z} = 0$ and the second condition is consideration that the θ angle as the co-polar angle, so the matrix used to convert from the original coordinates to projections coordinates is [60]:

$$\begin{bmatrix} x_r \\ y_r \\ z_r \end{bmatrix} = \begin{bmatrix} -\sin \varphi & \cos \varphi & 0 \\ -\cos \varphi \sin \theta & -\sin \varphi \sin \theta & \cos \theta \\ \cos \varphi \cos \theta & \sin \varphi \cos \theta & \sin \theta \end{bmatrix} \begin{bmatrix} x \\ y \\ z \end{bmatrix} \quad (2-25)$$

Based on the equation (2-25), the line integral projections along the line of response defined by $(x_r, y_r, \varphi, \theta)$ can be calculated by [60]:

$$P(x_r, y_r, \varphi, \theta) = \int_{-\infty}^{+\infty} f(x, y, z) dz_r \quad (2-26)$$

When taking a set of line integral projections for all (x_r, y_r) and constant orientation ($\hat{z}_r(\varphi, \theta)$ constant) will generate a 2D sinogram $P(x_r, y_r, \varphi, \theta)$ for the 3D object $f(x, y, z)$ as shown in figure (2-10) [60].

The $P(x_r, y_r, \varphi, \theta)$ can consider as a 2D sinogram when $\hat{z}_r(\varphi, \theta)$ is constant in a certain orientation, but when taking projections

$P(x_r, y_r, \varphi, \theta)$ for all orientation when $0 \leq \varphi < \pi$, $|\theta| < \frac{\pi}{2}$ for an object and the values of $|x_r, y_r| < \infty$ this leads to generation a 4D sinogram, so the X-ray transform for 3D object will increase the number of dimensions by one in projections domain, this causes redundancy in the data and distortion in the retrieved image [60].

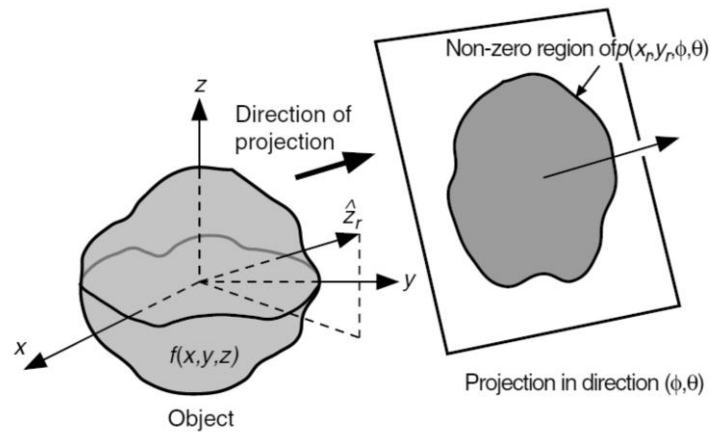


Figure 2-10 The projection taken by X-ray transform [60].

2.7 Method of Reconstruction 3D Object from X-Ray Projections

The following sections (2.7.1) and (2.7.2) show the equations of reconstruction object from 4D projections.

2.7.1 3D Back Projection for X-Ray Projections

Three-dimensional back-projection for X-ray projection is an extension to the two-dimensional back-projection for X-ray projection that shown in equation (2-20), and the back-projected image is given by [60]:

$$f(x, y, z) = \int_{-\theta}^{+\theta} \int_0^{\pi} P(x_r, y_r, \varphi, \theta) d\varphi \cos \theta d\theta \quad (2-27)$$

This process is called back-projection for X-ray projections, in which consider, the summation of $P(x_r, y_r, \varphi, \theta)$ passing through (x, y, z) for all θ and φ yields, the reconstructed image denoted $f(x, y, z)$ [60].

2.7.2 The 3D Fourier Slice Theorem for X-Ray Transform

This method also is known by central section theorem for the X-ray transform of the 3D object, for derivation, the mathematical equations for this method, initially applied the 2D Fourier transform to the first two variants (x_r, y_r) of the 4D projections as follows [60]:

$$P(u_{xr}, v_{yr}, \varphi, \theta) = \int_{-\infty}^{+\infty} \int_{-\infty}^{+\infty} P(x_r, y_r, \varphi, \theta) e^{-i2\pi(x_r u_{xr} + y_r v_{yr})} dx_r dy_r \quad (2-28)$$

If $F(u_x, v_y, w_z)$ is the 3D FFT of $f(x, y, z)$

$$F(u_x, v_y, w_z) = \int_{-\infty}^{+\infty} \int_{-\infty}^{+\infty} \int_{-\infty}^{+\infty} f(x, y, z) e^{-i2\pi(x u_x + y v_y + z w_z)} dx dy dz \quad (2-29)$$

Consequently, for obtaining the final equation of the Fourier slice theorem for X-ray transform based on equation (2-30) [60]:

$$P(u_{xr}, v_{yr}, \varphi, \theta) = F(u_x, v_y, w_z) \Big|_{w_z=0} \quad (2-30)$$

From equation (2-25) we have,

$$\begin{bmatrix} u_r \\ v_r \\ w_r \end{bmatrix} = \begin{bmatrix} -\sin \varphi & -\cos \varphi \sin \theta & \cos \varphi \cos \theta \\ \cos \varphi & -\sin \varphi \sin \theta & \sin \varphi \cos \theta \\ 0 & \cos \theta & \sin \theta \end{bmatrix} \begin{bmatrix} u_{xr} \\ v_{yr} \\ w_{zr} \end{bmatrix} \quad (2-31)$$

The meaning of the 3D Fourier slice theorem for the X-ray transform is identical to the 2D Fourier slice theorem where the 2D Fourier transform

for the projections perpendicular to $\hat{z}_r(\phi, \theta)$ be equivalent to the 3D Fourier transform for a section of the 3D object at the same orientation. This is shown in figure (2-11) [60].

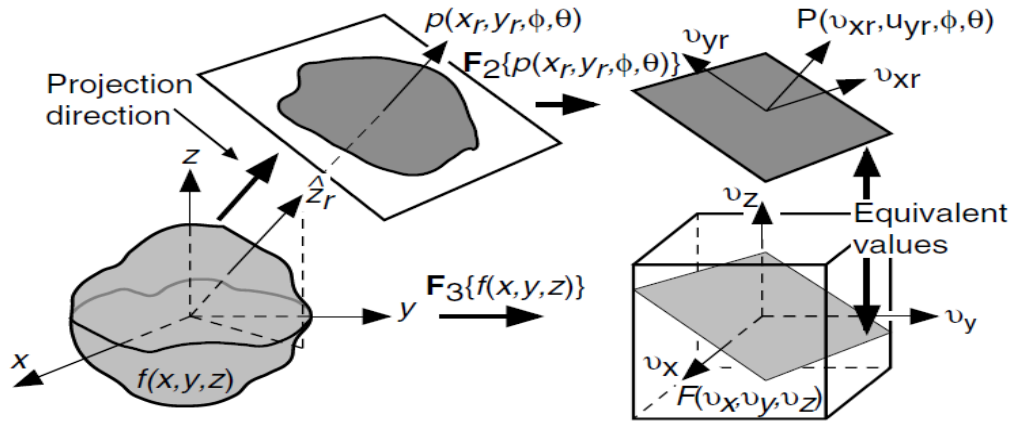


Figure 2-11 The 3D Fourier Slice Theorem for X-Ray Transform [60]

2.8 The Relationship between Radon Transform and X-Ray Transform

To produce projections for the 3D object there are two methods either by 3D Radon transform or X-ray transform. The Radon transform will integrate the 3D object across all two-dimensional planes as shown in figure (2-12) [60].

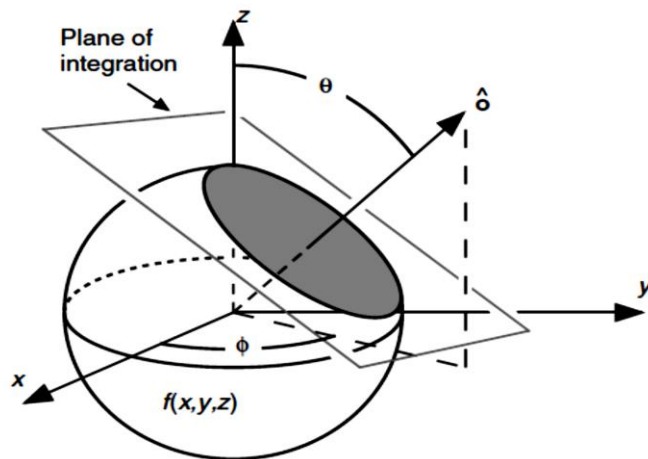


Figure 2-12 The Radon transform for 3D Object [60].

For an n -dimensional object $f(X)$, where $X = (x_1, x_2, \dots, x_n)$, the Radon transform of $f(X)$, is defined as the set of all integrals along the $(k = n - 1)$ dimensional hyperplanes intersecting the object [60].

Using the same notation, the X-ray transform of an n -dimensional object is defined as the set of all $(k = 1)$ dimensional line-integrals through the object as shown in figure (2-9) [60].

For two-dimensional objects, the X-ray and Radon transforms are equivalent, where $k = n - 1 = 1$ (that is, line integrals) for both, whereas for three (or higher) dimensional objects the X-ray transform remains a line-integral transform while the Radon transform becomes a plane integral for $n = 3$, and a hyperplane for $n > 3$ [60].

2.9 Ramp Filter In Frequency Domain

Ramp filter (RF) is the simplest type of filters, it is classified as a high-frequency filter, where it prevents the low frequencies from passing which causes blurring in the image and it allows the High frequencies passing. Its mathematical function is given by (2-32) [61]:

$$RF(v_x, v_y, v_z) = \sqrt{(v_x)^2 + (v_y)^2 + (v_z)^2} \quad (2-32)$$

The data at each frequency (v_x, v_y, v_z) is multiplied by the $RF(v_x, v_y, v_z)$.

2.10 Interpolation

The images of computed tomography obtained from a series of projections, and by collecting a set of projection data at different angles this will form the sinogram of a range of angle from 0° to 180° or 360° [1] [62].

In natural state when take scanning of object used angular interval for scanning (delta) equal to one consequently obtain full data sinogram but in this section, used different delta (angular interval for scanning) greater than one, thus this causes the loss of some data of sinogram, so to restored the lost data different methods interpolation are used on sinogram.

The interpolation in images is a widespread method in the image processing field and other fields. it was also used to improve the algorithms used to secure communication in mobile phones [63], Here, it used interpolation in tomography for image construction of an object from a little number of projections. Some of the interpolation purposes are to reduce the number of projections in a computed tomography scan to reduce the time of scan and exposure of radiation [64] [65] [66] [67]. There are many different types of interpolation methods, each of them has a different result for the final image. Will chose the best method depending on the quality, or visible distinction for each pixel.

The interpolation methods are used to find missing pixel values located in a known location, where this pixel is located between pixels and has known values. [68], [69]. Or as some have defined it as expanding data from limited data [70].

Three frequently interpolation methods used are the nearest neighbor interpolation, linear interpolation, and non-linear interpolation applied on the 2D sinogram that shown in figure (2-13) to determine the missing projections, for all three interpolation methods, the angular interval between two adjacent projections ($\Delta\theta$) is normalized to unity.

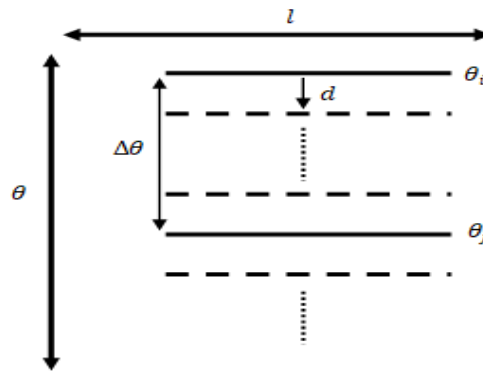


Figure 2-13 A schematic representation of the adopted geometry for the interpolation methods

The new value for the missing projections at distance d from the previous projection is calculated by finding the weighted sum of the previous projection at (θ_i) which is $P_{\theta_i,l}$ and the posturer projection at (θ_j) which is $P_{\theta_j,l}$, as equation (2-33):

$$P_{\theta,l} = w_i P_{\theta_i,l} + w_j P_{\theta_j,l} \quad (2-33)$$

Where $P_{\theta,l}$ is the projection at an angle fall between two adjacent projection at θ_i and θ_j , w_i is the summation weight for the previous projection at (θ_i) and w_j is the summation weight for posturer projection at (θ_j) .

The value of the two summation weights is always maintaining the following condition:

$$w_i + w_j = 1 \quad (2-34)$$

Where the value of the w_i is calculate for each interpolation method as follow:

- ✚ Nearest neighbor interpolation method

$$w_i = \begin{cases} 1 & \text{if } d < \frac{\Delta\theta}{2} \\ 0 & \text{elsewhere} \end{cases} \quad (2-25)$$

✚ Linear interpolation method

$$w_i = \frac{d}{\Delta\theta} \quad (2-36)$$

✚ Nonlinear interpolation method

$$w_i = \frac{1}{1+e^{-(6-12d)}} \quad (2-37)$$

The distribution for the summation weights is illustrated in the figure (2-14).

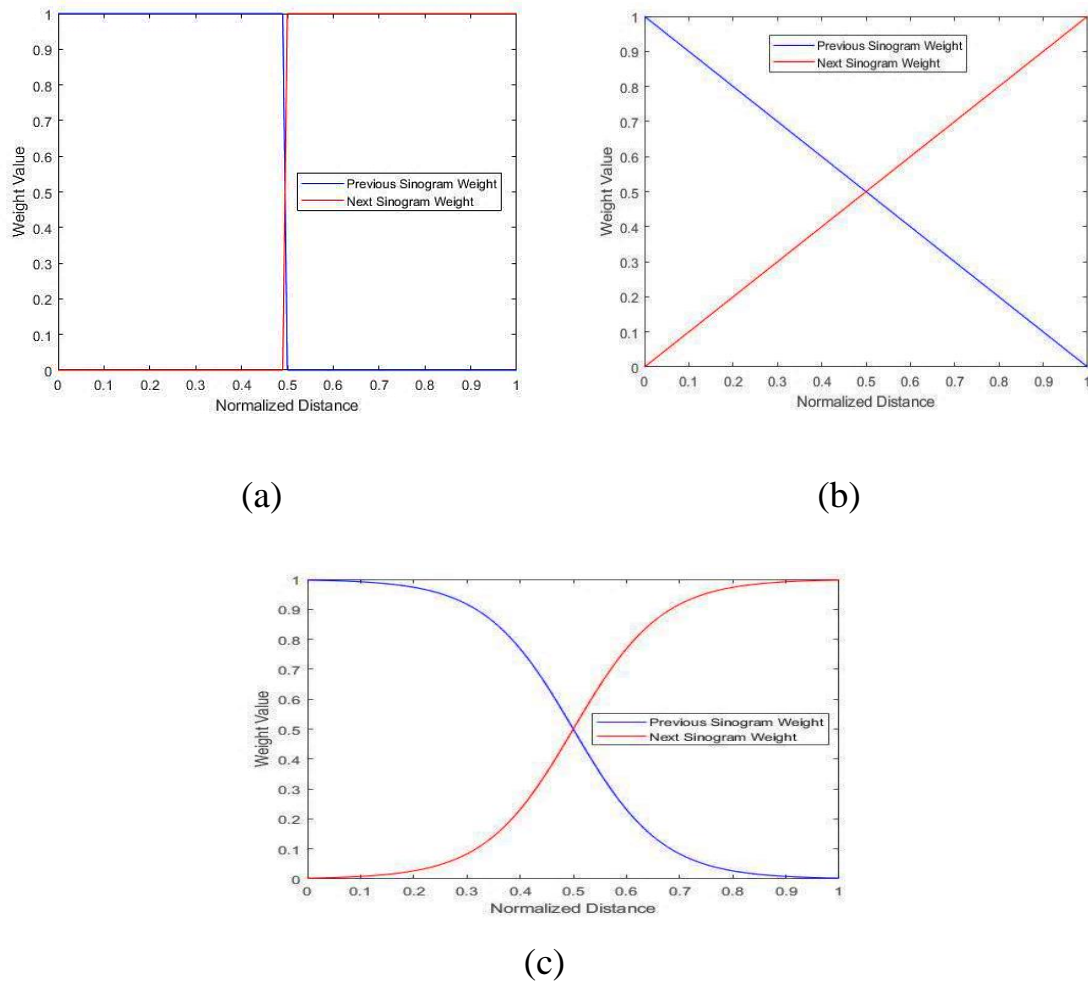


Figure 2-14 The distribution of the summation weights for three interpolation methods

(a) Nearest Neighbor (b) Linear (c) Nonlinear

2.11 Fidelity Criteria

Measure the fidelity criteria of an image after each processing method is necessary to estimate the quality of the image after processing and to estimate the performance of the processing method, there are two kinds of fidelity criteria are objective and subjective fidelity criteria. [71]

2.11.1 Objective Fidelity Criteria

Its mathematical measure applied to digital information to estimate the amount of error in information processed by comparing it with original information. Here the image represents the digital information, where $f(x, y, z)$ it represents the original image symbol and $\hat{f}(x, y, z)$ represents the retrieved image symbol [3]. For any values of x , y , and z the error (e) is [72]:

$$e = \hat{f}(x, y, z) - f(x, y, z) \quad (2-38)$$

The total error (e_T) of the retrieved image has a size ($N \times M \times W$) is [72]:

$$e_T = \sum_{x=0}^{N-1} \sum_{y=0}^{M-1} \sum_{z=0}^{W-1} (\hat{f}(x, y, z) - f(x, y, z)) \quad (2-39)$$

Care must be taken when using objective fidelity criteria because they may sometimes be inconsistent with the subjective fidelity criteria, where the image is judged to be bad or good after processing depends on the compatibility of the two fidelity criteria [3]. The common types of objective fidelity criteria are:

1- Mean Square Error (MSE)

It's an average of the sum of the square of the error between the image after and before processing [71].

$$MSE = \frac{1}{M \times N \times W} \sum_{x=0}^{N-1} \sum_{y=0}^{M-1} \sum_{z=0}^{W-1} ((f^{\wedge}(x, y, z) - f(x, y, z))^2) \quad (2-40)$$

When the value of the MAD or MSE high that means the processed image is bad compared to the original image, whereas when the value of the MAD or MSE is zero, it means that the method of processing is ideal. In these types of fidelity criteria, do not have negative values because of the effect of the quadratic and absolute operation [3].

2- Root Mean Square Error (RMSE)

It is calculated by taking the square root of Mean square error(MSE). When the value of RMSE small it means the processing method is ideal [73].

$$RMSE = \sqrt{\frac{1}{N \times M \times W} \sum_{x=0}^{N-1} \sum_{y=0}^{M-1} \sum_{z=0}^{W-1} ((f^{\wedge}(x, y, z) - f(x, y, z))^2)} \quad (2-41)$$

3- Signal to Noise Ratio (SNR)

It is calculated by taking the square root of MSNR as shown in equation (2-45). When the value of SNR high means the reconstructed image is good [3].

$$SNR = \sqrt{\frac{\frac{1}{N \times M \times W} \sum_{x=0}^{N-1} \sum_{y=0}^{M-1} \sum_{z=0}^{W-1} (f(x, y, z))^2}{MSE}} \quad (2-42)$$

Many times the SNR is calculated in decibel (1dB=one tenth of the logarithm) as below [71].

$$SNR = 10 \log_{10} \left(\frac{\frac{1}{N \times M \times W} \sum_{x=0}^{N-1} \sum_{y=0}^{M-1} \sum_{z=0}^{W-1} (f(x, y, z))^2}{MSE} \right) \quad (2-43)$$

4- Peaks- Signal to Noise Ratio (PSNR)

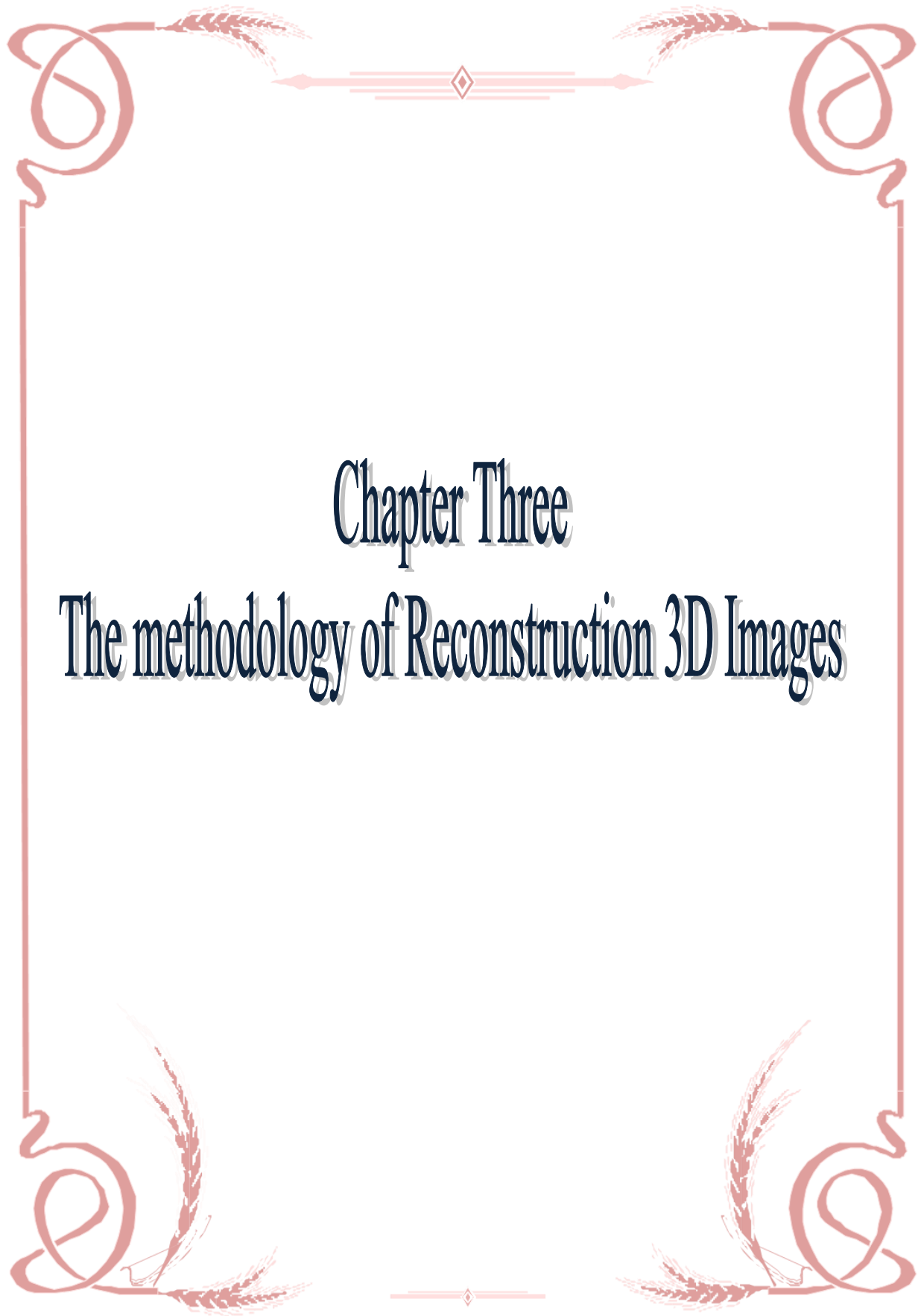
It is calculated by taking the ratio between the maximal value of the gray level in the image and the mean square error, it is also called the quantization noise. In many times, it is measured in units of decibel (1dB=one tenth of the logarithm), as below [74]:

$$PSNR = 10 \log_{10} \left(\frac{L^2}{MSE} \right) \quad (2-44)$$

Where, L is the maximum value of the gray levels.

2.11.2 Subjective Fidelity Criteria

The quality of retrieved images is evaluated based on the average rating of the group subjective evaluations of human experts. This can be done by display retrieved images to a collection of experts then calculate the averaging of their evaluations. The absolute rating scale may be used as evaluations, such as (excellent, fine, passable, marginal, inferior and unusable) [75] [76].



Chapter Three

The methodology of Reconstruction 3D Images

Chapter Three

The Methodology of Reconstructing 3D Images

3.1 Introduction

Computed tomography used to generate a three-dimensional representation of the inside object without affecting the structure of the object, the quality of the reconstructed images depends on several parameters in the reconstruction algorithms which will discuss in this chapter.

Most researches in the field of computed tomography focus on improving the quality of the reconstruction image. This chapter describes a review of algorithms of images reconstructed to improve its quality with using the least dose of radiation and least time.

3.2 summarize of methodology

The steps of reconstruct 3D object can summarize in figure (3-1)

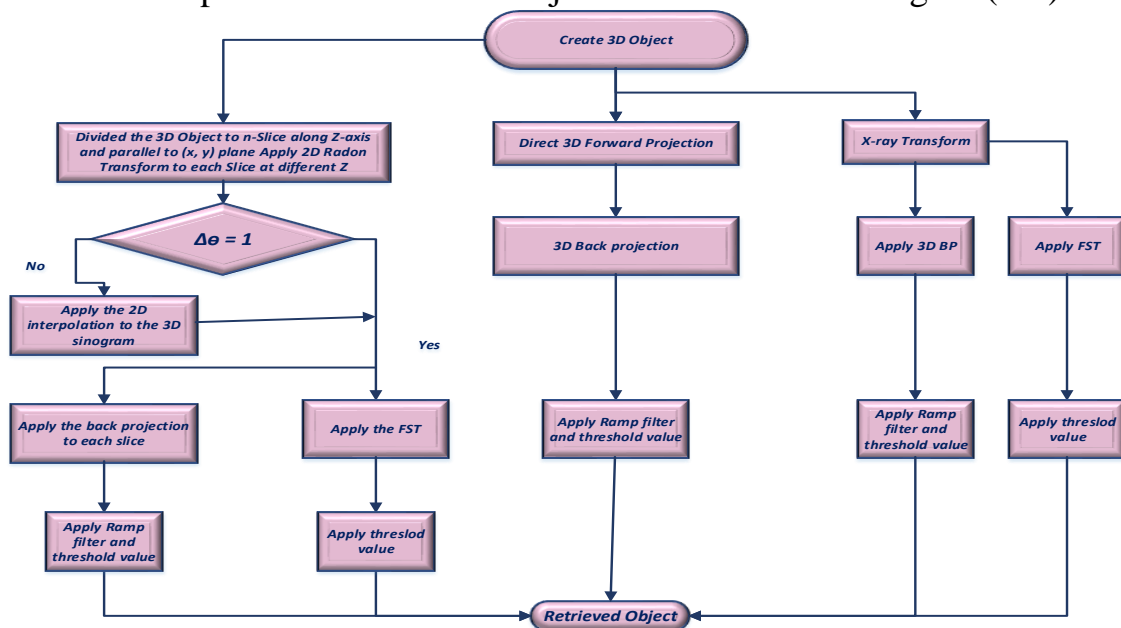


Figure 3-1 Summarize of methodology block diagram.

3.3 Creating 3D Object

The first step in our study is to create a three-dimensional object by using MATLAB programming language, as a sample to apply and test the algorithms.

Here, initially will create two objects, the first object is the first object is a symmetrical solid sphere have a hollow sphere in the center of a solid sphere as shown in figure (3-2a, b). This is done by using the sphere equation and choice the radius of the spheres and the position of the spheres in the three-dimensional space by controlling on the space dimensions (x, y, and z). Where the centers, radius and the density of each sphere are listed in table (3-2), this sketch in dimension's space is (33, 33, 33).

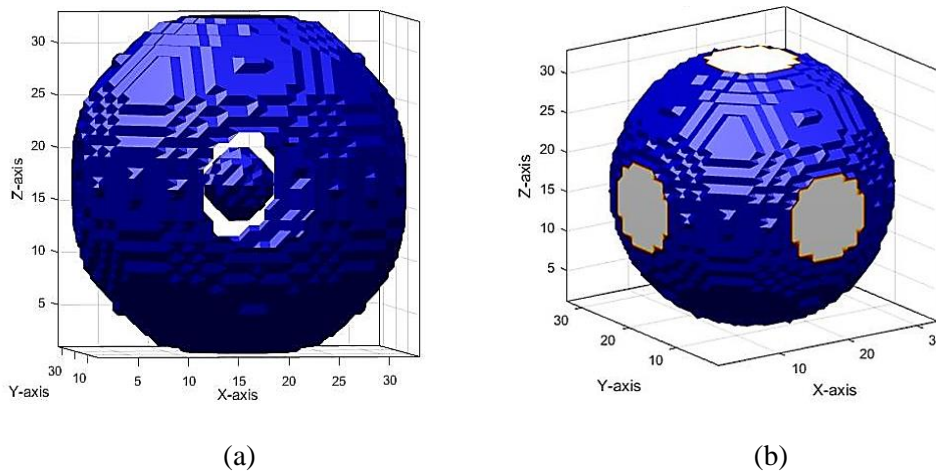


Figure 3-2 (a) hollow sphere inside solid sphere
(b) Solid sphere

Table 3-1 the location, dimension, and density of the spheres that consist of the object

<i>Sphere No.</i>	<i>Center</i>	<i>radius</i>	<i>Density</i>
<i>1 (The solid sphere)</i>	<i>(17,17,17)</i>	<i>17</i>	<i>1</i>
<i>2 (The hollow sphere)</i>	<i>(17,17,17)</i>	<i>3.5</i>	<i>0</i>

The second object is asymmetrical, which is almost similar to the outer structure of the Mickey Mouse head with a hollow small sphere in the center of it as shown in figure (3-3 a, b), where the big sphere and the ears of mickey Mouse are solid spheres. This is done in the similar way of the first object also based on sphere equation as well as the choice the radius of the spheres and the position of the spheres in the three-dimensional space by controlling the space dimensions (x, y and z). Where the centers, radius and the density of each sphere are listed in table (3-3), this sketch in dimension's space is (33, 33, 33).

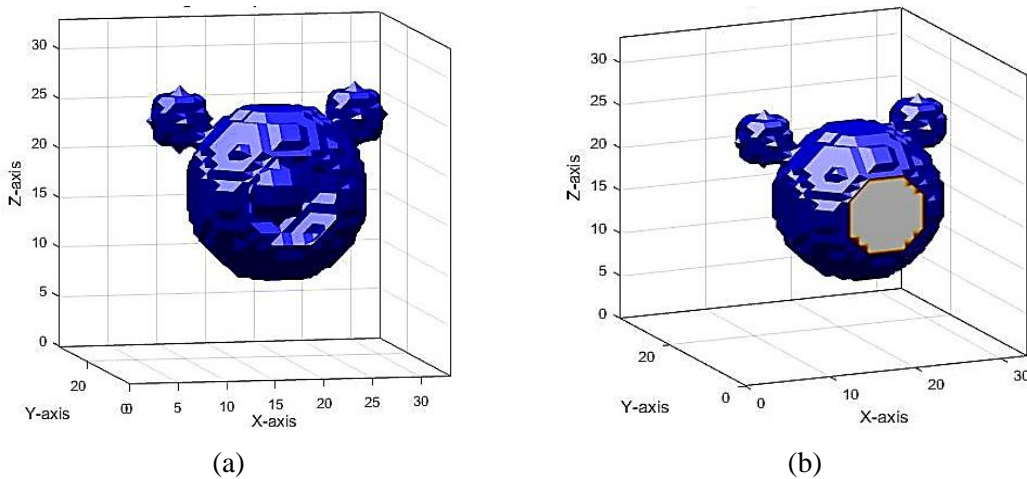


Figure 3-3 (a) hollow sphere inside head Mickey Mouse & (b) the solid head for Mickey Mouse

Table 3-2 The location, dimension, and density of the spheres that consist of Mickey Mouse

<i>Sphere No.</i>	<i>Center</i>	<i>radius</i>	<i>Density</i>
<i>1 (the main)</i>	<i>(17,8.5,18)</i>	<i>9</i>	<i>1</i>
<i>2 (small right)</i>	<i>(26,13,25)</i>	<i>3</i>	<i>1</i>
<i>3 (small left)</i>	<i>(8, 13, 25)</i>	<i>3</i>	<i>1</i>
<i>4 (the Hollow)</i>	<i>(17,8.5,18)</i>	<i>3</i>	<i>0</i>

3.4 Methods of Forward projections

The second step after creating a three-dimensional object, it is done by taking the forward projections of the three-dimensional object. In this research, it was done by three methods depending on how the image is reconstructed.

3.4.1 Slicing Method

The object is divided in a certain direction into several two-dimensional layers in this method, for example, an object $O(x,y,z)$ can be considered to be composed of several two-dimensional layers (n) have the same thickness along the z-axis, all these layers are perpendicular to z-axis as shown in figure (3-4). Each layer in three dimensional object is considered as a two-dimensional function $f(x,y)$.

According to the above paragraph, the three-dimensional object reconstruction can be done by taken a number of two dimensional Radon transform of a 3D object along different heights as shown in figure (3-4) by applying the equation of two-dimensional projections (2D Radon transform) (see equation 2-3) separately for each two-dimensional slice at different heights for the three-dimensional object the orientation of the two-dimensional projection is identified by angle (θ), where the range of theta angle has the range $(0 - \pi)$. The two dimensional radon transform (that discussed in section 2-2 in chapter two) will generate sinogram (i.e. two-dimensional projection) for each slice of the object.

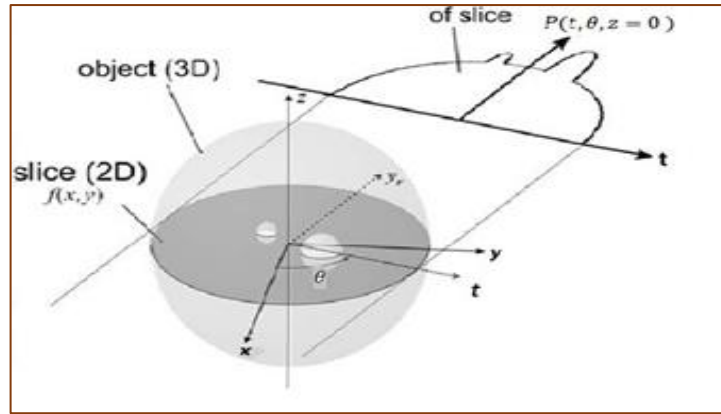


Figure 3-4 The 2D radon transform for one plane of 3D object [60].

After the implementation completed of the forward projections on all the slides starting from $Z=1$ to $Z=33$, the two-dimensional projections (sinogram) has resulted from each two-dimensional slice are stacking at different heights to produce the three-dimensional projections of the three-dimensional object, the block diagram of this method illustrated in figure (3-5).

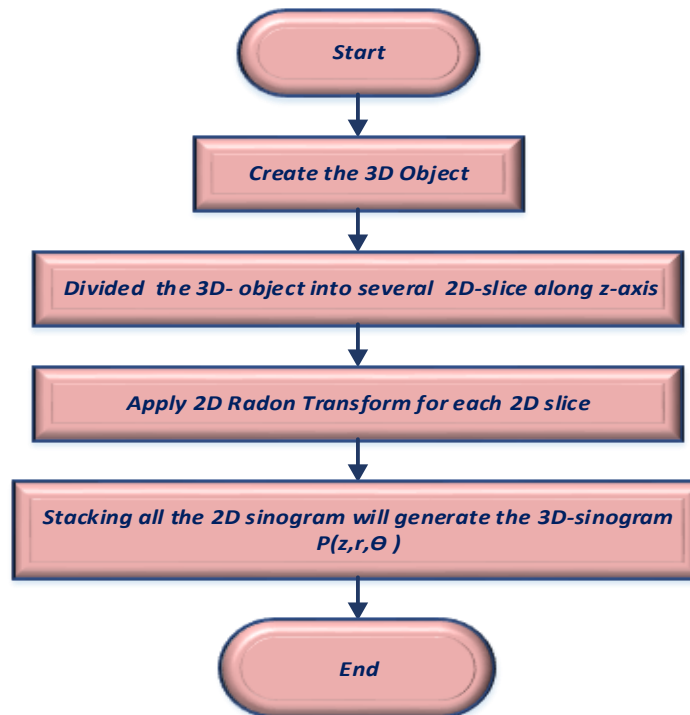


Figure 3-5 The forward slicing method block diagram.

3.4.2 Direct 3D Projections Method

In the second method, apply the equation of the three-dimensional projections (three dimensional Radon transform) that shown in equation (2-23) for the three-dimensional object, the orientation of the three-dimensional projection is identified by a pair of angles (θ, φ) , rather than one angle as done in two-dimensional projections. Where the range of theta angle is $(0 - \pi)$, while the range of Phi is $(0 - 2\pi)$. The block diagram of this method illustrated in figure (3-6).

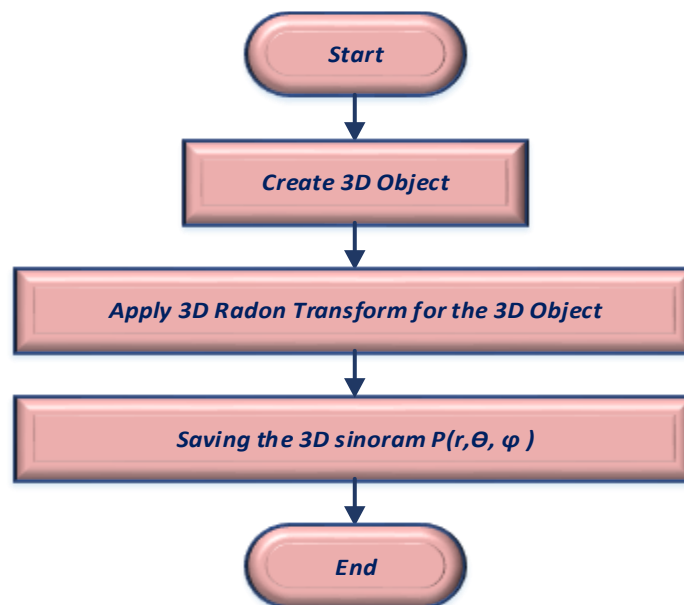


Figure 3-6 The Forward the Direct 3D Projections block diagram.

3.4.3 X-Ray Transform Method (X-Ray Projections)

The third method, is done by taking X-ray projections (seen equations 2-25 and 2-26) for a three-dimensional object where the object is stationary while the X-ray rotate around the object, the orientation of the X-ray projections is identified by a pair of angles (θ, φ) Where the range of theta angle has $|\pi/2|$ degrees while the range of Phi is $(0 - \pi)$. and pair of

coordinate (x, y) to locate the position of projections, the block diagram of this method illustrate in figure (3-7).

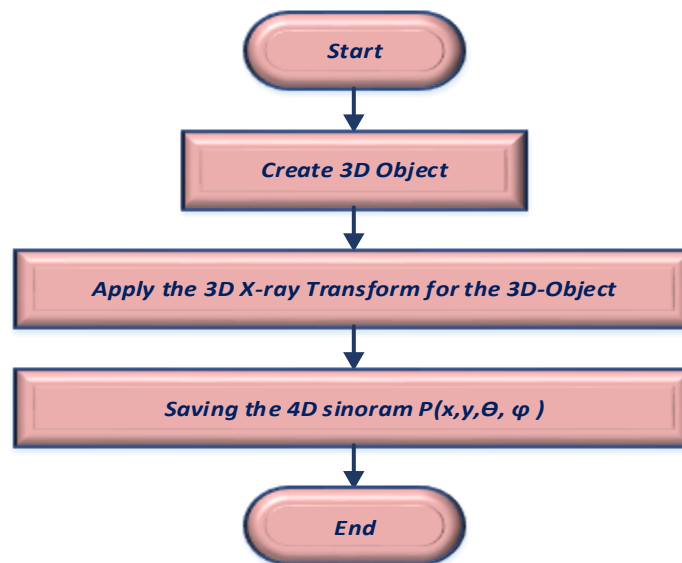


Figure 3-7 The Forward X-Ray Transform block diagram.

3.5 3D Object Reconstruction Methods

There are many methods to reconstruction images from its projections, in this research work, three types of reconstruction methods are used, two of them are Back-Projections (BP) (or Inverse Radon Transform) and Fourier Slice Theorem (FST), each of these methods is applied depending on the method of taking these projections for the three-dimensional object as explained in sections (3.3.1 and 3.3.2). The third method is X-ray transform to reconstruction the three dimension object from projections that obtained by using the method in section (3.3.3), there are two methods to complete the last method either Three-Dimensional Back Projections for X-Ray Projections or the Three-Dimensional Central Section Theorem for X-Ray Projections, therefore it is necessary to study and determine the best method in order to make an accurate reconstruction by considering devices that available, time consumption and cost for the method.

3.5.1 Reconstructing the 3D Object from 2D Projection

It is designed for the two-dimensional Computed Tomography (CT) models, the Back-Projection process is very useful in three-dimensional reconstruction field, in order to reconstruct the images from its sinogram obtained as results from Radon transform calculation explained in chapter two. If the 3D sinogram of the 3D object is obtained by applying the method in section (3.3.1). In this case, the appropriate reconstruction method is either by using a back-projection method, which is done by applying the two dimensional back projection by using equation (2-20) for all slices at different heights, this leads to reconstructed several slices for the object at different heights, the figure (3-8) illustrates the block diagram of this method.

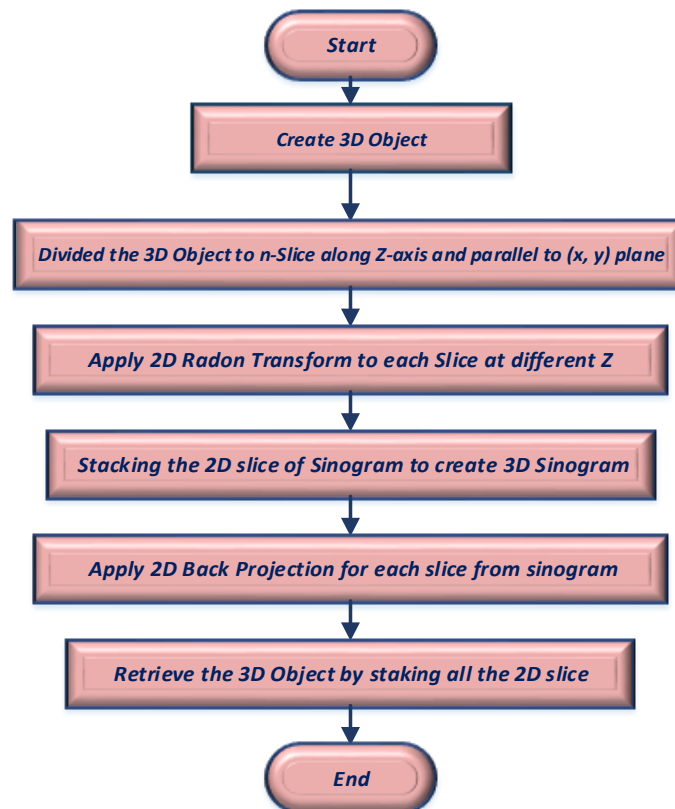


Figure 3-8 The Reconstructed 3D Object by back-projection method block diagram.

Or using Fourier Slice Theorem, it is done by applying the one dimensional Fourier transform for all one-dimensional projections by using equation (2-5) for all slices at different heights. After that filtering is applied for each result, that leads to obtaining the slices at different heights for 3D object in frequency domain, the 2D inverse Fourier transform is implemented for each slice by using equation (2-16) this leads to reconstruct several slices for an object at different heights. All slices are stacked in its position corresponding to each (x, y, z) to reconstruct the 3D object, the figure (3-9) illustrates the block diagram of this method.

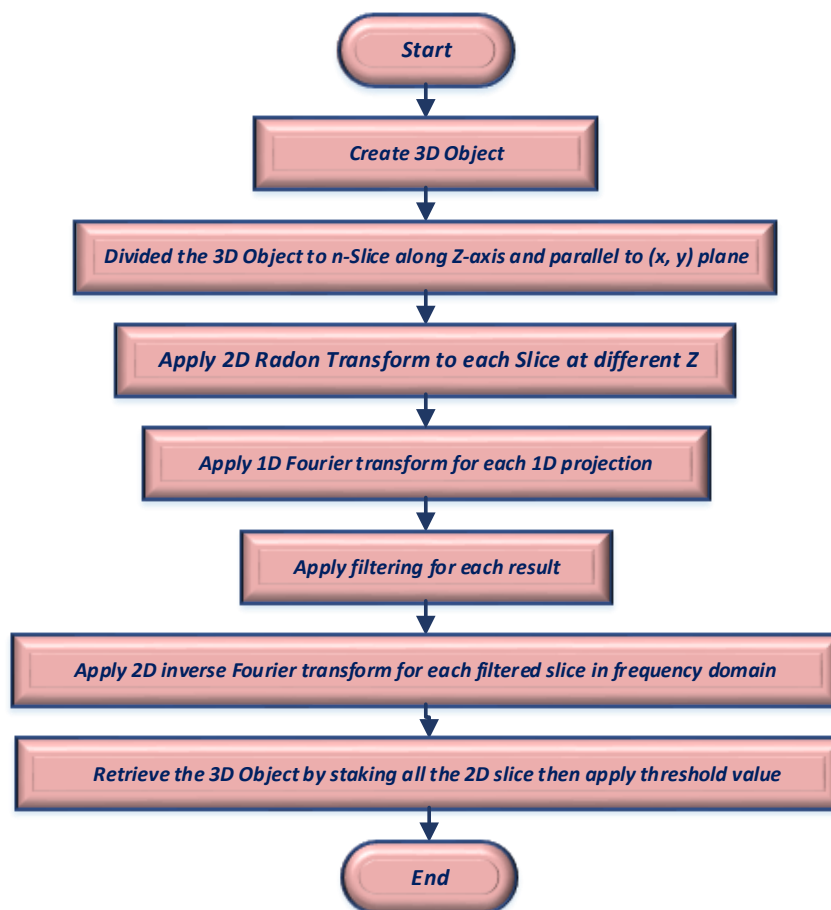


Figure 3-9 The Reconstructed 3D Object by FST method block diagram.

The object obtained by Fourier slice theorem has too many points because of the blurring artifact thus by apply a threshold value to the

reconstructed object, in which all point with magnitude less than the average value of the all reconstructed points will be eliminated.

3.5.2 Reconstructing the 3D Object from 3D Projection

The appropriate reconstruction method is used a 3D back-projection method utilizing equation (2-24) on the 3D sinogram of the 3D object, which is obtained by implementing the direct 3D forward projection method in section (3.3.2), the figure (3-10) illustrates the block diagram of this method.

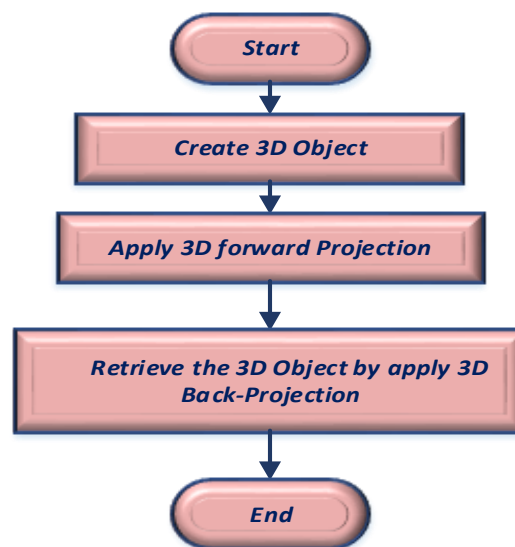


Figure 3-10 The 3D BP block diagram.

3.5.3 Reconstruction the 3D Object from 4D Projection

When the X-ray transform used to obtain the 4D projections, the appropriate images reconstruction methods are either 3D Back Projection for X-ray Projections described in equation (2-27). Figure (3-11) illustrates the block diagram of this method.

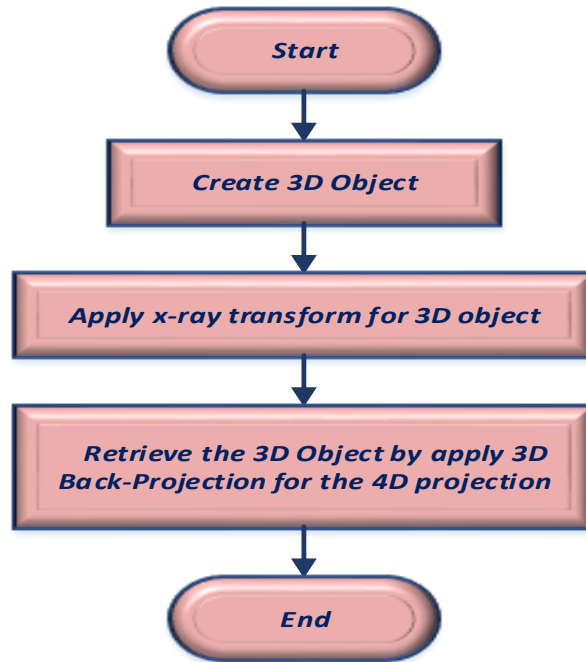


Figure 3-11 The 3D BP for x-ray projections block diagram.

Or the central section theorem for the X-ray projection of a 3D, which applied the 2D forward Fourier transform to 4D projection. The 4D projections in frequency domain are transformed to 3D projection also in frequency domain by matrix transformation, then the 3D inverse Fourier transform is applied to retrieve 3D object, this method described in the section (2.7.2), the figure (3-12) illustrates the block diagram of this method.

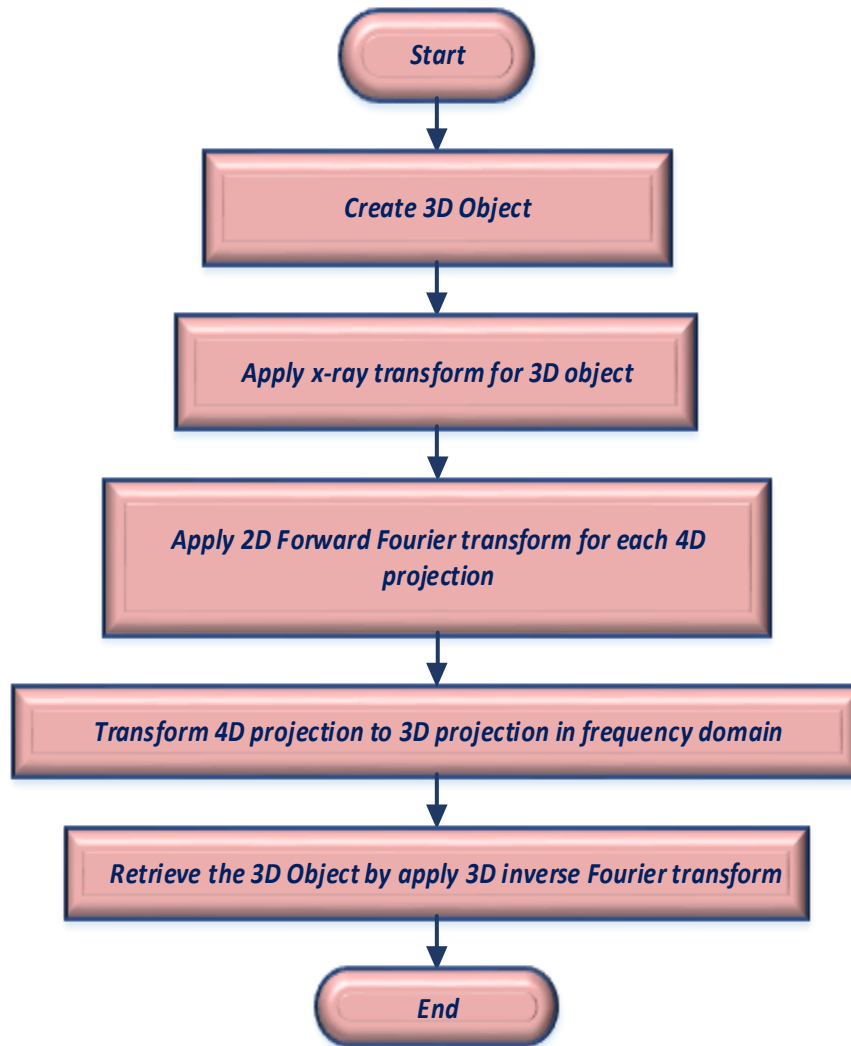


Figure 3-12 The central section theorem for the X-ray projection block diagram.

3.6 The Methodology of Interpolation

For the purpose of explaining the effect on asymmetric object of the interpolation methods adopted in this study, an asymmetrical body is used, such as the head of the Mickey Mouse shown in figure (3-3).

The interpolation methods applied to the 3D projections obtained by using the forward method illustrated in section (3.3.1), but it must be taken

into account that the equal angular distance ($\Delta\theta$) is greater than one degree that is used to obtain the 3D projections.

To enhance the 3D projection and estimate the values of the missing projection data, three equation of interpolation methods are used (see section (2-8)). The reconstruct object from interpolation sinogram by applying the methods of reconstruction object for each two-dimensional slice from its sinogram. To study the object features and estimate how much the improvement compared to the object reconstruction from sinogram in terms of missing data.

The signal-to-noise (SNR) ratio is used to evaluate the reconstructed object, besides that the number voxel that constructs the 3D object after using a threshold value to decide whether the voxel belongs to the object. The interpolation method illustrated in the block diagram (3-13) by using Back projection to reconstruct object and (3-14) by using Fourier slice theorem to reconstruct object.

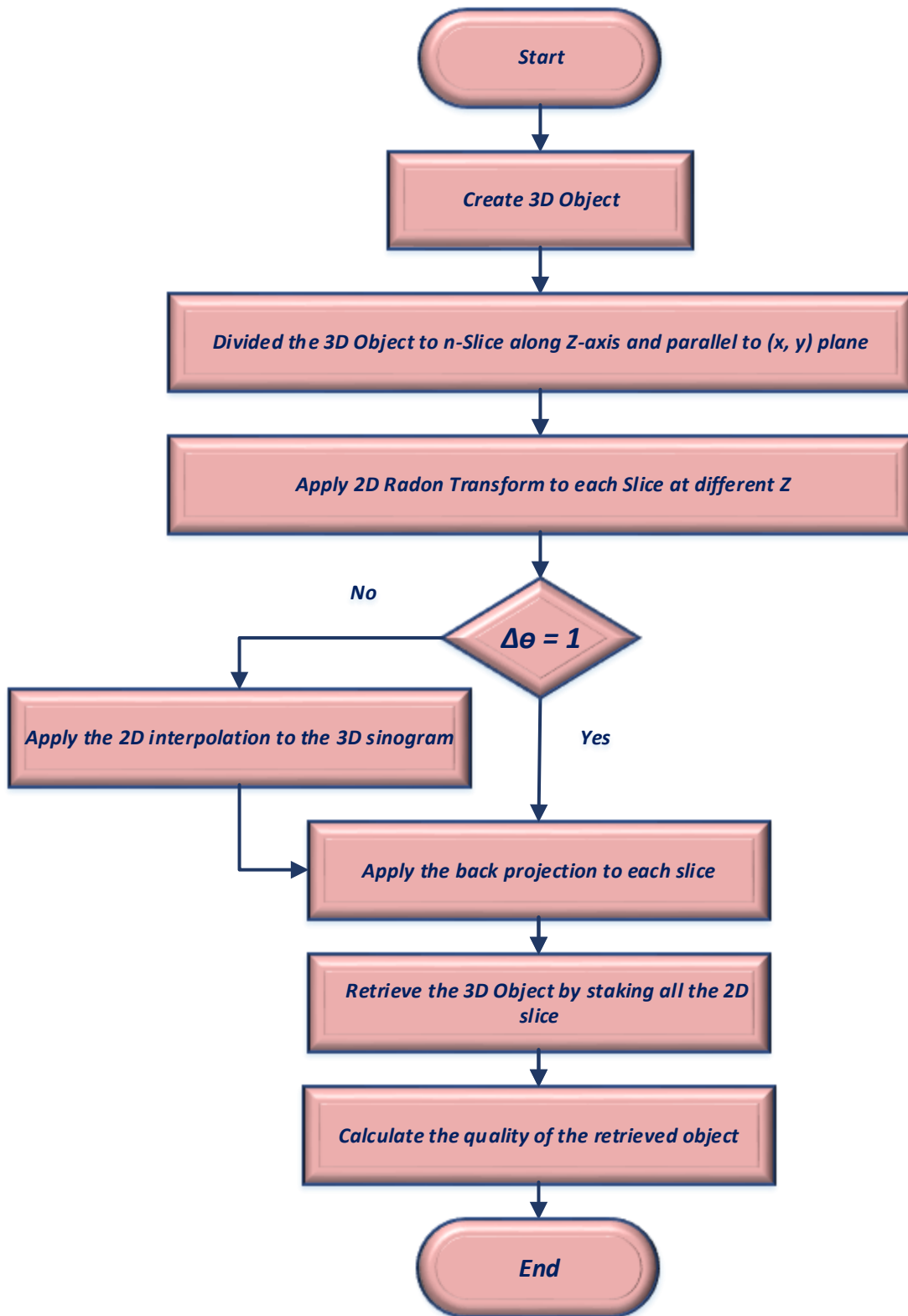


Figure 3-13 The interpolation method by using Back projection to reconstruct object block diagram.

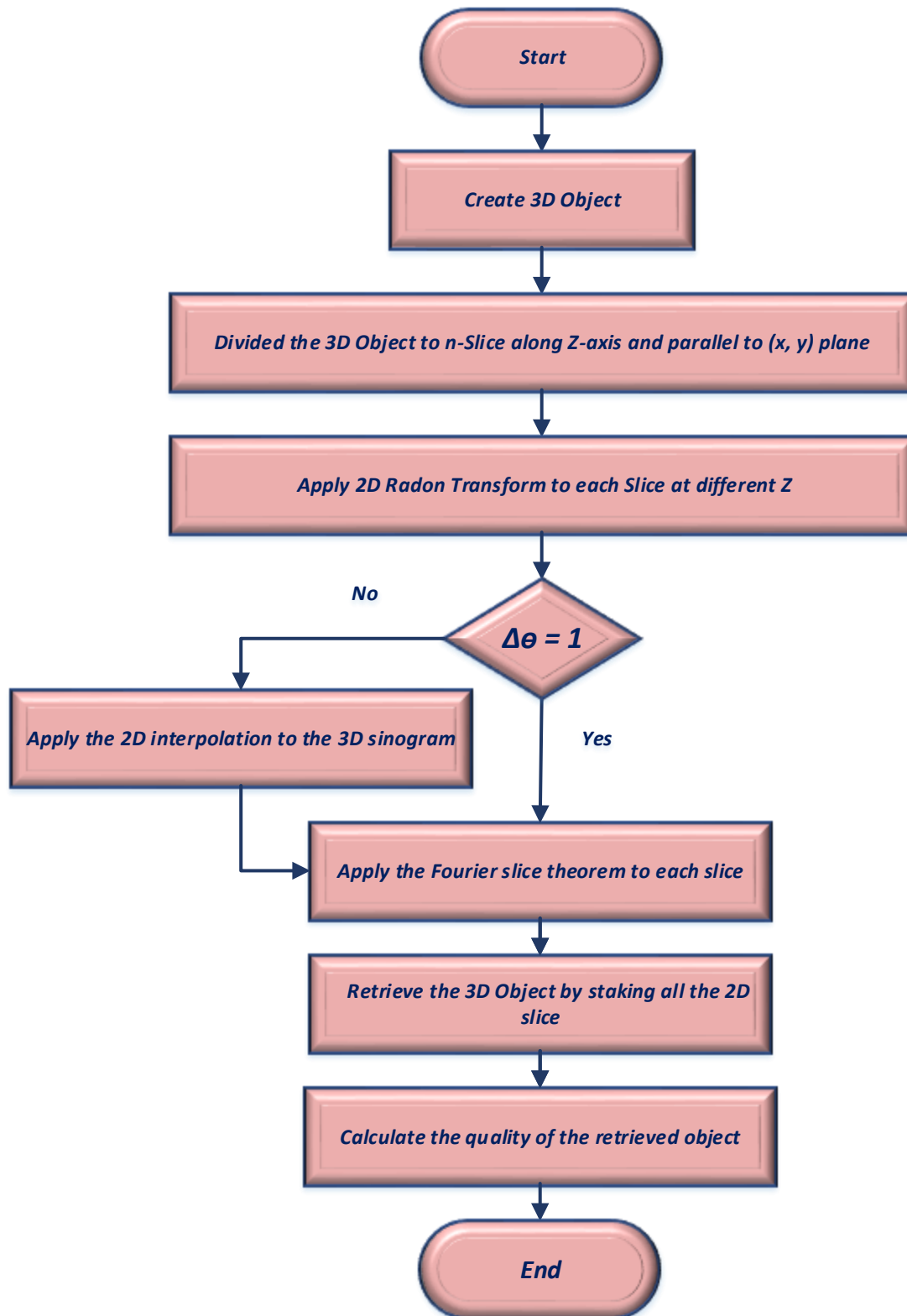
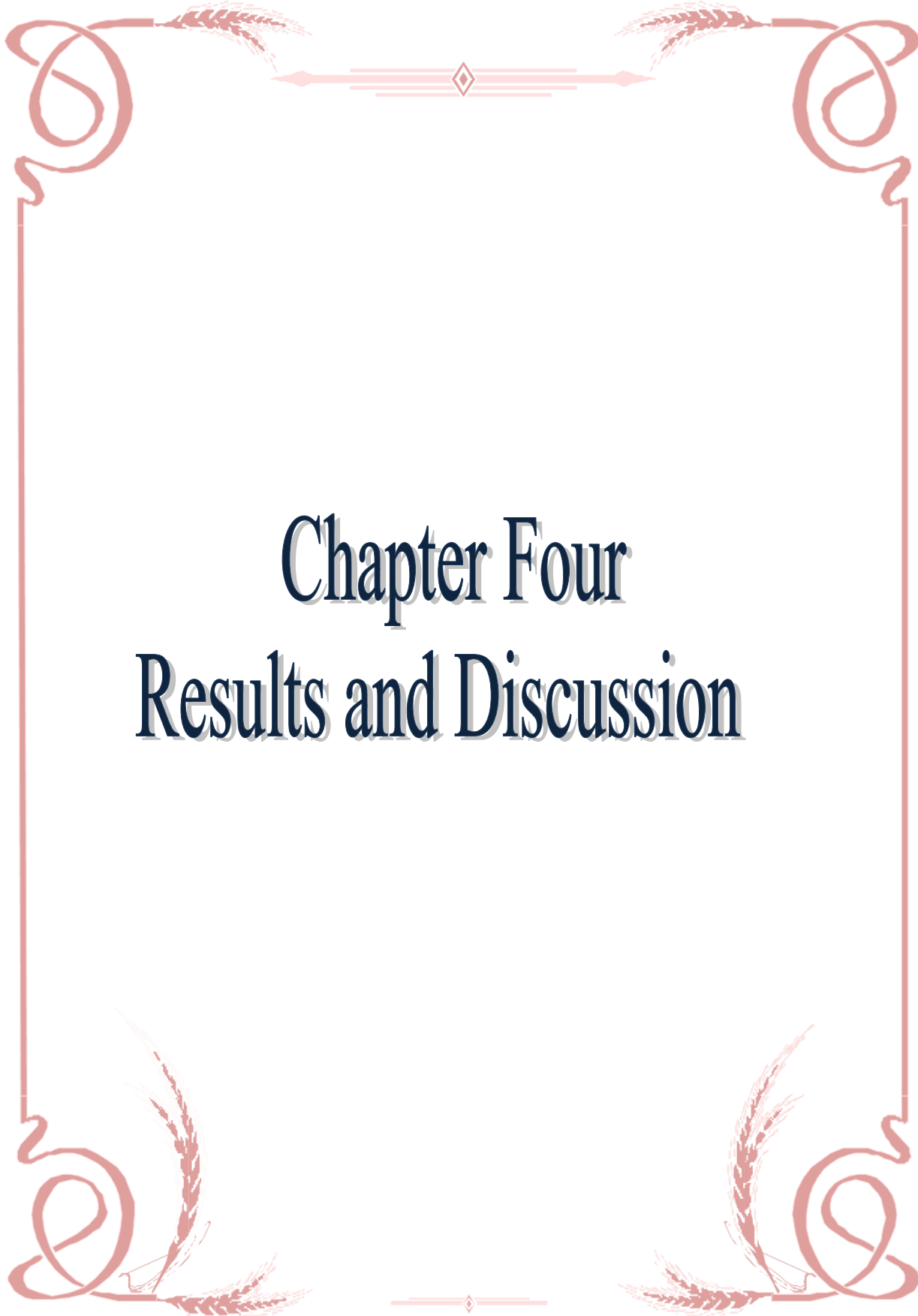


Figure 3-14 The interpolation method by using FST to reconstruct object block diagram.



Chapter Four
Results and Discussion

Chapter Four

Results and Discussion

4.1 Introduction

In this chapter the results are given to illustrate the reconstruction images and the improvements in the performance of the suggested method.

4.2 Results of the Forward projections

The following results obtained by applying the adopted forward methods.

4.2.1 Forward Projection using Slicing Method

In the first method, the object is divided into several two-dimensional slides along the Z-axis (height) and these slices are parallel to the plane (x , y) see figure (4-1 a, b), the 2D slices also are shown in figure (4-2 a, b), then apply the equation of two-dimensional projections (2D Radon transform) separately for each two-dimensional slice at different heights for the three-dimensional object.

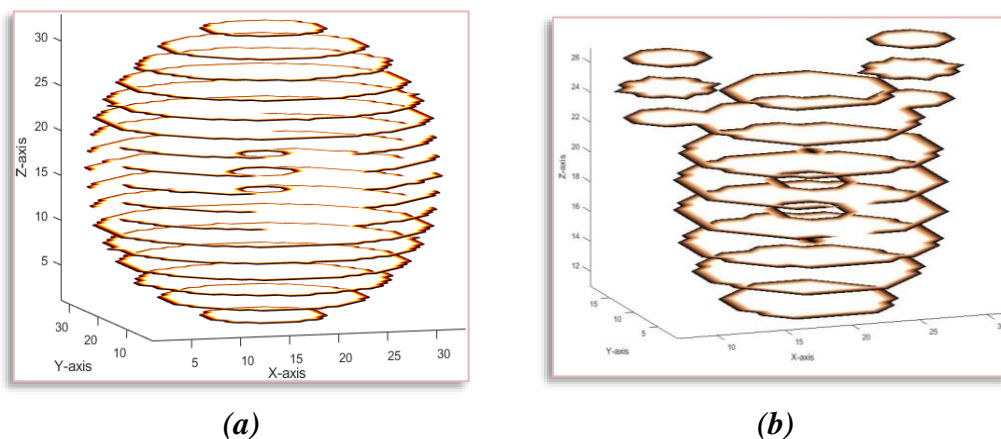
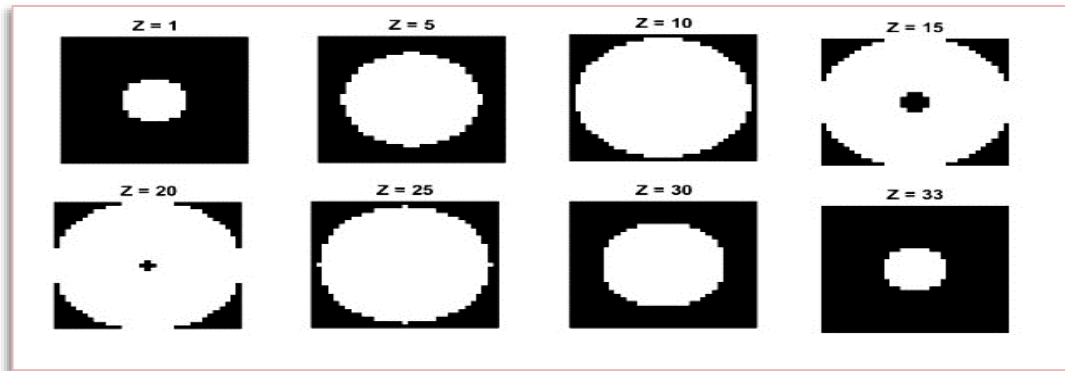
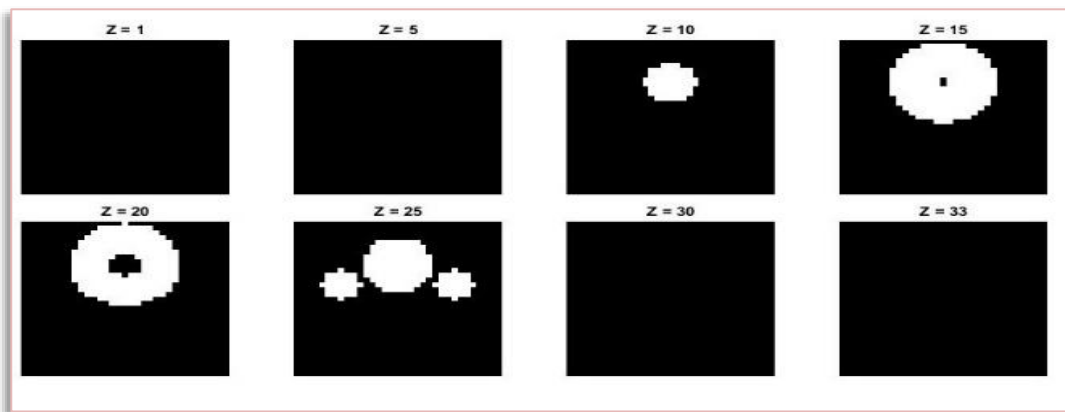


Figure 4-1 The 2D slices along the Z-axis for (a) for hollow sphere inside the solid sphere (b) for the head of Mickey Mouse



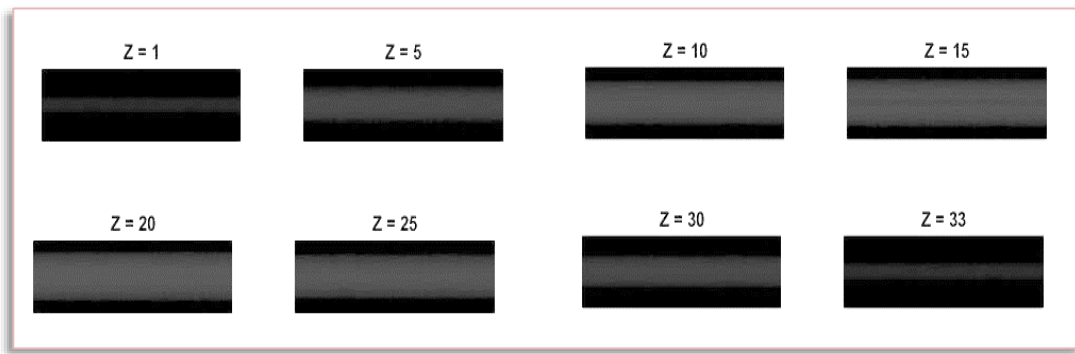
(a)



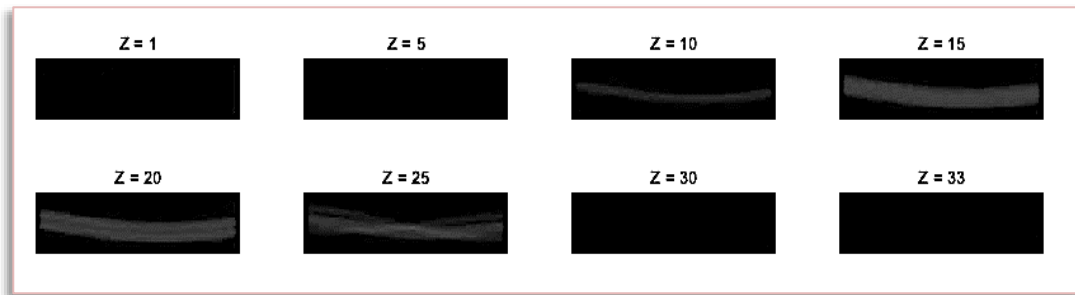
(b)

Figure 4-2 (a) 2D slice of the sphere at different heights & (b) 2D slice of the head of Mickey Mouse at different heights

After completing the implementation completed of the forward projections on all the slides starting from $Z=1$ to $Z=33$, stacking the two-dimensional projections has resulted from each two-dimensional slice at different heights as represented in figure (4-3 a, b) to produce the three-dimensional projections of the three-dimensional object as shown in figure (4-4 a, b).

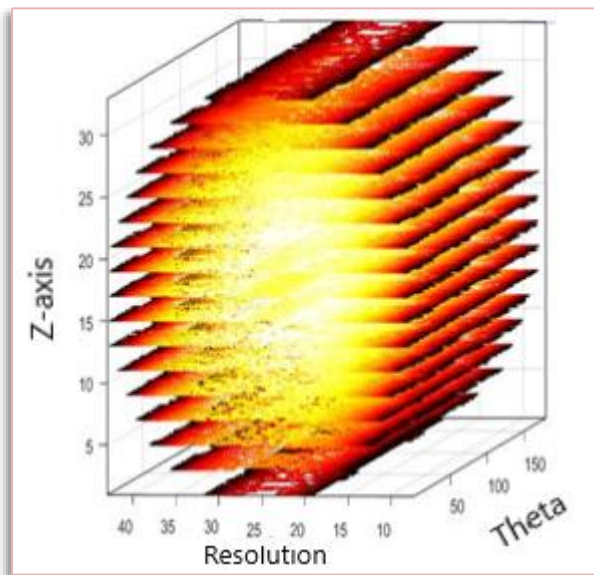


(a)

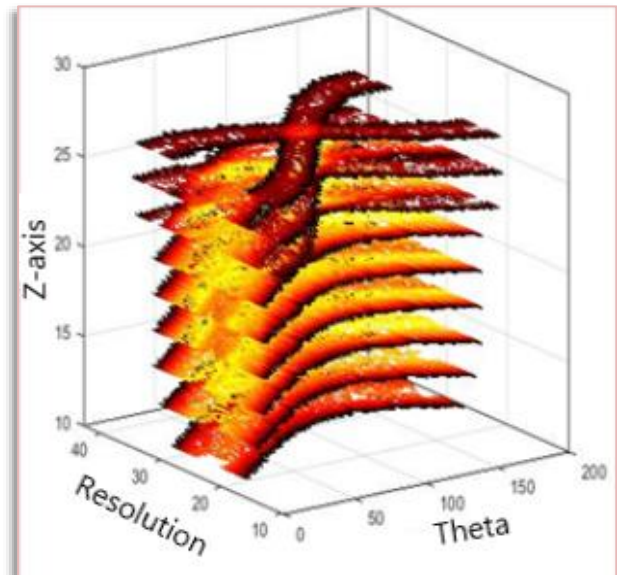


(b)

Figure 4-3 a 2D projection for some 2D slice of the (a) sphere at different heights and (b) head of Mickey mouse



(a)



(b)

Figure 4-4 Staking the 2D slices of projections for (a) sphere and (b) head of Mickey Mouse.

4.2.2 Forward Projection using Direct 3D Projections Method

In the second method, apply the equation of the three-dimensional projections (three dimensional Radon transform) for the three-dimensional object. See figures (4-5 a, b) and (4-6 a, b) represent the three-dimensional projections and the two-dimensional slice of the three-dimensional projections at different heights. The figure (4.7 a, b) represents the mesh for three-dimensional projection for the head of Mickey Mouse and sphere.

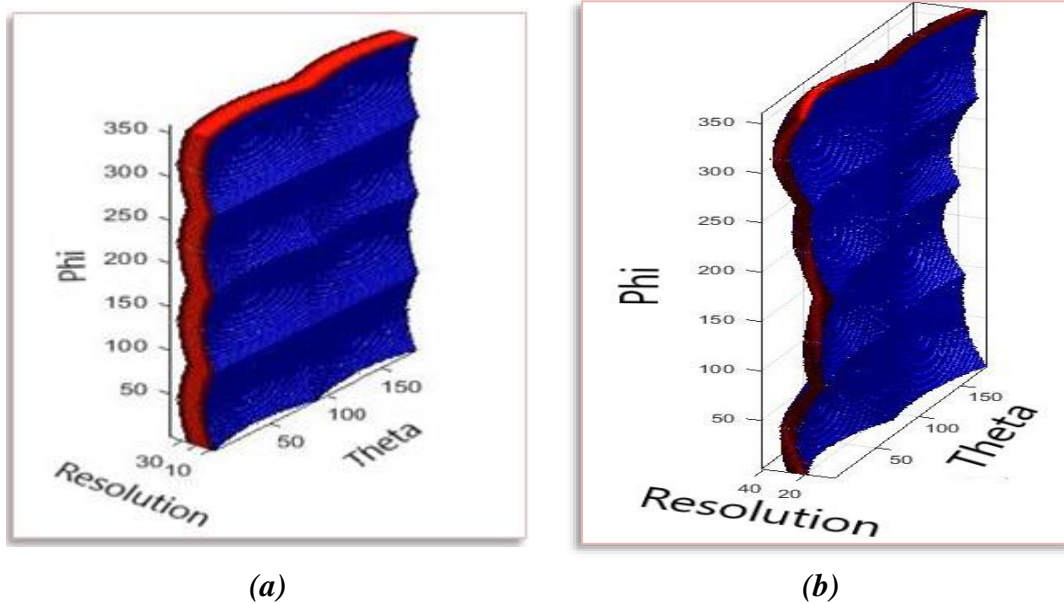
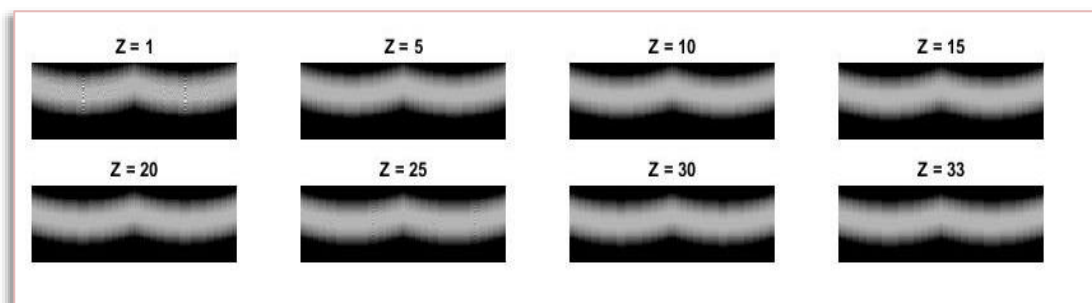
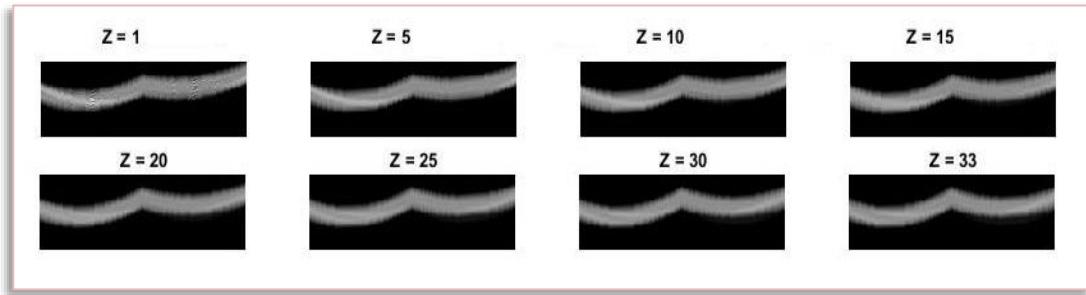


Figure 4-5 The 3D projections for (a) sphere and (b) head of Mickey Mouse.

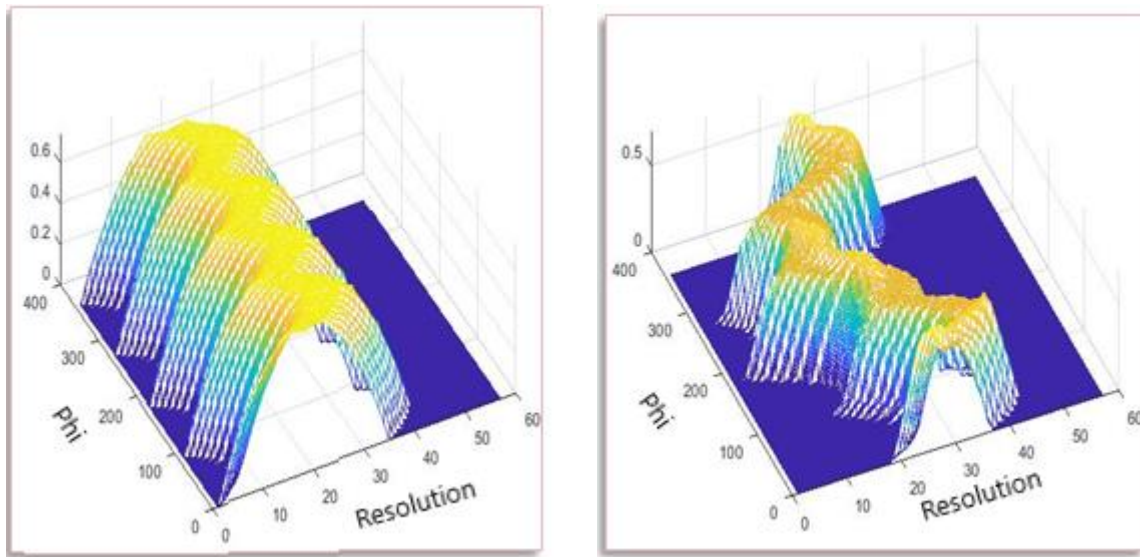


(a)



(b)

Figure 4-6 a 2D slices projection from 3D projections for (a) sphere and (b) head of Mickey Mouse.



(a) for sphere

(b) for Mickey Mouse

Figure 4-7 a mesh for 3D Projections.

4.2.3 Forward Projection using X-Ray Transform Method

The third method, this method is done by taking X-ray transform to obtain the 4D projection for a three-dimensional object, see figure (4-8), (4-9), (4-10) and (4-11) represent the three-dimensional X-ray projections and several of two dimensional slices that taken from three-dimensional X-ray projections at different heights for different object.

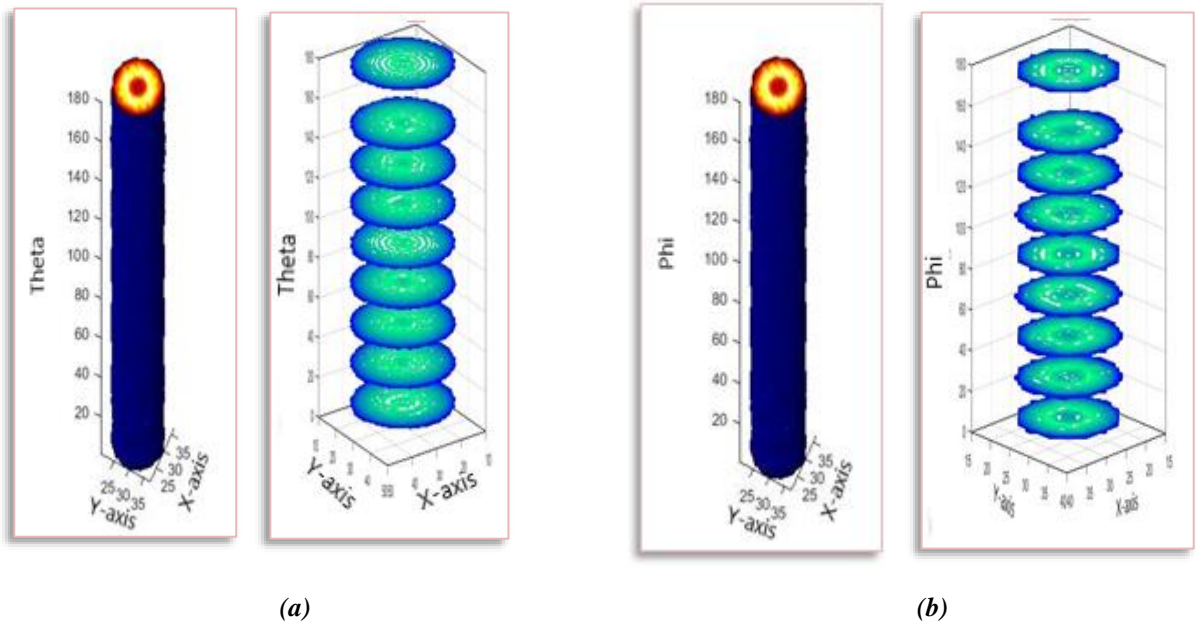


Figure 4-8 The 3D X-ray projections of the 3D sphere for (a) all range of Theta and specific Phi and (b) all range of Phi and specific Theta.

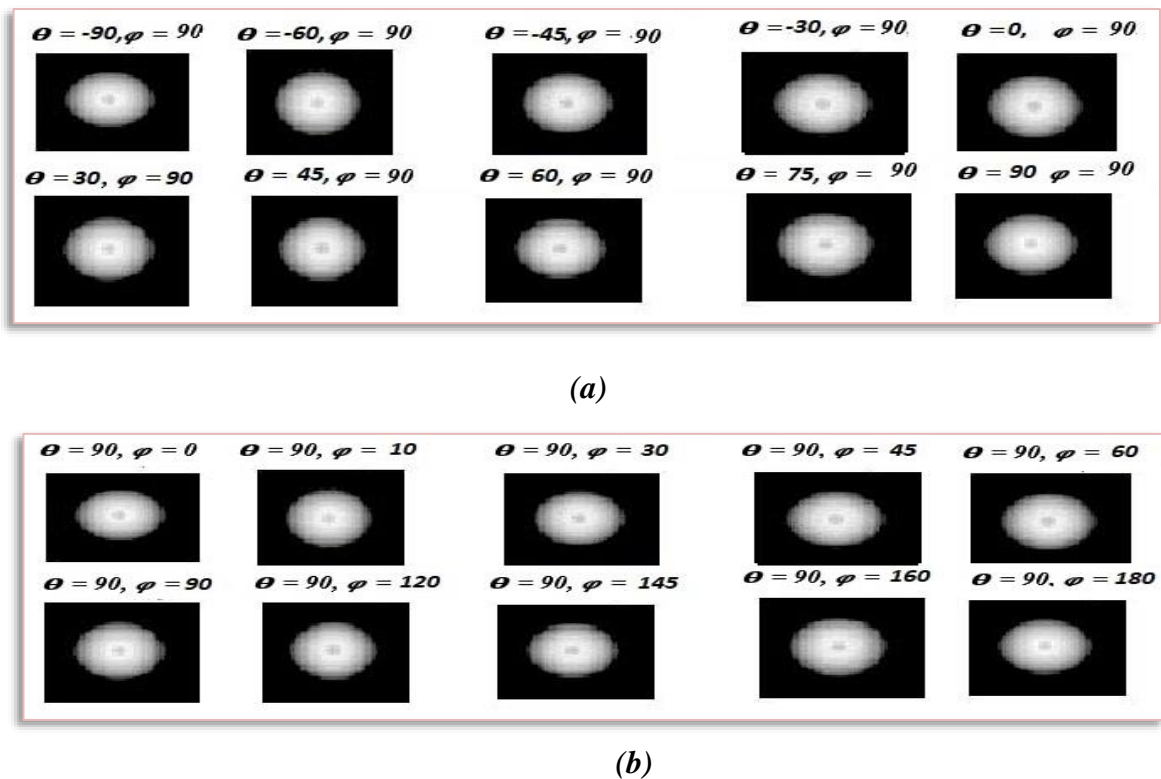


Figure 4-9 A 2D slice projections from 4D X-ray projections for the sphere at (a) specific Phi and several degrees of Theta and (b) specific Theta and several degrees of Phi.

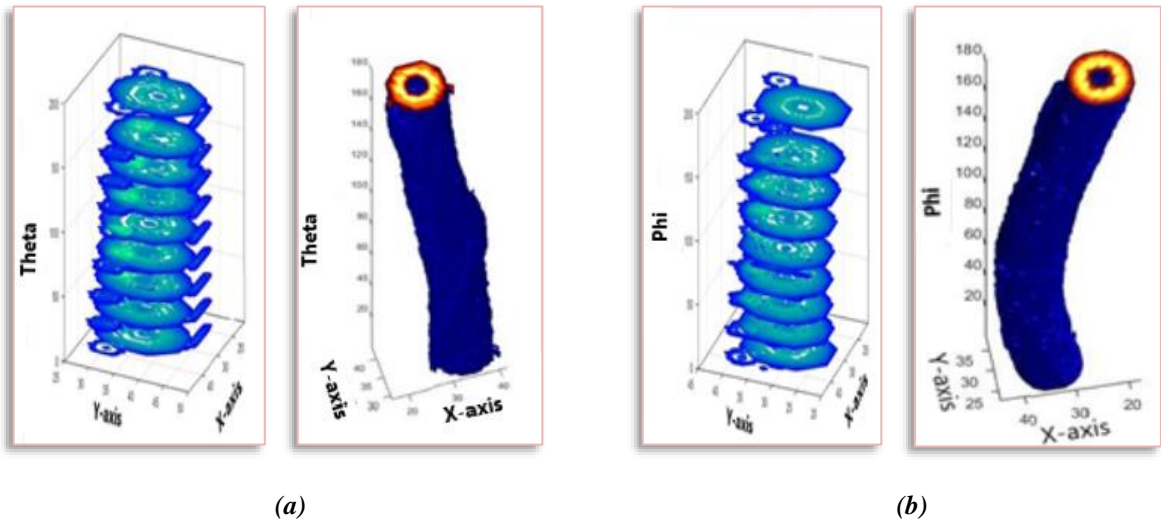


Figure (4-10) a 3D X-ray projections of the head of Mickey Mouse at (a) specific Phi and several degrees of Theta and (b) specific Theta and several degrees of Phi.

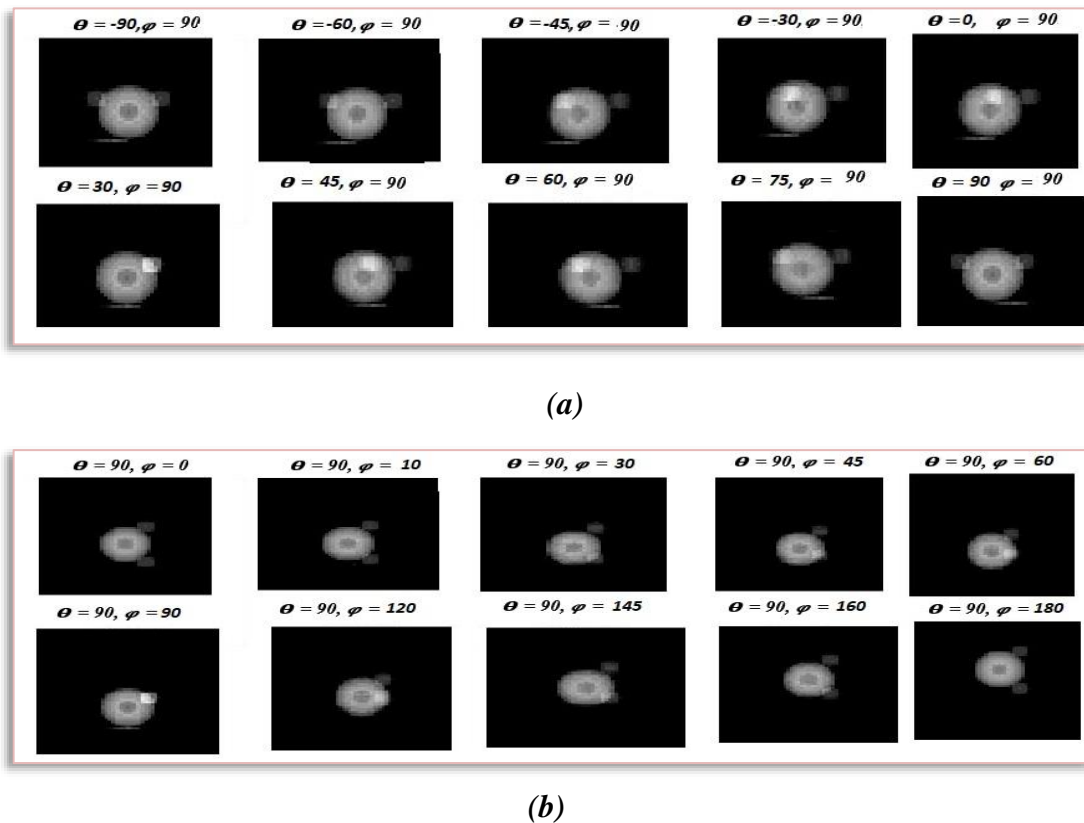


Figure 4-11 The 2D slice projections from 4D x-ray projections for the head of Mickey Mouse at (a) specific Phi and several degrees of Theta and (b) specific Theta and several degrees of Phi.

4.3 The Results of Reconstruction Methods

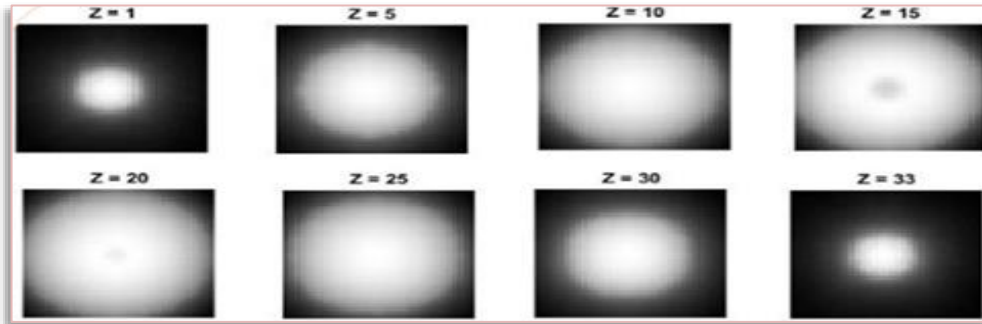
The following results obtained by applying the adopted reconstruction methods.

4.3.1 Reconstruct 3D Object from the 2D projection

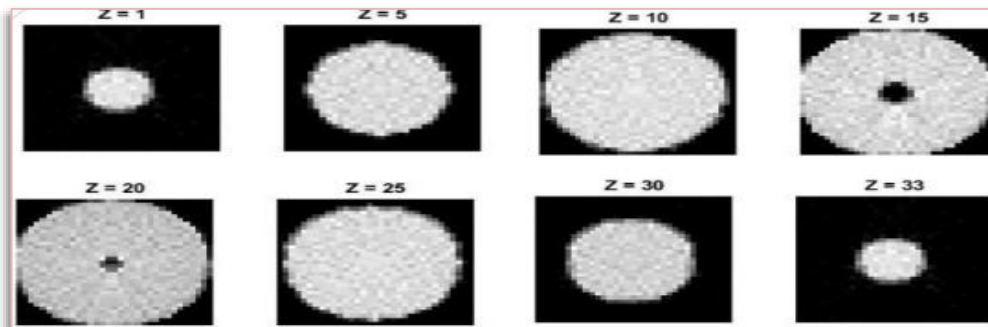
The following results obtained by applying the adopted reconstruction methods from the 2D projection with and without an applied filter.

4.3.1.1 The Results of Reconstruction Without Filtering

The 2D reconstruction methods are applied to the 2D projection of the 2D slices of the 3D object to restore the object slices, it is done by taking each two dimensional slice of projections as shown in figures (4-3 a) and (4-3 b) and then applied the two dimensional back projection equations for all slices at different heights, this led to reconstructed several slices for an object at different heights as shown in figures (4-12 a) and (4-13 a), or by using Fourier Slice Theorem, it is done by taking each two dimensional slice of projections as shown in figures (4-3 a) for sphere and (4-3 b) for head of Mickey Mouse and apply the one dimensional Fourier transform for all one-dimensional projections for all slices at different heights then filtering each result, that led to obtaining slices at different heights for object in frequency domain, and by applying the 2D inverse Fourier transform for each slice this led to reconstructed several slices for an object at different heights as shown in figures (4-12 b) and (4-13 b). it is clear from figures that the blurring artifact that the Back Projection method suffers from, miss the internal hollow sphere in both two objects, while using the Fourier Slice Theorem the reconstructed image eliminated from the blurring artifact, therefore, the interior hollow sphere become obvious in both two objects.

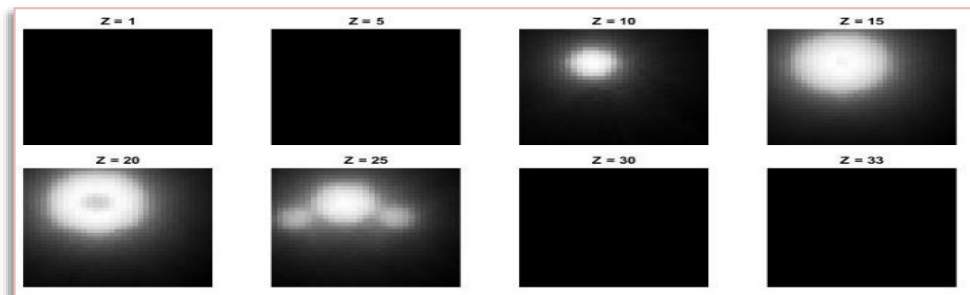


(a)

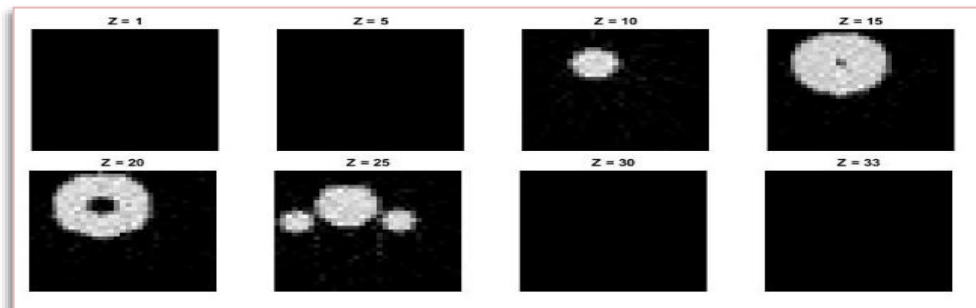


(b)

Figure 4-12 The 2D reconstructed Slices from the 2D projection of the 3D Sphere for different Z values, reconstructed by (a) BP and (b)FST.



(a)



(b)

Figure 4-13 the 2D reconstructed Slices from the 2D projection of the 3D head of Mickey Mouse for different Z values, reconstructed by (a) BP and (b) FST.

As mentioned in chapter three to restore the 3D object, the 2D reconstructed slices are stacked back together again, see figures (4-14 a, b) for sphere and (4-15 a, b) for Mickey Mouse. It is clear that the internal hollow sphere is absent in the Back Projection method, due to blurring artifact.

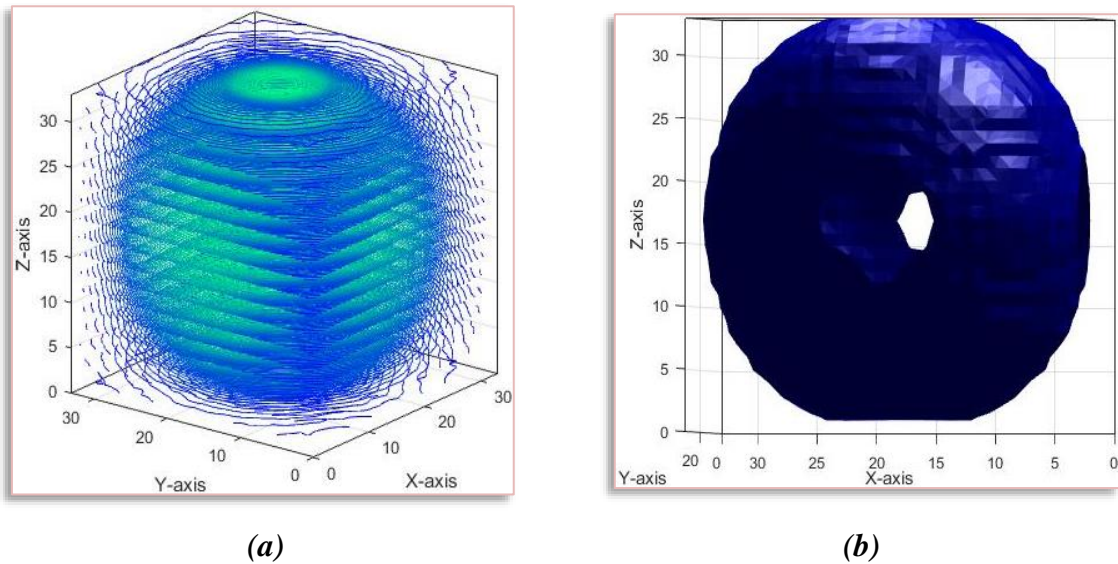


Figure 4-14 The 3D reconstructed sphere from the 2D projection using BP method, (a) representing the stacked 2D slices and (b) the 3D representation where there is no internal sphere.

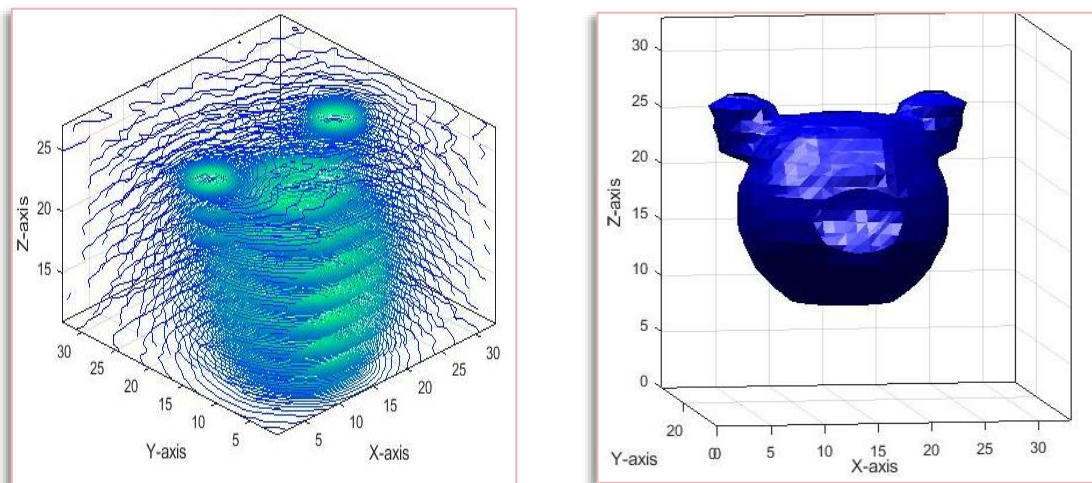


Figure 4-15 The 3D reconstructed head of Mickey Mouse from the 2D projection using BP method, (a) representing the stacked 2D slices, and (b) the 3D representation where there is no internal sphere.

While the Fourier Slice Theorem success to reconstruct the 3D object with the precence of the internal hollow sphere as illustrated in figures (4-16 a, b) for sphere and (4-17 a, b) for Mickey Mouse, since it eliminates most of the blurring effect by correcting the contribution weight of the object points that contribute in the back projection integral.

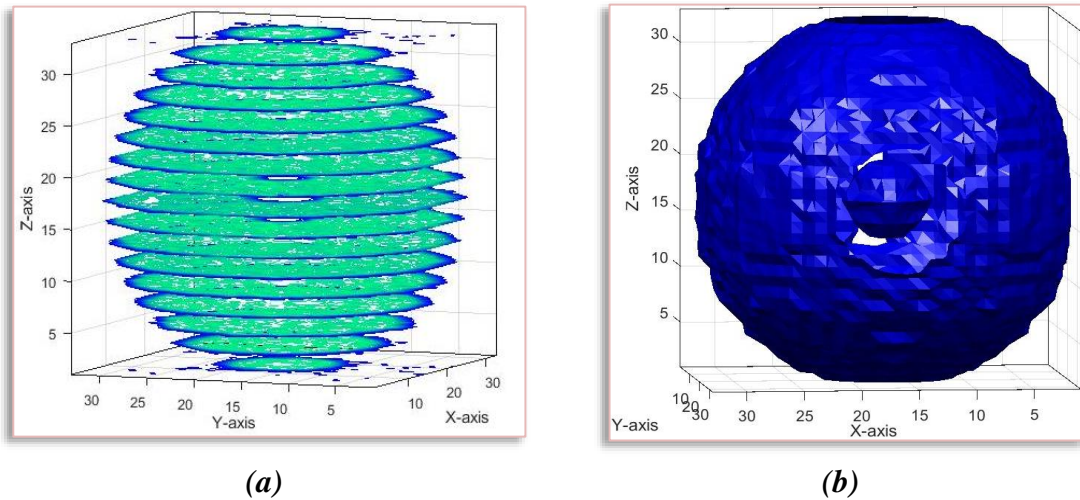


Figure 4-16 The 3D reconstructed sphere from the 2D projection using FST method, (a) representing the stacked 2D slices and (b) the 3D representation where there is the internal sphere

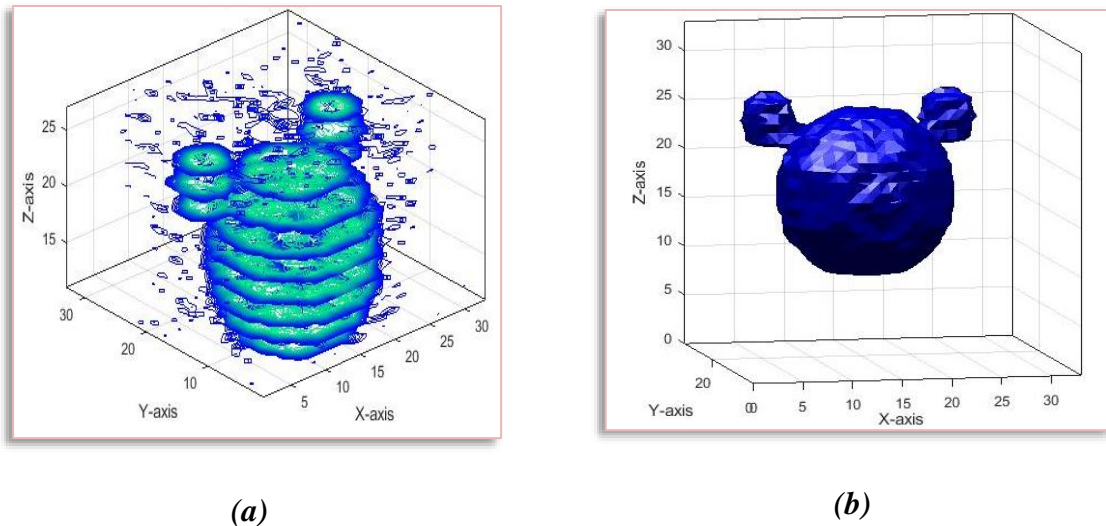


Figure 4-17 The 3D reconstructed Mikey Mouse from the 2D projection using FST method, (a) representing the stacked 2D slices, and (b) the 3D representation where there is the internal sphere

4.3.1.2 The Results of Reconstruction With Filtering

It is clear from the figures (4-16) and (4-17) that the objects reconstructed by FST have excessive points, so, to eliminate the excessive points that related to the blurring artifact that the FST couldn't remove, will apply a threshold value for both objects that reconstructed, in which all point with magnitude less than the average value (0.4630) of the all reconstructed point will be eliminated for sphere while for head of Mickey Mouse all point with magnitude less than the average value (0.0775) multiplied by 4 of the all reconstructed point will be eliminated, It is clear from figures (4-18 a, b) and (4-19 a, b) by using subjective criteria the reconstructed object will greatly improve when applying the threshold value.

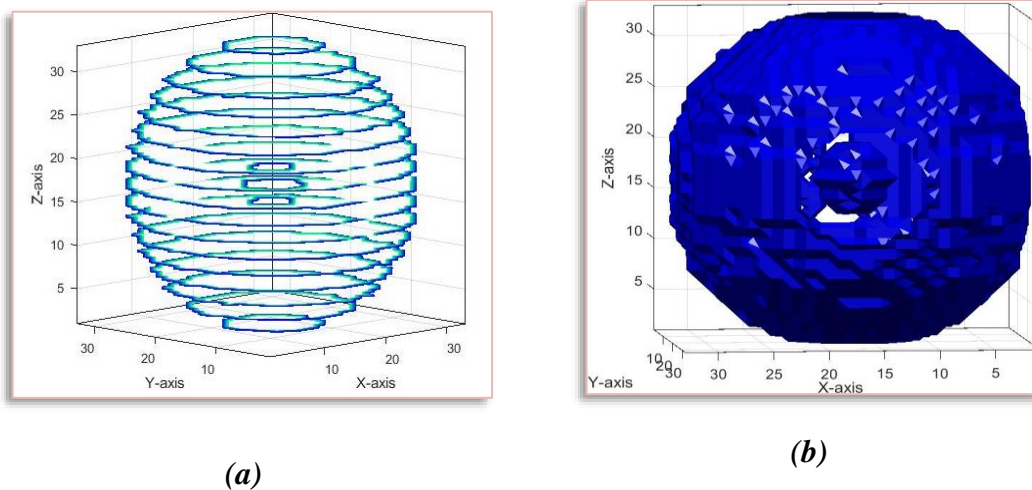


Figure 4-18 The 3D reconstructed sphere from the 2D projection using FST method after applying the threshold value, (a) representing the stacked 2D slices and (b) the 3D representation.

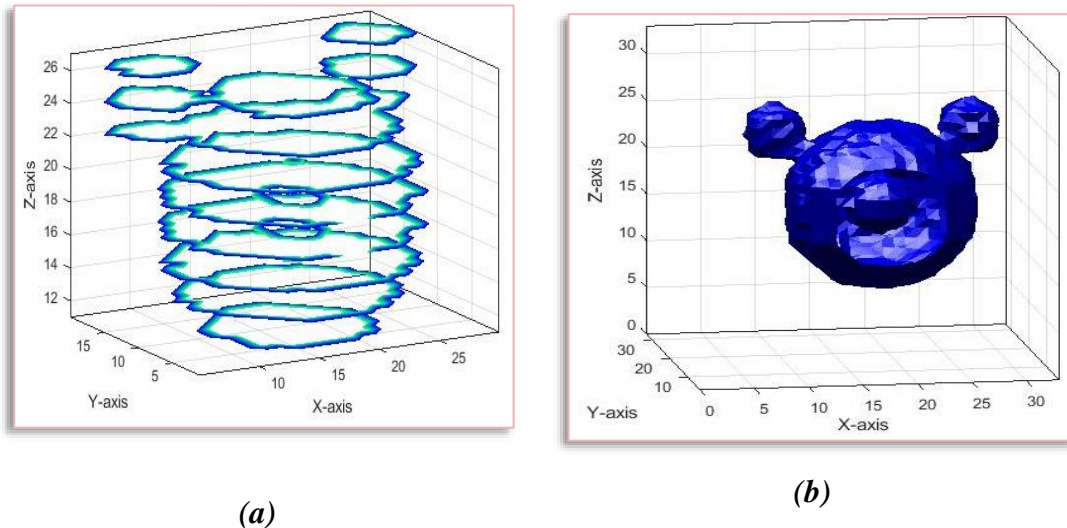


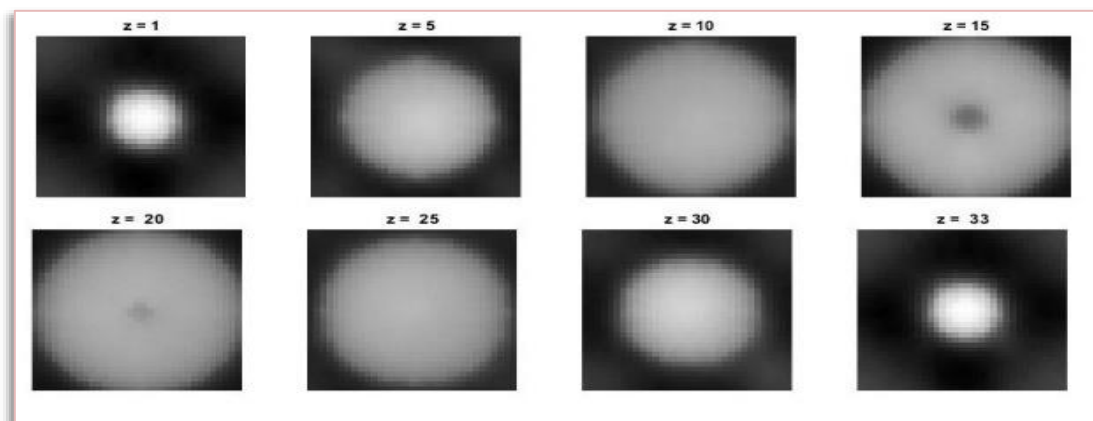
Figure 4-19 The 3D reconstructed head of Mickey Mouse from the 2D projection using FST method after applying the threshold value, (a) representing the stacked 2D slices and (b) the 3D representation.

Table 4-1 The SNR, PSNR and RMSE before and after applying the threshold for both reconstructed objects from the 2D projection by FST method

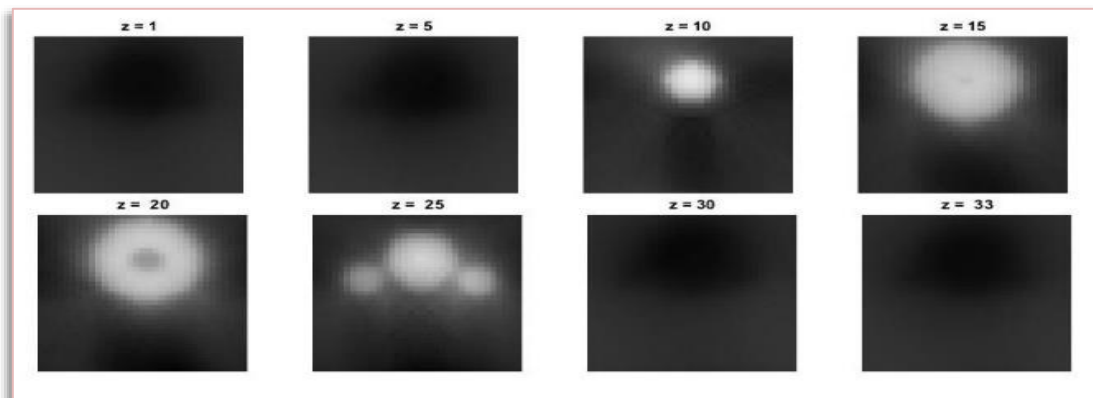
Retrieved 3D object by FST	Without Threshold			With Threshold			
	SNR	PSNR	RMSE	Threshold	SNR	PSNR	RMSE
Sphere Without Filtering	11.8311	14.3060	0.1926	0.4630	12.7142	15.1891	0.1740
Head of Mickey Mouse Without Filtering	9.5247	20.0805	0.0991	0.0775 *4	8.1601	18.7159	0.1159

From table (4-1) can notice that the SNR increases for sphere and decreases for Mickey Mouse after applying the threshold value while the RMSE decreases for sphere and increases for the head of Mickey Mouse after applying the threshold value. This means that the recovered sphere after applying the threshold value has improved in comparison to the recovered sphere without applying the threshold value while the recovered Mickey Mouse after applying the threshold value has not improved in comparison to the recovered Mickey Mouse without applying the threshold.

As shown from the figures (4-14) and (4-15) that the objects reconstructed by BP the blurring were removed by applying the filter in the frequency domain called the ramp filter in the frequency domain. The figures (4-20) and (4-21) have shown the result from applying the filtering, from the figure (4-20) can see the filtering success to retrieve the internal hollow sphere inside both objects. While the figure (4-21) shows the three-dimensional object drawing algorithm was unable to build the inner hollow sphere in the head of Mickey Mouse due to blurring while the algorithm in the large solid sphere succeeded in building the internal hollow sphere. On the other hand, the filtering caused some defects of the external structure of a big solid sphere.



(a)



(b)

Figure 4-20 The slices of the reconstructed object from the 2D projection after applying the filter for (a) sphere and (b) head of the mickey mouse

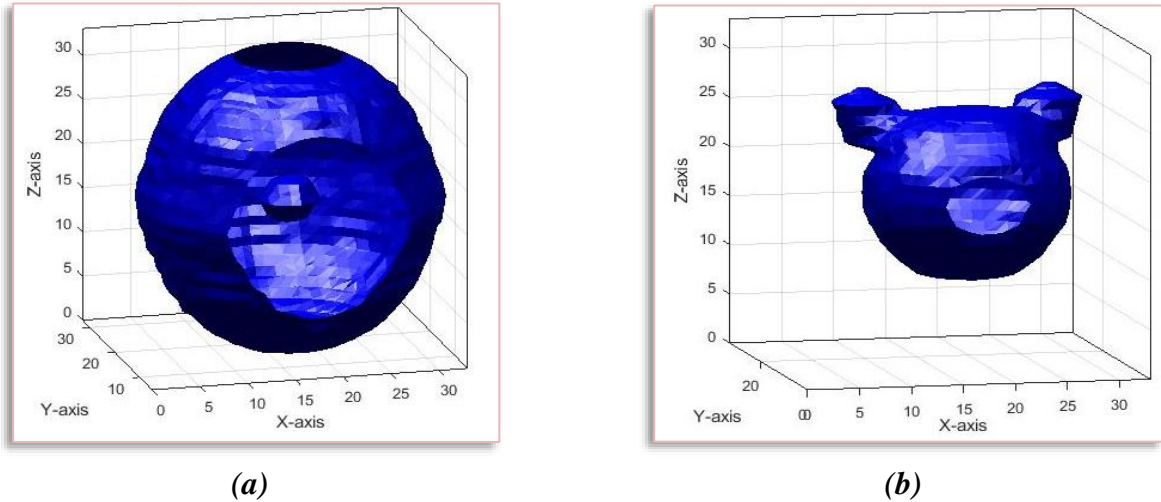


Figure 4-21 The 3D reconstructed from the 2D projection after applying the filter for (a) sphere and (b) head of the mickey mouse

In order to evaluate the accuracy of each method in the reconstruction process, by calculating the volume of the solid sphere, the volume of the head of Mickey Mouse and the volume of the hollow sphere inside them by counting the points that belong to each of them. The results are shown in Table (4-2).

Table 4-2 The volume of the reconstruction 3D object from 2D projection

<i>Type of object</i>	<i>Original</i>	<i>Reconstruction by BP</i>	<i>Reconstruction by FST</i>	<i>Reconstruction by BP after apply filtering</i>
<i>Solid Sphere</i>	<i>20326</i>	<i>18871</i>	<i>19664</i>	<i>16720</i>
<i>Internal Hollow Sphere</i>	<i>147</i>	<i>Zero</i>	<i>172</i>	<i>98</i>
<i>Head Mickey Mouse</i>	<i>3162</i>	<i>3561</i>	<i>3349</i>	<i>3145</i>
<i>Internal hollow sphere in head Mikey Mouse</i>	<i>126</i>	<i>Zero</i>	<i>101</i>	<i>1</i>

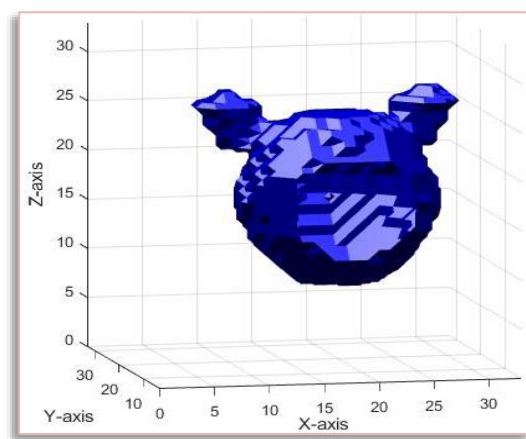
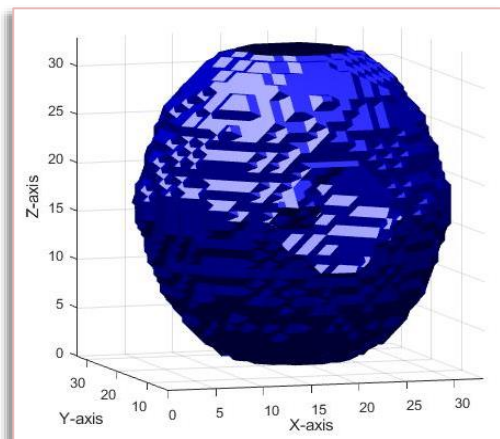
From table (4-2) the volume of each object (sphere and head of Mickey Mouse) that reconstructed by FST is closer to the original object volume compared to the calculated volumes of reconstructed objects by BP method.

After applying the filtering on the results of back-projection now calculate the SNR, PSNR and RMSE of the retrieved object before and after filtering and threshold. The results are shown in Table (4-3).

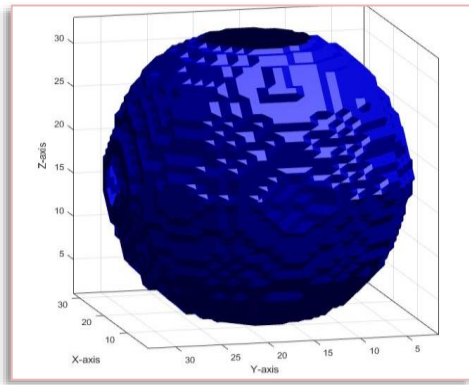
Table 4-3 The SNR, PSNR and RMSE before and after apply Filtering for objects reconstructed by back-projection method from the 2D projection

Retrieved 3D object by BP	Without Threshold			With Threshold			
	SNR	PSNR	RMSE	Threshold	SNR	PSNR	RMSE
Sphere Without Filtering	8.9835	11.4584	0.2673	0.55	9.3921	11.8670	0.2551
Sphere With Filtering	6.9714	9.4463	0.3370	0.5	7.3541	9.8290	0.3225
Head of Mickey Mouse Without Filtering	4.5529	15.1087	0.1756	0.55	7.0687	17.6245	0.1315
Head of Mickey Mouse With Filtering	3.1029	13.6587	0.2075	0.5	7.2691	17.8249	0.1285

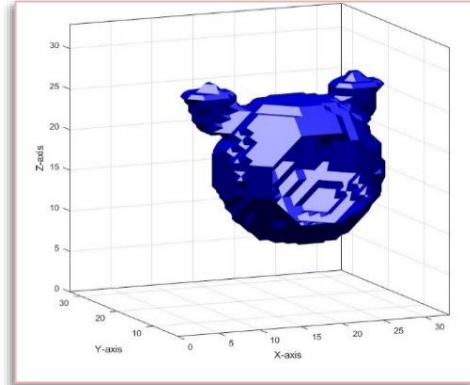
From the table (4.3), the SNR decreases and the RMSE increases after the filter for both objects can be noticed. This means that the recovered objects after applying the filter have not improved in comparison to the recovered objects without applying the filter. But after applying the threshold value the values of SNR increase and RMSE decreases this means the recovered objects improved after applying the threshold value for each object (sphere and Mickey Mouse) and in each state (with and without filtering). The figures (4-22) and (4-23) have shown the results from applying the threshold values on the objects with filter and without the filter.



(a)



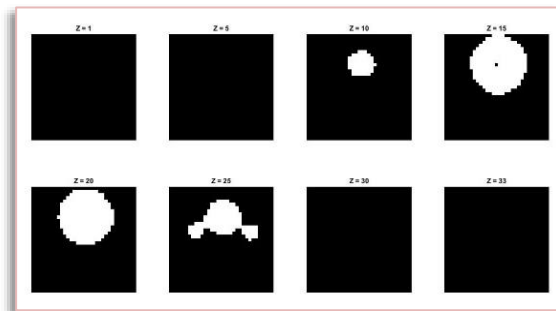
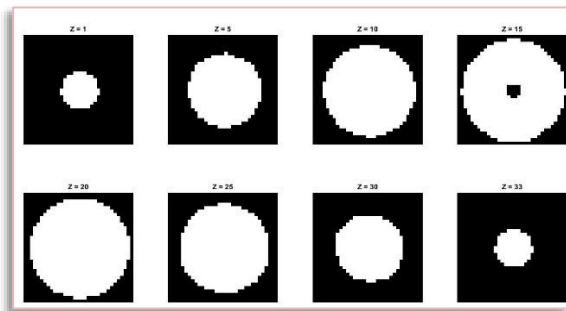
Sphere



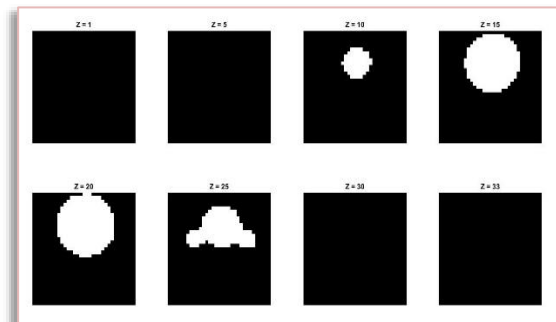
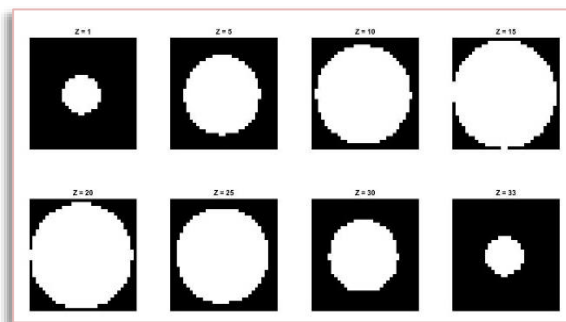
head of the mickey mouse

(b)

Figure 4-22 (a)The 3D reconstructed from the 2D projection after applying a threshold on filter object and (b)The 3D reconstructed from the 2D projection after applying a threshold on no filter object



(a)



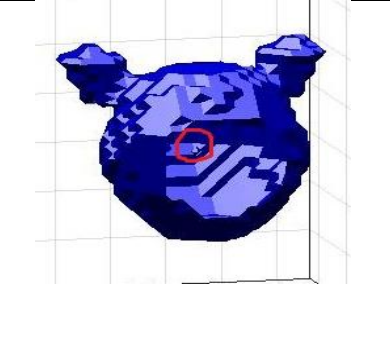
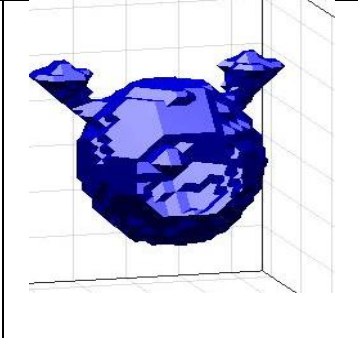
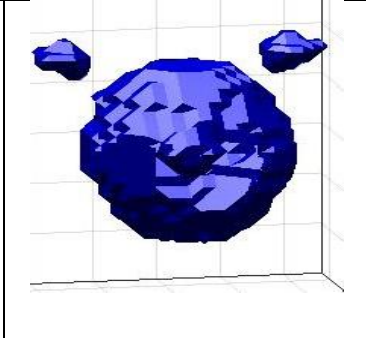
(b)

sphere

head of the mickey mouse

Figure 4-23 (a) The slices of the 3D reconstructed from the 2D projection after applying a threshold on filter object and (b) The slices of the 3D reconstructed from the 2D projection after applying a threshold on no filter object

Table 4-4 The change in external structure with change the threshold value for filtered head of Mickey Mouse reconstructed by back-projection method from the 2D projection

Threshold	0.5	0.55	0.6
SNR	7.2691	6.7910	5.5548
object			

From table (4.4) can note when increasing the threshold value of the filtered Mickey Mouse, the inner sphere starts to appear beginning from threshold value equal to (0.5) but with continuing increase the threshold value leads to distortion in the external structure, so from the subjective criteria, the best result for head of Mickey Mouse can be obtained when the threshold value is 0.5.

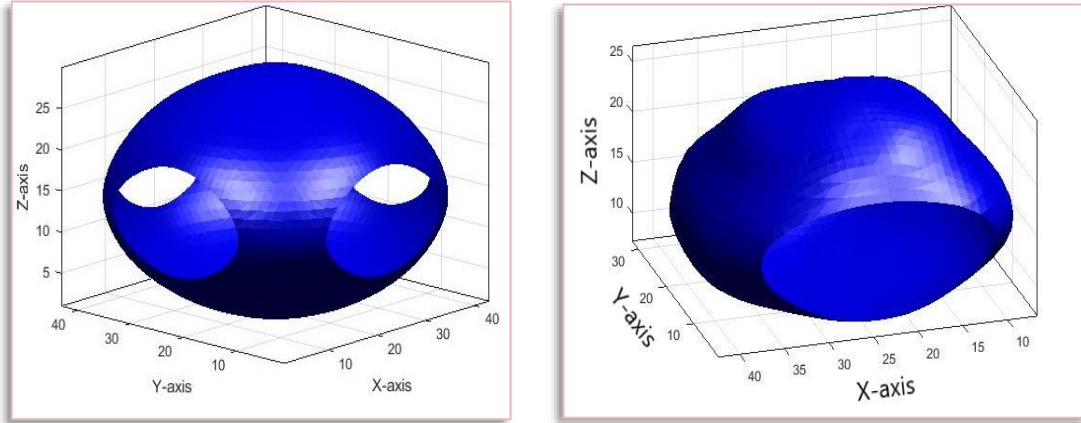
4.3.2 Reconstruct 3D Object from the 3D Projection

The following results obtained by applying the adopted reconstruction methods from the 3D projection with and without an applied filter.

4.3.2.1 The Results of Reconstruction Without Filtering

The 3D reconstruction method is a 3D Back-Projection is applied to the 3D projections that shown in figure (4-5), the 3D object retrieved by using 3D Back Projection is shown in figures (4-24 a, b) and (4-25 a, b) shows the slices of retrieved objects from these figures, it is clear that the 3D Back Projection method greatly suffers from the blurring artifact, that causes to miss the internal hollow sphere in both two objects and miss the external

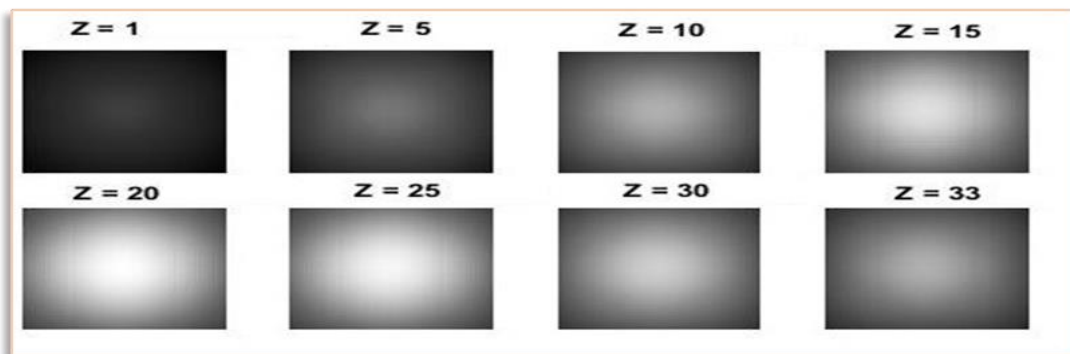
features of both two objects where can see the ears of head of Mickey Mouse appear like scars.



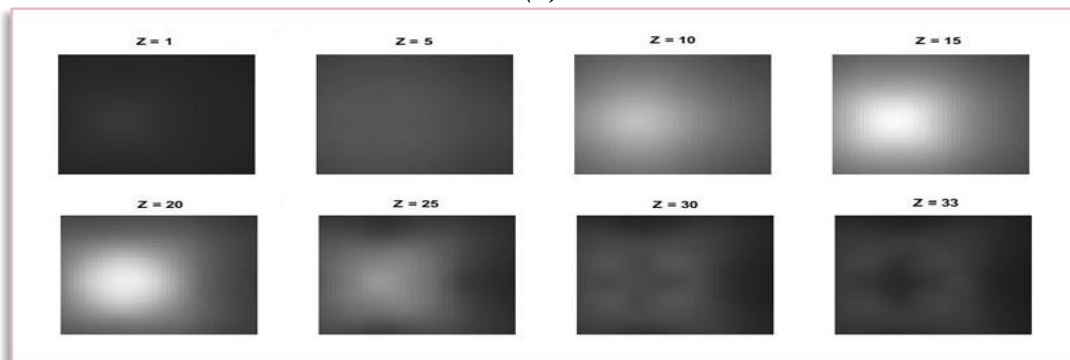
(a)

(b)

Figure 4-24 The 3D reconstructed object by 3D BP from the 3D Projection for (a) sphere and (b) head of the mickey mouse



(a)

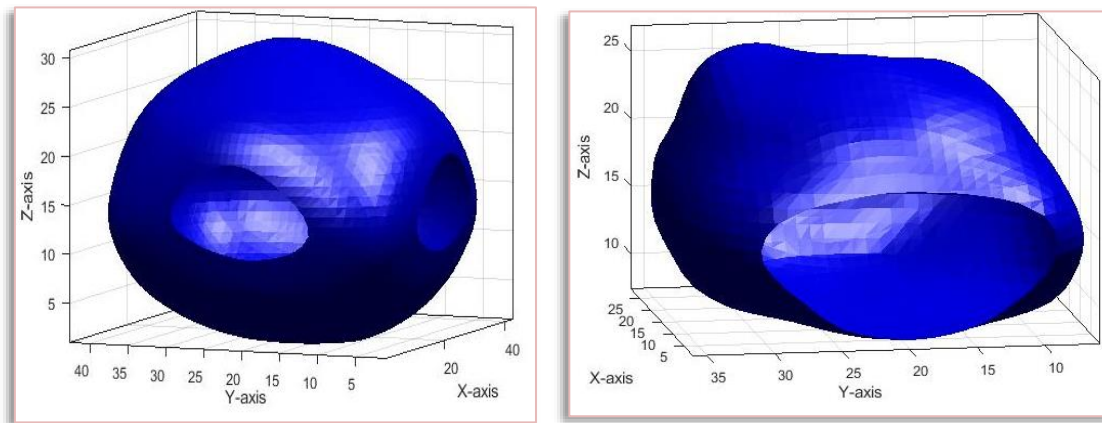


(b)

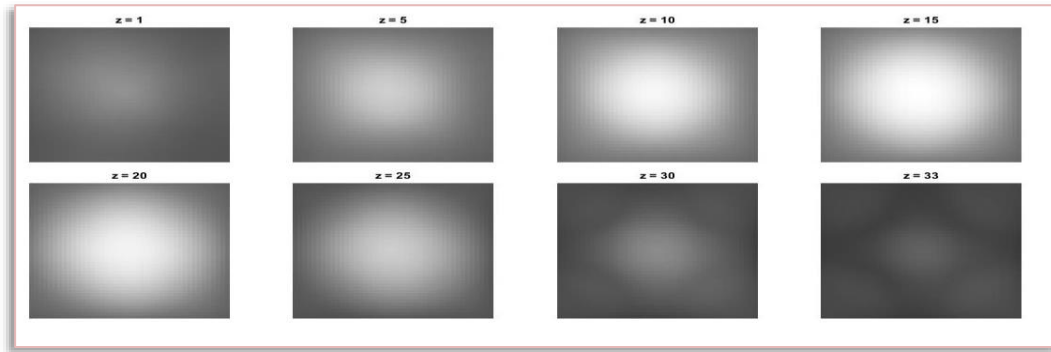
Figure 4-25 The 3D reconstructed object using 3D BP method from the 3D Projection for (a) sphere and (b) head of the mickey mouse.

4.3.2.2 The Results of Reconstruction With Filtering

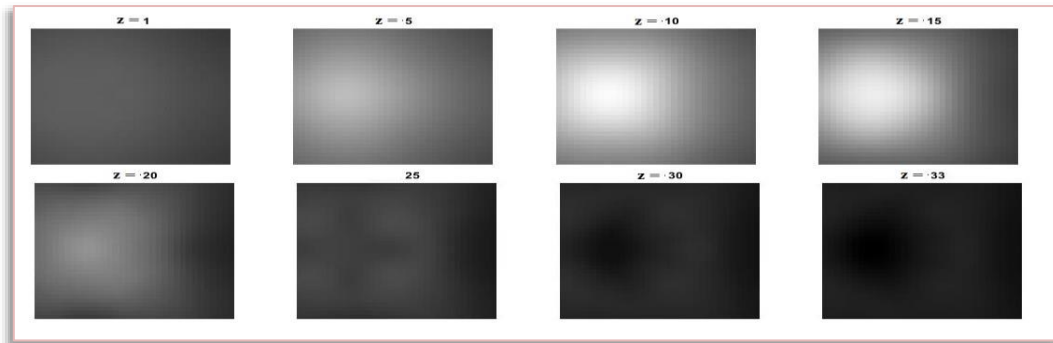
The retrieved object by 3D back Projection can be improved by applying the filter in the frequency domain called the ramp filter in the frequency domain. The figures (4-26) and (4-27) have shown the result from applying the filtering, from these figures shows that the impact of the filter on improve retrieved object is very little, where the effect of blurring is still clear on the lack of clarity of the external structure of the two objects and also on the disappearance of an internal hollow sphere, Where the scars on Mickey Mouse's head seem clearer but they remain unclear enough to classify them as ears for head of Mickey Mouse because of the effect of blurring.



(a) (b)
Figure 4-26 The 3D reconstructed object by BP after filtering from the 3D Projection for (a) sphere and (b) head of the mickey mouse



(a) Sphere



(b)

Figure 4-27 (a) The 3D reconstructed object using 3D BP method from the 3D Projection after filtering for (a) sphere and (b) head of the mickey mouse

In order to evaluate the accuracy of each method in the reconstruction process, by calculating the volume of the solid sphere, the volume of the head of Mickey Mouse and the volume of the hollow sphere inside them by counting the points that belong to each of them. The results are shown in Table (4-5).

Table 4-5 The volume of the 3D retrieved object from 3D projection

Type of object	Original	Reconstruction by BP	Reconstruction by BP after apply filtering
Solid Sphere	20326	19860	23675
Internal Hollow Sphere	147	Zero	Zero
Head Mickey Mouse	3162	8994	9900
Internal hollow sphere in head Mickey Mouse	126	Zero	Zero

From table (4-5) the volume of each object that reconstructed by BP before apply filtering is closer to the volume of the original object compared

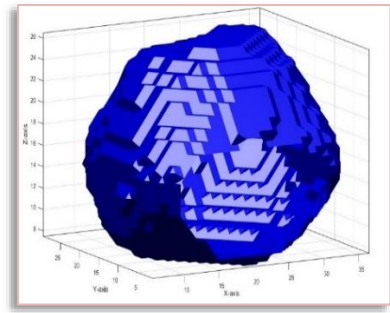
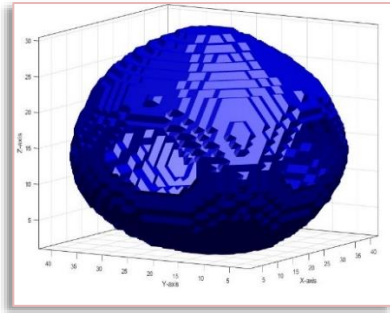
to the calculated volume of reconstructed objects by BP method with filtering, while the volume of the inner sphere is zero in each reconstructed method.

After applying the filtering on the results of back-projection now calculate the SNR, PSNR and RMSE of the retrieved object before and after filtering and threshold. The results are shown in Table (4-6).

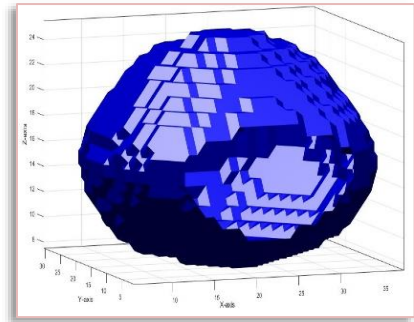
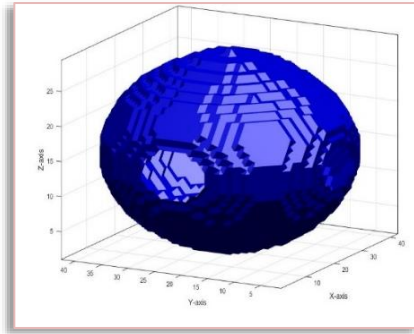
Table 4-6 The SNR and RMSE before and after apply Filtering on the 3D retrieved object from 3D projection

<i>Retrieved 3D object by BP</i>	<i>Without Threshold</i>			<i>With Threshold</i>			
	<i>SNR</i>	<i>PSNR</i>	<i>RMSE</i>	<i>Threshold</i>	<i>SNR</i>	<i>PSNR</i>	<i>RMSE</i>
<i>Sphere Without Filtering</i>	2.0240	7.9475	0.4005	0.55	0.6447	6.5682	0.4694
<i>Sphere With Filtering</i>	1.7745	7.6981	0.4122	0.5	-0.076	5.8467	0.5101
<i>Head of Mickey Mouse Without Filtering</i>	-4.916	9.0883	0.3512	0.55	-4.333	9.6712	0.3284
<i>Head of Mickey Mouse With Filtering</i>	-5.192	8.8123	0.3626	0.5	-3.253	10.7511	0.2900

From the table (4.6), can notice that the SNR decreases and the RMSE increases after the filtering for both objects and after applying the threshold value on the solid sphere, while the SNR increases and RMSE decreases after applying the threshold value on the head of Mickey Mouse in each state (with and without filtering), that means the solid sphere has not improved after applying the filtering and applying the threshold value, while the head of Mickey Mouse is badly after applying the filtering but is very little improved after applying the threshold value in each state (with and without filtering). The figures (4-28) and (4-29) have shown the results from applying the threshold values on the objects with filter and without the filter.



(a)

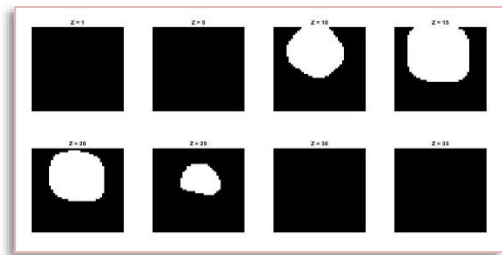
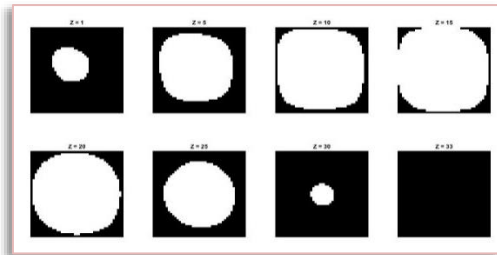


(b)

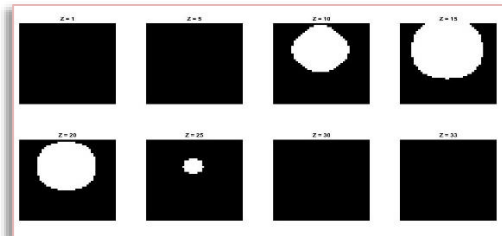
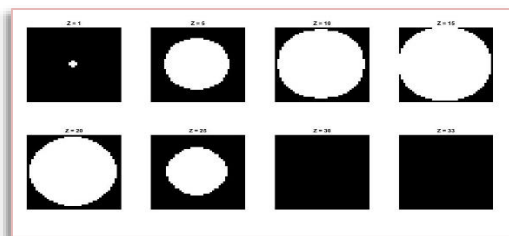
Sphere

head of the mickey mouse

Figure 4-28 (a)The 3D reconstructed from the 3D Projection after applying a threshold on filter object (b)The 3D reconstructed from the 3D Projection after applying a threshold on no filter object.



(a)



(b)

Sphere

head of the mickey mouse

Figure 4-29 (a)The slices of the 3D reconstructed from the 3D Projection after applying a threshold on filter object and (b)The slices of the 3D reconstructed from the 3D Projection after applying a threshold on no filter object

4.3.3 Reconstruct 3D Object from the 4D Projection

The following results obtained by applying the adopted reconstruction methods from the 4D projection with and without an apply the filtering.

4.3.3.1 The Results of Reconstruction Without Filtering

The reconstructed 3D object from 4D projection (X-Ray Projections) by apply either three-dimensional Back Projection for X-Ray Projections or apply the central section theorem for the X-ray projection, the retrieved 3D objects from applied three-dimensional Back Projection are shown in figure (4-30 a, b) and the slices of retrieved object are shown in figure (4-31 a, b), from these figures, it is clear that the internal hollow sphere inside the solid sphere and inside head of Mickey Mouse is absence, due to blurring.

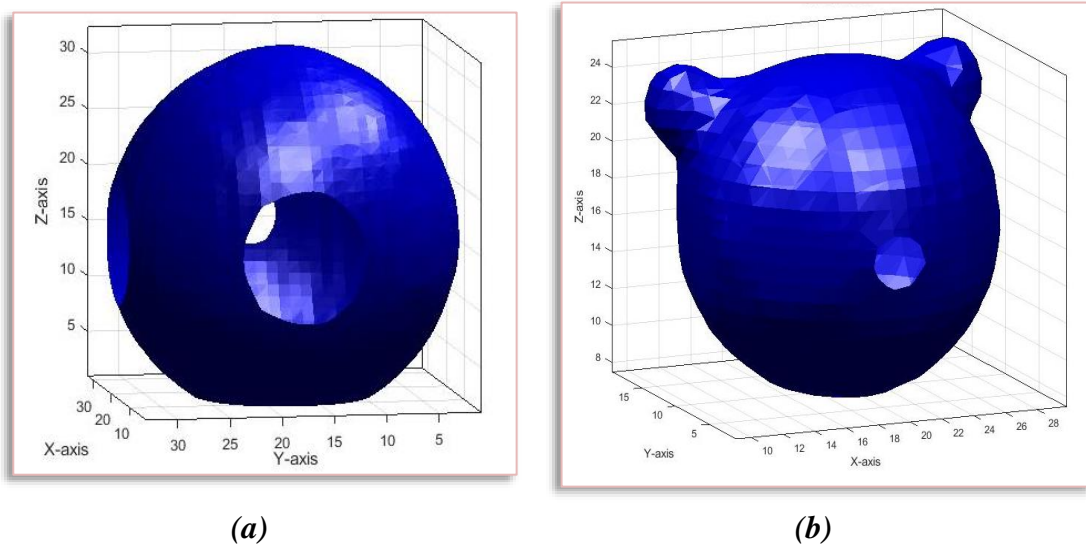
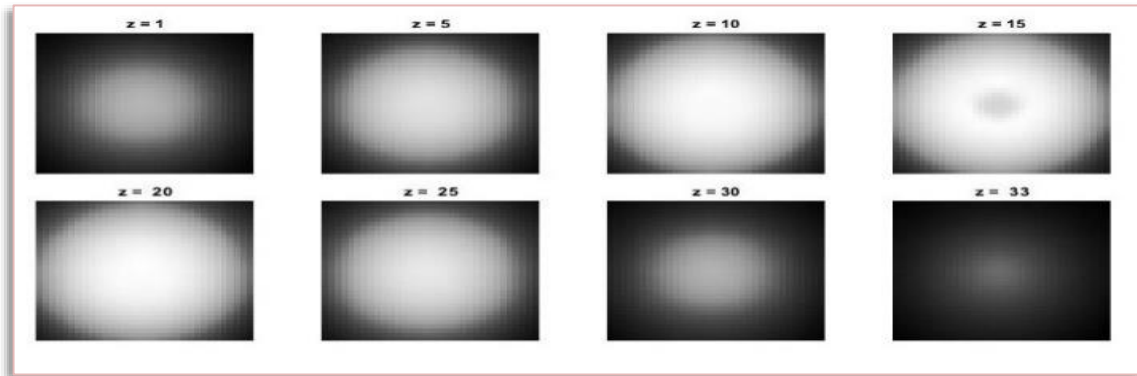
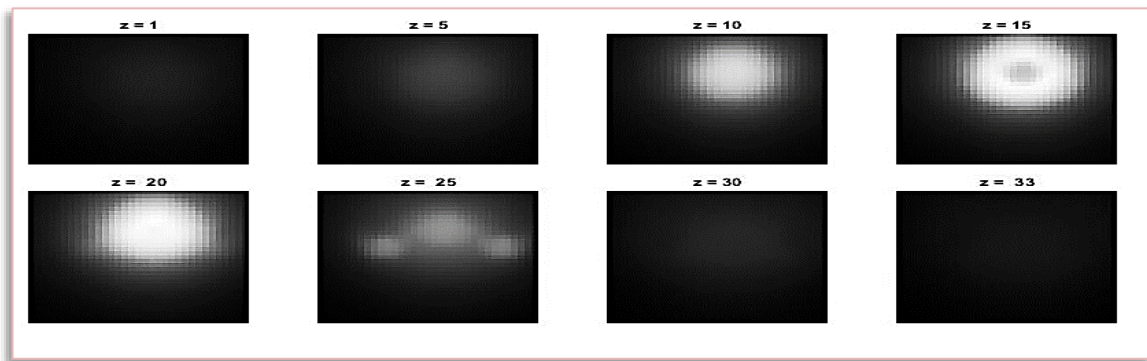


Figure 4-30 The 3D reconstructed by using 3D BP from x-ray projections for (a) sphere and (b) head of mickey mouse



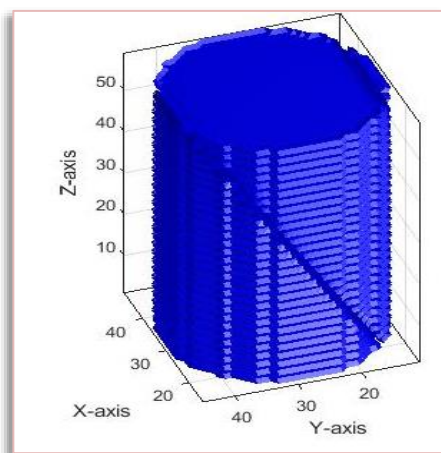
(a)



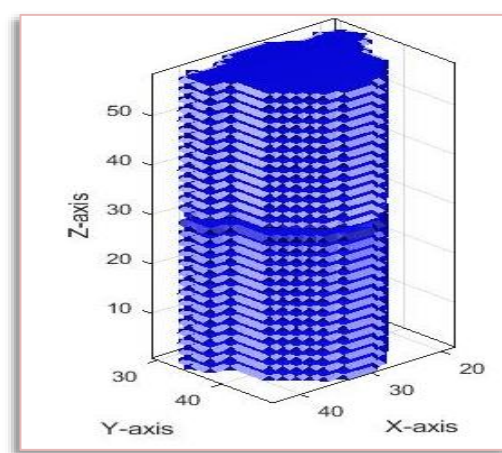
(b)

Figure 4-31 (a) The slices of 3D reconstructed by using 3D BP from x-ray projections for (a) sphere and (b) head of the mickey mouse

When apply the central section theorem for the X-ray projection (4D Projection), the retrieved 3D objects from applying this method are shown in figure (4-32 a, b) and the slices of the retrieved object are shown in figure (4-33 a, b).



(a)



(b)

Figure 4-32 The 3D reconstructed from x-ray projections by central section theorem at Fai (0°) and Theta (45°) for (a) sphere and (b) head of the mickey mouse.

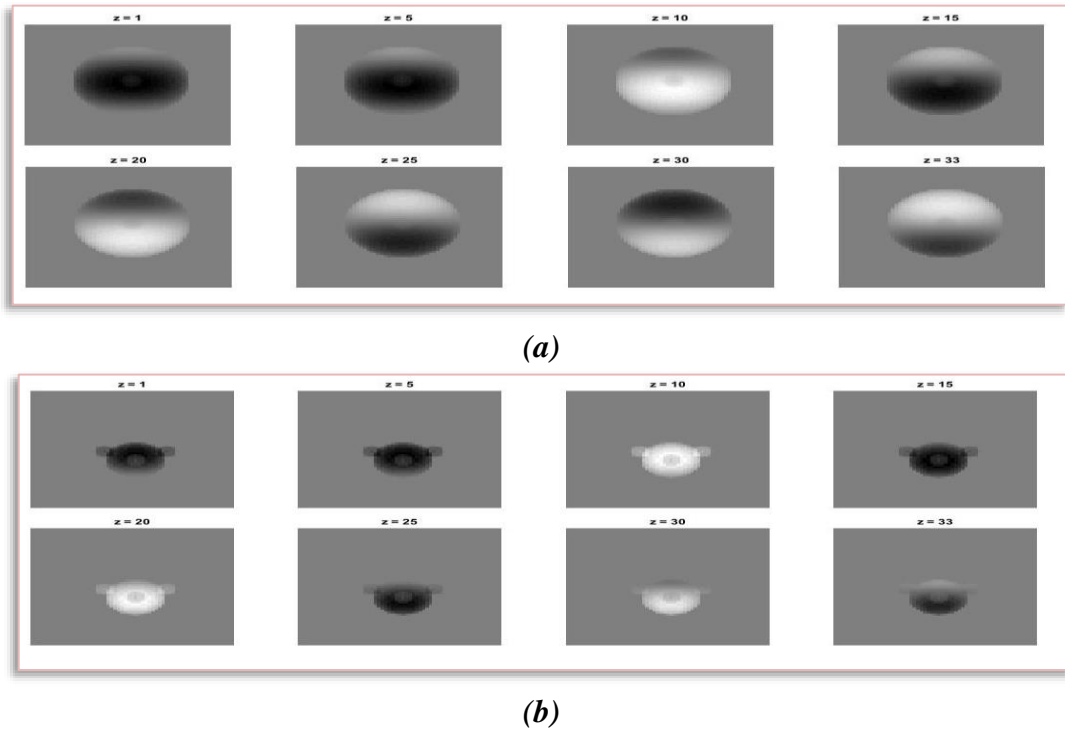


Figure 4-33 The slices of 3D reconstructed from x-ray projections by central section theorem at $\text{Phi} (0^\circ)$ and $\text{Theta}(45^\circ)$ for (a) sphere and (b) head of the mickey mouse.

These retrieved objects obtained from applying this method on the plane of projection at a certain angle of phi and a certain angle of theta this a plane of projections will occupy the frequency space correctly as shown in figure (4-34).

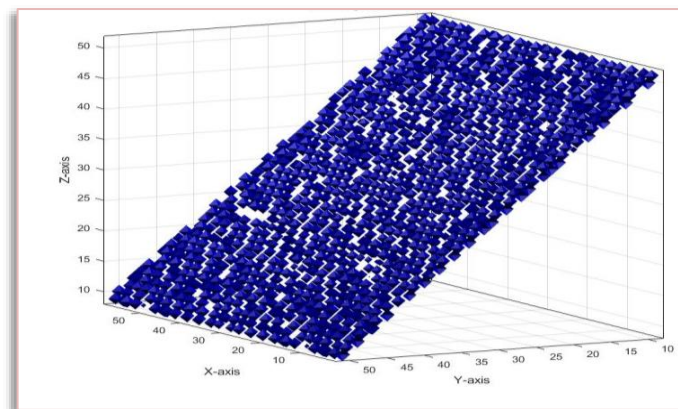


Figure 4-34 The Plane Projection at $\text{Phi} (0^\circ)$ and $\text{Theta} (45^\circ)$.

While if adding other planes of projections at different Phi and theta with the plane above will intersect in the frequency space at which the frequency values will be distorted along the line between the two planes because the values of frequencies of the first plane will be replaced with the values of the frequencies of the second plane as shown in figure (4-35), This will lead to distorting the retrieved object during reconstruction as shown in figure (4-36) and (4-37).

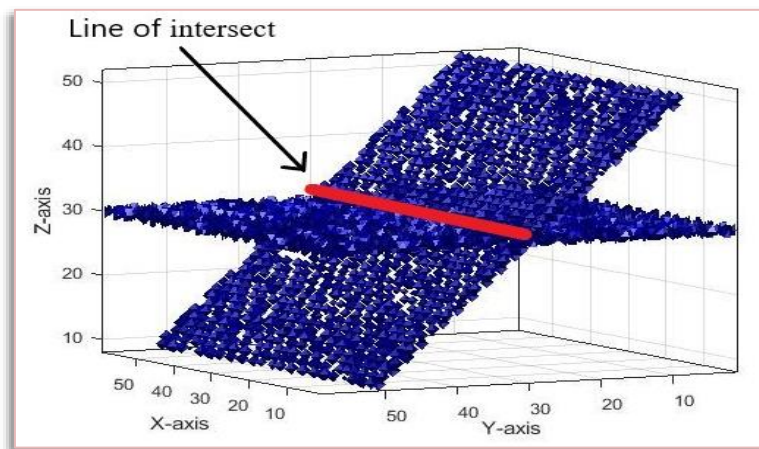
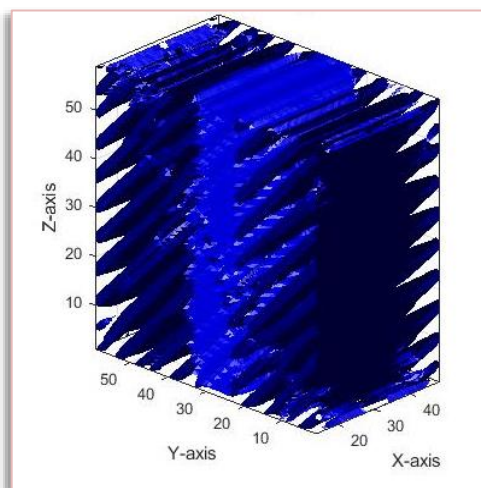
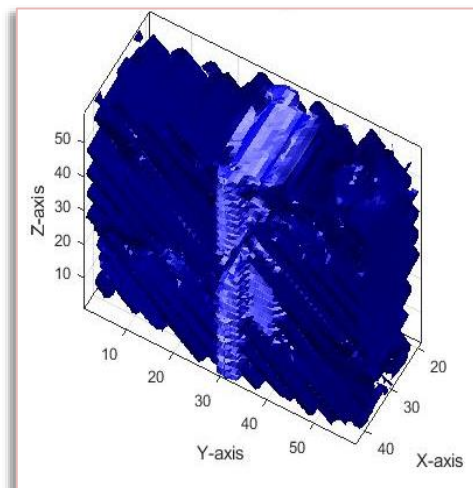


Figure 4-35 The Planes of Projection at Fai (0°) and Theta($45^\circ, 90^\circ$).



(a)



(b)

Figure 4-36 The 3D reconstructed Object from x-ray projections by central section theorem at Fai (0°) and Theta($45^\circ, 90^\circ$) for (a) sphere and (b) head of mickey mouse

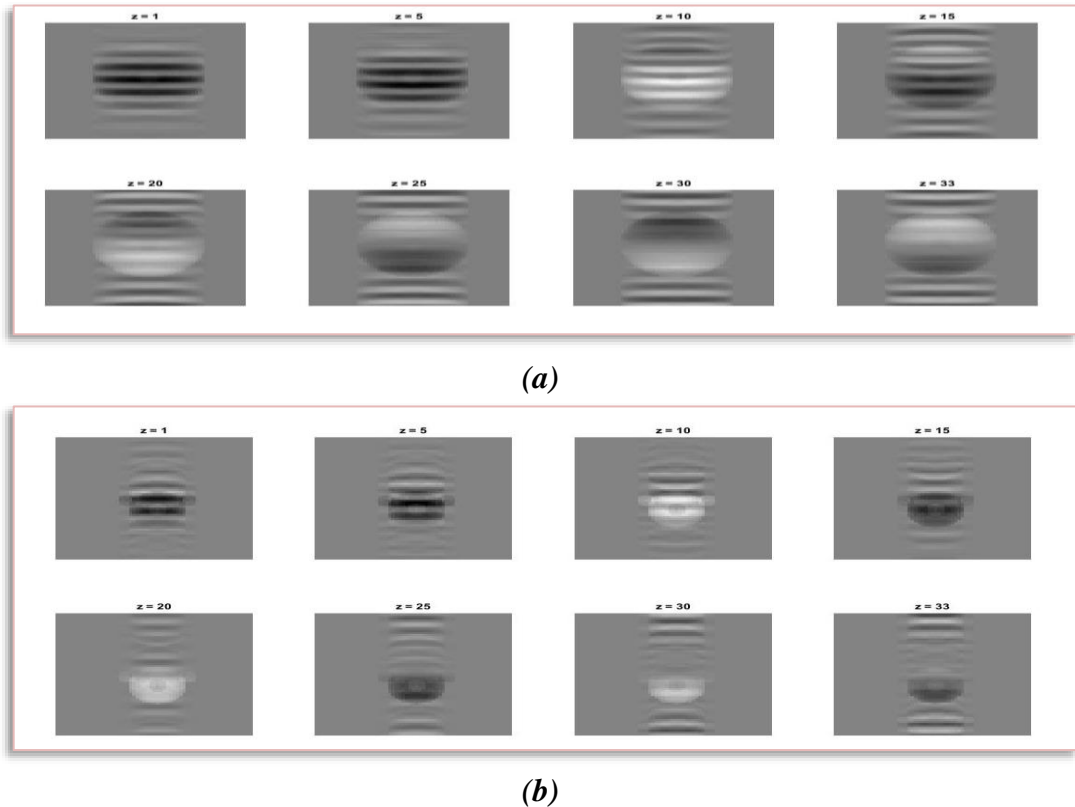
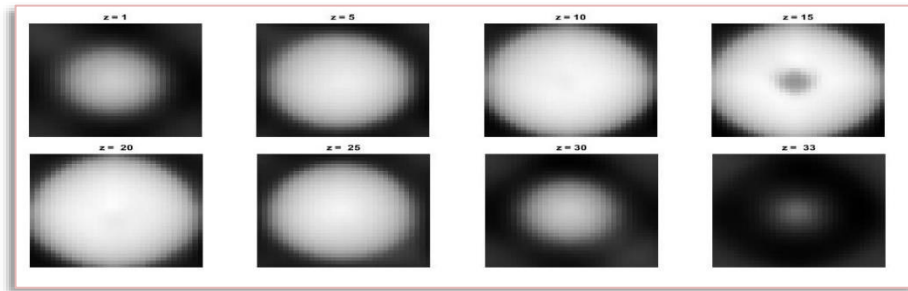


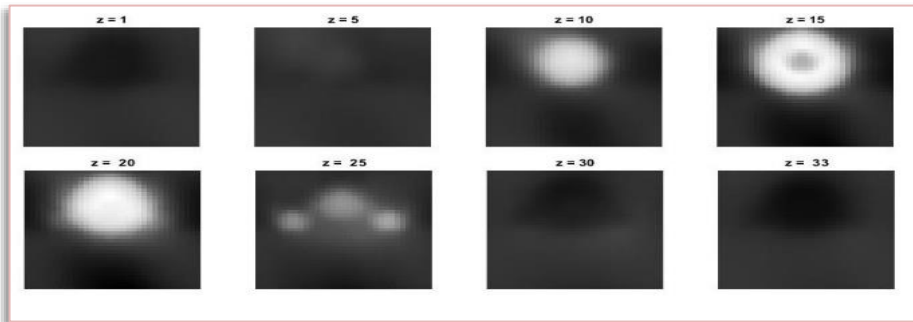
Figure 4-37 The slices of 3D reconstructed 3D Object from x-ray projections by central section theorem at Fai (0°) and Theta (45° , 90°) for (a) sphere and (b) head of mickey mouse

4.3.3.2 The Results of Reconstruction With Filtering

The blurring shown in figures (4-30 a, b) and (4-31 a, b) can be removed by applying the filter in the frequency domain called the ramp filter in the frequency domain. The slice of retrieved objects as shown in figures (4-38 a, b) and the 3D objects as shown in figure (4-39 a, b). From the figure (4-38) can see the filtering success to retrieve the internal hollow sphere inside both objects. While the figure (4-39) shows the three-dimensional object drawing algorithm was unable to build the inner hollow sphere in both objects due to blurring. The effect of the filter on both objects was not clear, where the object after filtering and the object before the filter were very close to each other in structure and details.

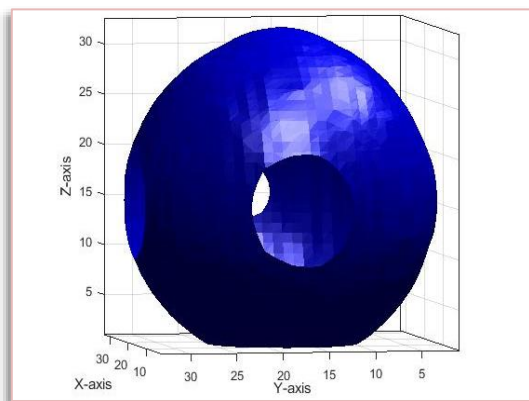


(a)

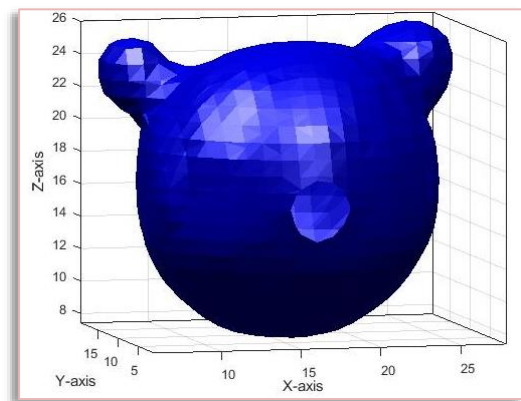


(b)

Figure 4-38 The slices of 3D Object reconstructed from x-ray projections after filtering for (a) sphere and (b) head of mickey mouse



(a)



(b)

Figure 4-39 The 3D reconstructed Object from x-ray projections after filtering for (a) sphere and (b) head of mickey mouse

In order to evaluate the accuracy of each method in the reconstruction process, by calculating the volume of the solid sphere, the volume of the head of Mickey Mouse and the volume of the hollow sphere inside them by counting the points that belong to each of them. The results are shown in Table (4-7).

Table 4-7 The volume of the 3D retrieved object from X-ray Transform

<i>Type of object</i>	<i>Original</i>	<i>Reconstruction by BP</i>	<i>Reconstruction by BP after apply filtering</i>
<i>Solid Sphere</i>	<i>20326</i>	<i>20266</i>	<i>20984</i>
<i>Internal Hollow Sphere</i>	<i>147</i>	<i>Zero</i>	<i>Zero</i>
<i>Head Mickey Mouse</i>	<i>3162</i>	<i>3133</i>	<i>3563</i>
<i>Internal hollow sphere in head Mikey Mouse</i>	<i>126</i>	<i>Zero</i>	<i>Zero</i>

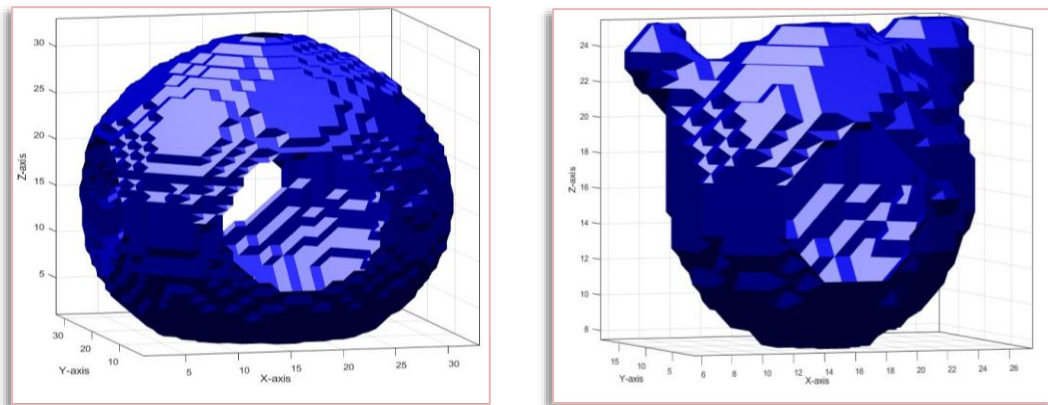
From table (4-7) the volume of each object (sphere and Mickey Mouse) that reconstructed by BP without filtering is closer to the original object volume compared to the calculated volumes of reconstructed objects by BP with filtering. While the volume of the inner sphere inside each object is zero in both the reconstruction method. but by using the subjective criteria, it can be noticed that the objects reconstructed by Back-Projection with filtering are better than the objects reconstructed by Back-Projection without filtering where the internal hollow spheres that are shown in figure (4-38 a, b) are more clearly than the internal hollow spheres without filtering that are shown in figure (4-31 a, b).

After applying the filtering on the results of back-projection now calculate the SNR, PSNR and RMSE of the retrieved object before and after filtering and the threshold value. The results are shown in table (4-8).

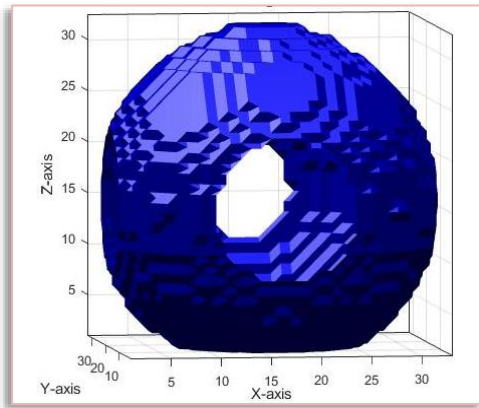
Table 4-8 The SNR and RMSE of reconstruct objects from X-ray Transform before and after apply Filtering

<i>Retrieved 3D object by BP</i>	<i>Without Threshold</i>			<i>With Threshold</i>			
	<i>SNR</i>	<i>PSNR</i>	<i>RMSE</i>	<i>Threshold</i>	<i>SNR</i>	<i>PSNR</i>	<i>RMSE</i>
<i>Sphere Without Filtering</i>	<i>7.7888</i>	<i>10.2637</i>	<i>0.3068</i>	<i>0.45</i>	<i>8.1140</i>	<i>10.5889</i>	<i>0.2955</i>
<i>Sphere With Filtering</i>	<i>8.3517</i>	<i>0.8266</i>	<i>0.2875</i>	<i>0.35</i>	<i>8.0535</i>	<i>0.5284</i>	<i>0.2976</i>
<i>Head of Mickey Mouse Without Filtering</i>	<i>3.7023</i>	<i>14.2580</i>	<i>0.1937</i>	<i>0.55</i>	<i>4.1112</i>	<i>4.6670</i>	<i>0.1848</i>
<i>Head of Mickey Mouse With Filtering</i>	<i>1.8274</i>	<i>12.3832</i>	<i>0.2403</i>	<i>4.0689</i>	<i>14.6247</i>	<i>0.1857</i>	<i>0.55</i>

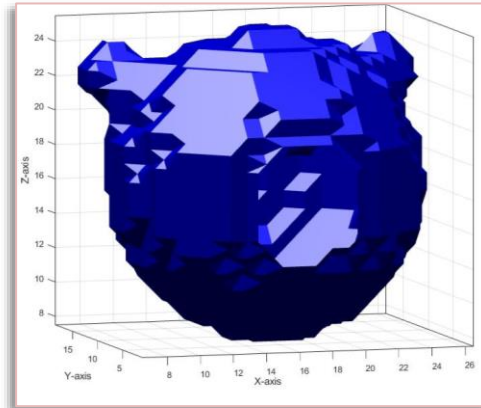
From the table (4-8), note that the SNR increases and the RMSE decrease after applying the filtering for Sphere, while after applying the threshold value for each sphere before and after applying the filter the SNR and the RMSE are very little change, using the subjective criteria can not notice any change in the solid sphere in comparison to the recovered Sphere without applying the threshold value. While the SNR decreases and that RMSE increases after applying the filtering for Mickey Mouse, this means that the recovered head of Mickey Mouse after applying the filter has not improved in comparison to the recovered head of Mickey Mouse without applying the filter, while the SNR increases and the RMSE decrease after applying the threshold value for head of Mickey Mouse in each state (before and after applying the filtering), this means that the recovered head of Mickey Mouse after applying the threshold value has improved in comparison to the recovered head of Mickey Mouse without applying the threshold value. The figures (4-40) and (4-41) have shown the results from applying the threshold values on the objects with filter and without the filter.



(a)



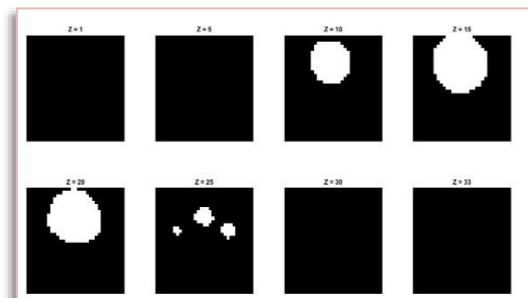
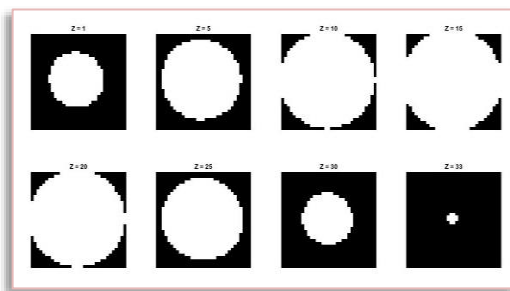
Sphere



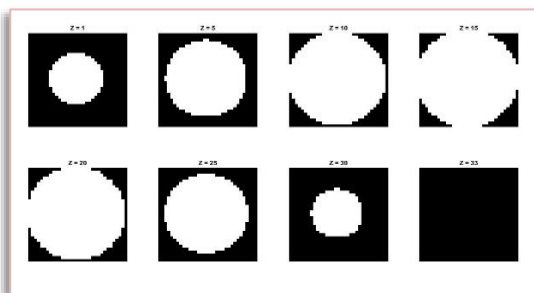
head of the mickey mouse

(b)

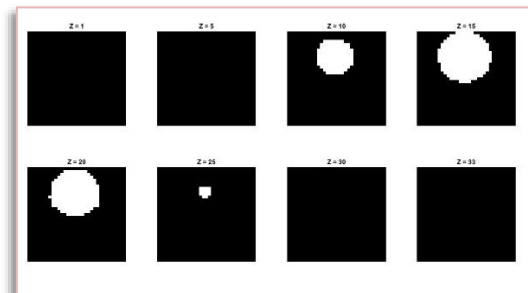
Figure 4-40 (a)The 3D reconstructed from x-ray projections after applying a threshold on filter object and (b)The 3D reconstructed from x-ray projections after applying a threshold on no filter object



(a)



Sphere



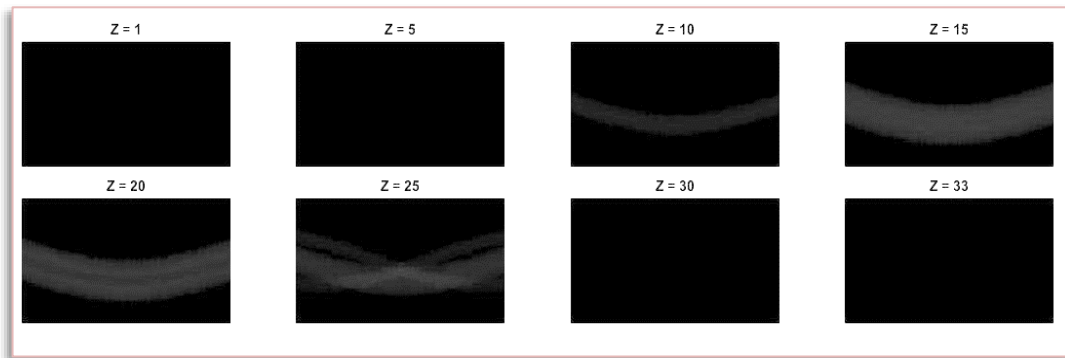
head of the mickey mouse

(b)

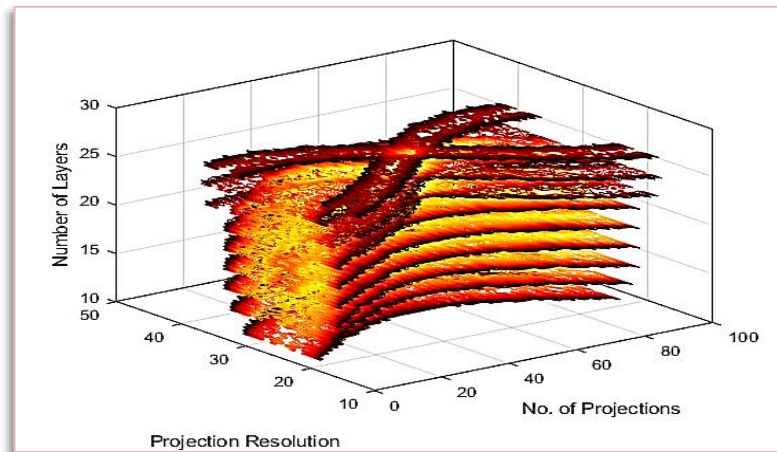
Figure 4-41 (a)The slices of the 3D reconstructed from x-ray projections after applying a threshold on filter object and (b)The slices of the 3D reconstructed from x-ray projections after applying a threshold on no filter object.

4.4 The Results of the Interpolation

The three-dimensional asymmetric object (head of Mickey Mouse) is used as a test sample for this section. The interpolation is applied in sequential steps as following, the first step, apply 2D Radon transform for each slice at different heights of the three-dimensional object using equal angular interval ($\Delta\theta$) and greater than one degree, see figure (4-42 a, b).



(a)



(b)

Figure 4-42 (a) A slice of projection at different heights and at $\Delta\theta = 2^\circ$.
 (b) 3D sinogram obtain from stacking the 2D projection and at $\Delta\theta = 2^\circ$.

In the second step, a prediction of the values of missing data of projections by using the three interpolation methods (as mention in section (2-9)). Table (4-9) shows the SNR and the RMSE before and after apply

interpolation methods at different delta and the figure (4-43) shows comparing the quality of the 3D sinogram before and after interpolation for each method of interpolation.

Table 4-9 The SNR and RMSE before and after applying the interpolation methods for projection at different delta.

<i>Delta</i>	<i>Extend Projection</i>		<i>Nearest Neighbour</i>		<i>Linear</i>		<i>Non-linear</i>	
	<i>RMSE</i>	<i>SNR</i>	<i>RMSE</i>	<i>SNR</i>	<i>RMSE</i>	<i>SNR</i>	<i>RMSE</i>	<i>SNR</i>
2	0.0135	3.0519	0.0013	23.3251	0.0011	25.183	0.0013	23.3419
3	0.0156	1.7929	0.0017	21.0693	0.0013	23.2799	0.0014	22.9039
4	0.0165	1.2782	0.0021	19.272	0.0015	22.082	0.0017	21.1721
5	0.0171	0.9992	0.0023	18.2544	0.0016	21.4136	0.0018	20.6975
10	0.0181	0.482	0.0036	14.4374	0.0018	20.358	0.0021	19.3724
15	0.0185	0.3238	0.005	11.7191	0.0021	19.362	0.0023	18.2992
20	0.0186	0.2458	0.0062	9.7388	0.0024	18.0012	0.0027	17.1518
30	0.0188	0.1695	0.0085	7.0913	0.0031	15.8433	0.0035	14.7878
45	0.0189	0.121	0.0111	4.7085	0.0042	13.1966	0.0046	12.4231

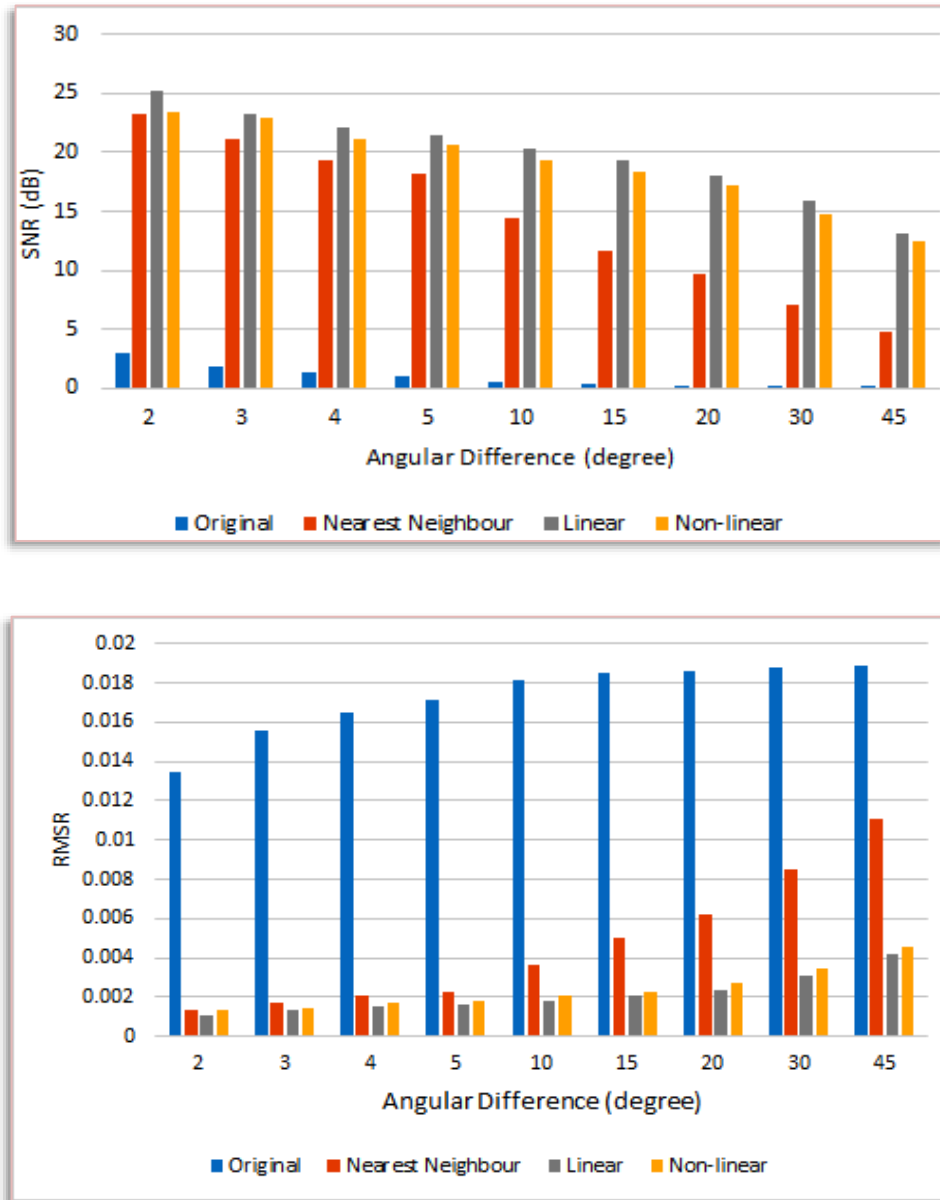


Figure 4-43 The quality of the interpolated 3D sinogram

As it is evident from the table (4.9) and figure (4-43), the SNR for the 3D sinogram before interpolation is decreased dramatically with an increase in the angular interval greater than 10°, in other words, the reduction of the number for projections leads to a decrease in SNR of the 3D sinogram before interpolation, while the SNR for the 3D sinogram reinforced after interpolation, where the linear and Non-Linear are more resistance to the

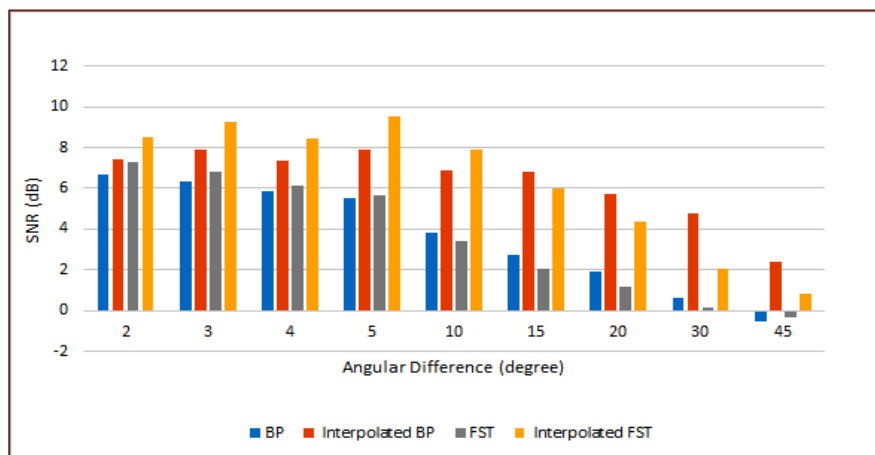
reduction of the number for projections more than the Nearest Neighbor method which decrease with the increase in the angular interval.

Table 4-10 The SNR and RMSE before and after apply the interpolation methods for object at different delta.

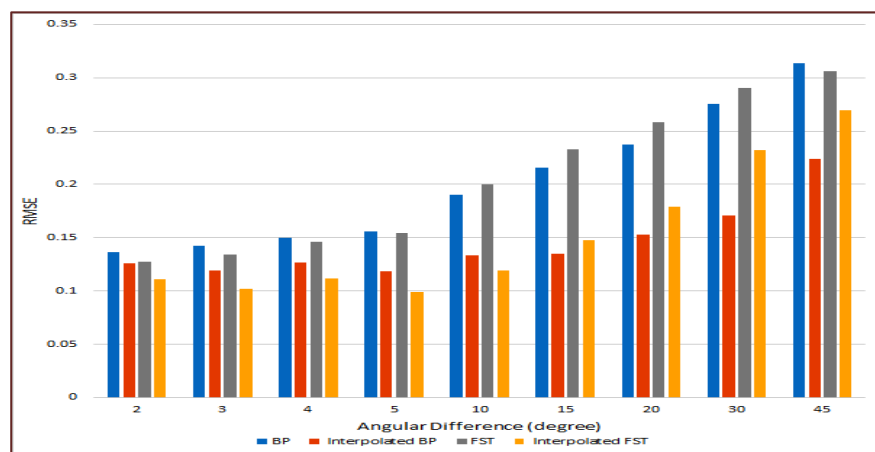
<i>Delta</i>			2	3	4	5	10	15	20	30	45
<i>WithOut Interpolation</i>	<i>BP</i>	<i>RMSE</i>	0.1363	0.1421	0.1499	0.1559	0.19	0.2156	0.2372	0.2757	0.3137
		<i>SNR</i>	6.7063	6.3447	5.8799	5.5439	3.8247	2.7269	1.8962	0.5908	-0.532
	<i>FST</i>	<i>RMSE</i>	0.1275	0.1344	0.1459	0.1545	0.1998	0.2331	0.2586	0.2908	0.3065
		<i>SNR</i>	7.2899	6.8316	6.1174	5.6192	3.3855	2.0493	1.1465	0.1267	-0.328
<i>Nearest Neighbor interpolation</i>	<i>BP</i>	<i>RMSE</i>	0.1256	0.1192	0.1267	0.1188	0.1335	0.135	0.1531	0.1709	0.2241
		<i>SNR</i>	7.4182	7.8698	7.3423	7.904	6.8923	6.7916	5.7009	4.7422	2.3917
	<i>FST</i>	<i>RMSE</i>	0.1109	0.1019	0.112	0.0987	0.1189	0.1477	0.1793	0.2325	0.2692
		<i>SNR</i>	8.4998	9.237	8.4123	9.5134	7.8954	6.0109	4.3282	2.0693	0.7976
<i>Linear interpolation</i>	<i>BP</i>	<i>RMSE</i>	0.1299	0.1289	0.132	0.1302	0.1339	0.1329	0.1395	0.1421	0.1628
		<i>SNR</i>	7.1293	7.1943	6.9883	7.1079	6.8652	6.9263	6.5093	6.3447	5.1631
	<i>FST</i>	<i>RMSE</i>	0.1188	0.1175	0.1233	0.1165	0.1225	0.1226	0.1353	0.1546	0.1783
		<i>SNR</i>	7.904	7.9992	7.5821	8.0699	7.6382	7.6301	6.7718	5.6141	4.3774
<i>Non-Linear interpolation</i>	<i>BP</i>	<i>RMSE</i>	0.1255	0.1238	0.1261	0.1239	0.1274	0.1266	0.1332	0.134	0.1522
		<i>SNR</i>	7.4259	7.5425	7.3877	7.5347	7.2974	7.3498	6.9058	6.8585	5.7476
	<i>FST</i>	<i>RMSE</i>	0.1109	0.1091	0.1118	0.1098	0.1156	0.1139	0.1285	0.1482	0.174
		<i>SNR</i>	8.4998	8.6396	8.4316	8.5892	8.1416	8.2702	7.2235	5.9833	4.5878

As it is evident from the table (4-10) and figure (4-44), The quality of the reconstructed object from the 3D sinogram before and after interpolation by using the Back-projection and FST methods, where the reconstructed object from the interpolated 3D sinogram by the Linear interpolation and Non-Linear interpolation is better in comparison with the reconstructed object from the 3D sinogram without interpolation. The results of using the nearest neighbor interpolation method, in fact, the FST and BP methods give the best results at the angular interval less than 10 °, and it deteriorates after the angle interval greater than 10° and the degradation is faster in the FST method compared to the BP method.

SNR Vs. Angular Difference

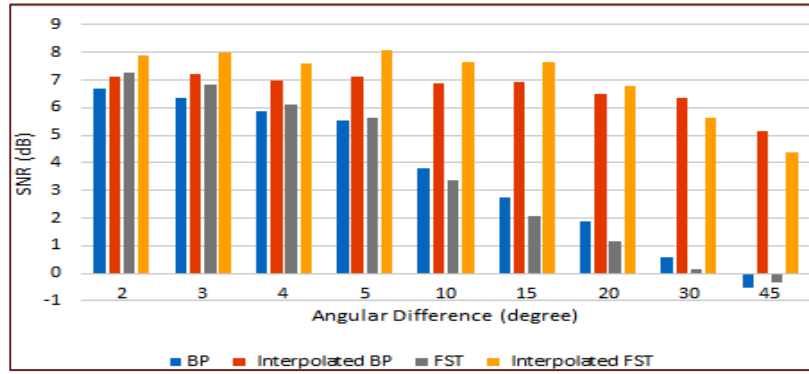


RMSE Vs. Angular Difference

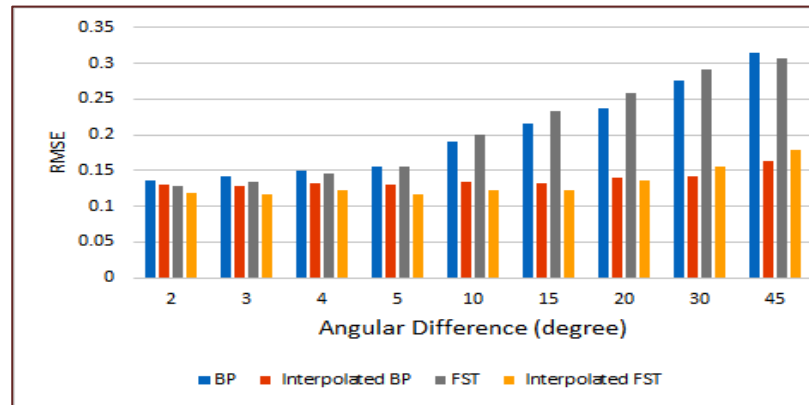


(a) Nearest Neighbor interpolation

SNR Vs. Angular Difference

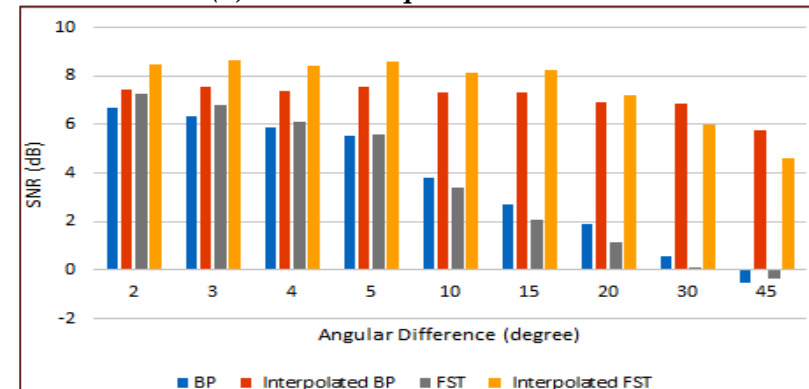


RMSE Vs. Angular Difference

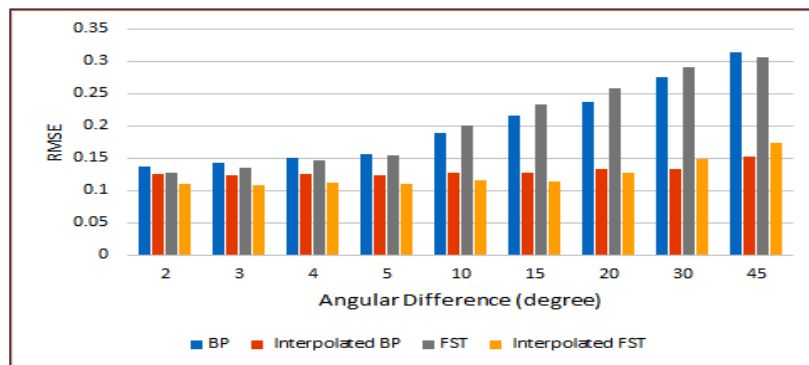


(b) Linear interpolation

SNR Vs. Angular Difference



RMSE Vs. Angular Difference



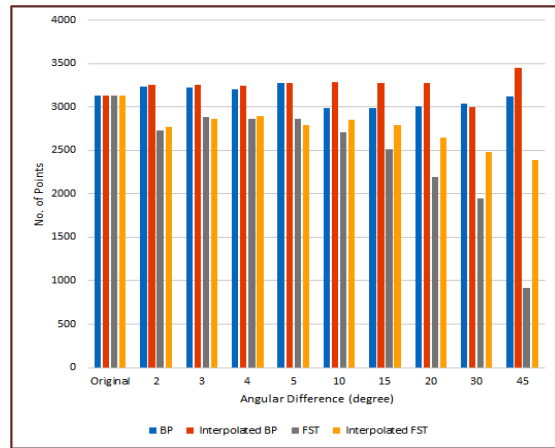
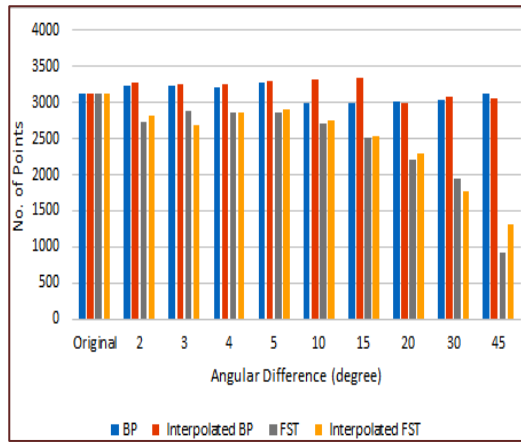
(c) Non-Linear Interpolation

Figure 4-44 The quality of the reconstructed object before and after the interpolation process.

To consider the deformation in the retrieved object, the number of points that belong to the object (the volume) and the number of points that belong to the hollow sphere inside the object is calculated using a threshold value that calculated empirically, its value is ranging between (0.50 -0.65), as illustrated in the table (4-11) and figure (4-45).

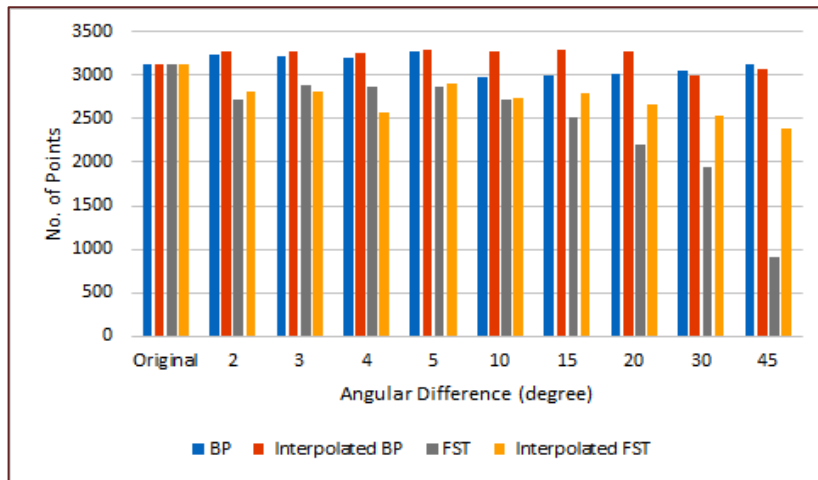
Table 4.11 The No. of point Of the Out and internal object before and after applying the interpolation methods at different delta.

		<i>Delta</i>		<i>Orig.</i>	<i>2</i>	<i>3</i>	<i>4</i>	<i>5</i>	<i>10</i>	<i>15</i>	<i>20</i>	<i>30</i>	<i>45</i>
		<i>BP</i>	<i>Out</i>										
<i>Without Interpolation</i>	<i>BP</i>	<i>Out</i>	3129	3239	3223	3207	3278	2986	2989	3007	3042	3118	
		<i>internal</i>	118	0	0	0	0	0	0	0	19	81	
	<i>FST</i>	<i>Out</i>	3129	2725	2880	2860	2865	2712	2517	2198	1946	916	
		<i>internal</i>	118	145	124	131	126	126	121	134	137	241	
<i>Nearest Neighbor interpolation</i>	<i>BP</i>	<i>Out</i>	3129	3274	3262	3256	3300	3307	3334	2991	3071	3061	
		<i>internal</i>	118	0	0	0	0	0	0	0	0	0	
	<i>FST</i>	<i>Out</i>	3129	2811	2678	2868	2897	2761	2523	2298	1776	1303	
		<i>internal</i>	118	130	157	125	120	131	136	123	108	105	
<i>Linear interpolation</i>	<i>BP</i>	<i>Out</i>	3129	3255	3258	3241	3274	3287	3278	3280	3001	3452	
		<i>internal</i>	118	0	0	0	0	0	0	0	0	0	
	<i>FST</i>	<i>Out</i>	3129	2776	2861	2893	2787	2852	2787	2651	2486	2393	
		<i>internal</i>	118	138	132	131	135	125	133	150	141	130	
<i>Non-Linear interpolation</i>	<i>BP</i>	<i>Out</i>	3129	118	3129	118	3129	118	3129	118	3129	118	
		<i>internal</i>	3273	0	3273	0	3273	0	3273	0	3273	0	
	<i>FST</i>	<i>Out</i>	3129	2811	2815	2574	2898	2733	2795	2668	2528	2385	
		<i>internal</i>	118	130	136	177	122	139	135	148	140	147	



(a) Nearest Neighbor interpolation

(b) Linear interpolation

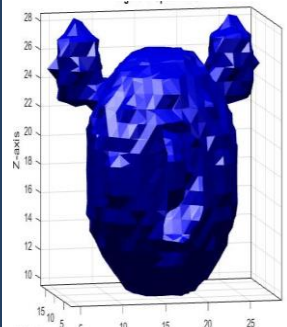
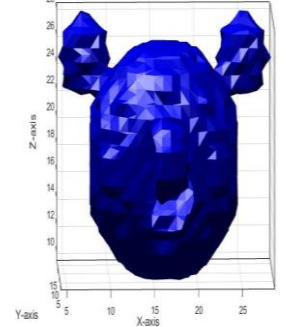
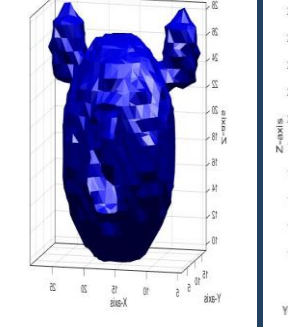
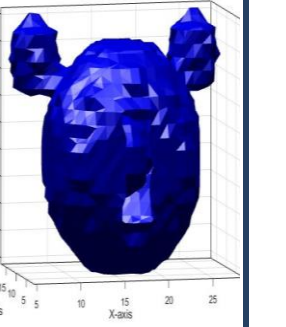
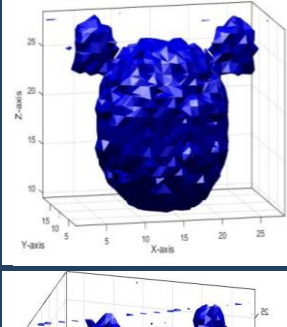
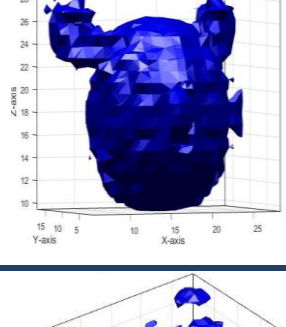
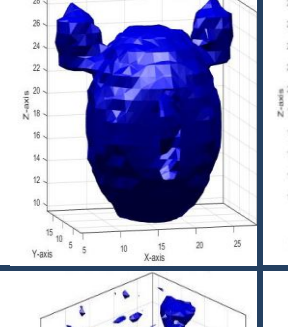
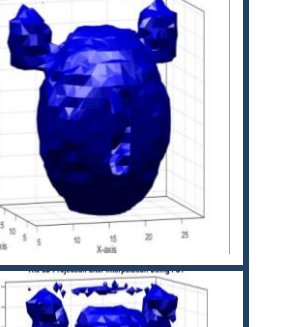
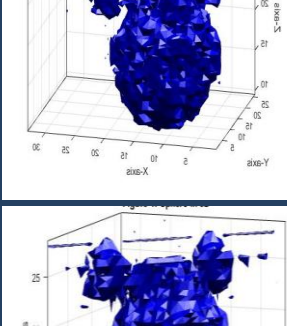
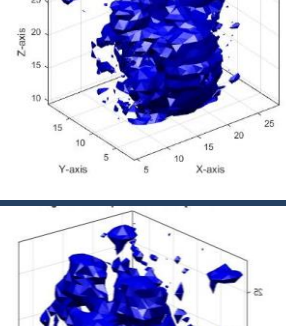
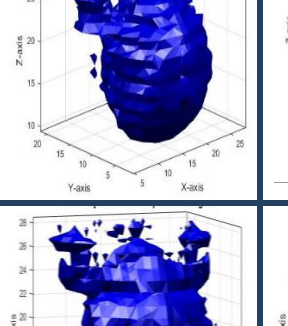
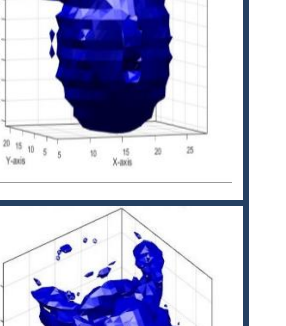
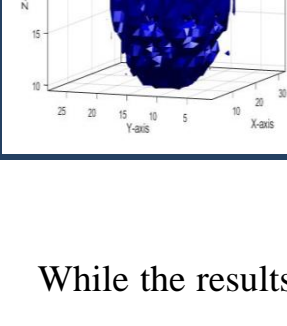
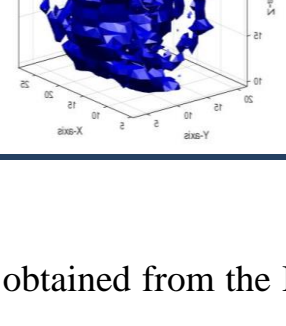
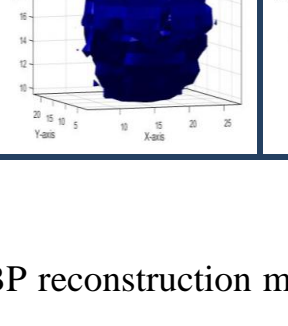
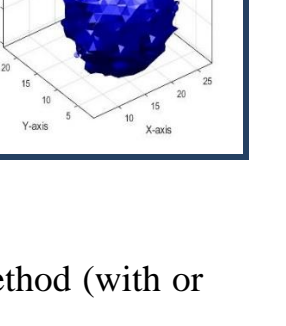


(c) Non-Linear interpolation

Figure 4-45 Number of points that belong to the object

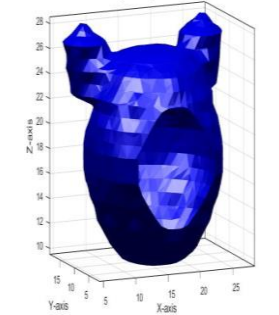
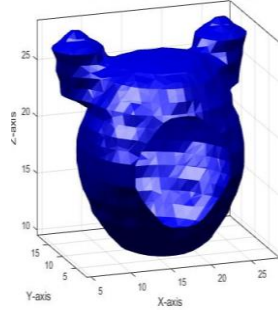
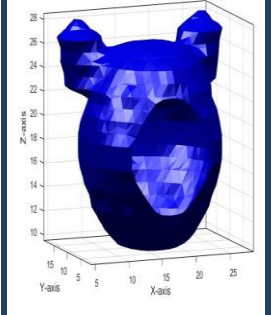
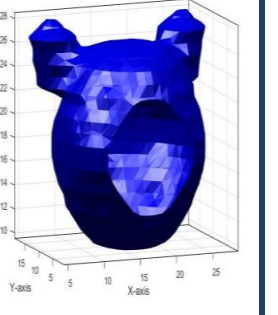
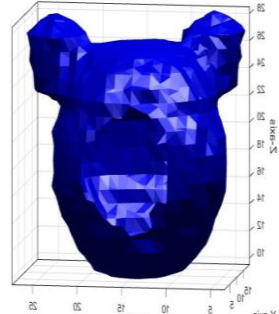
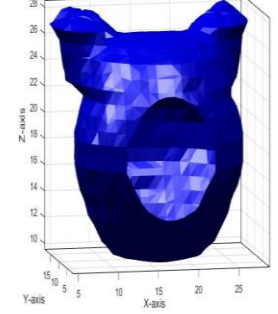
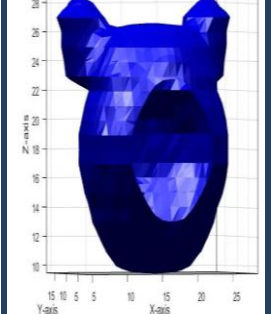
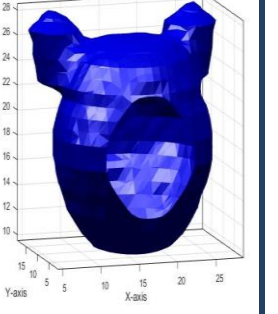
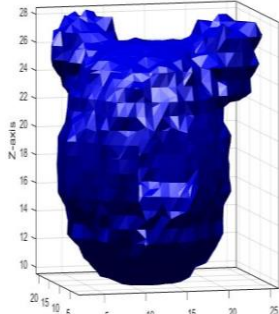
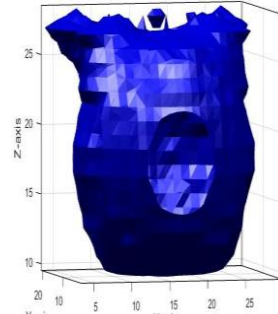
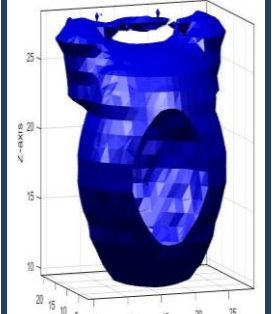
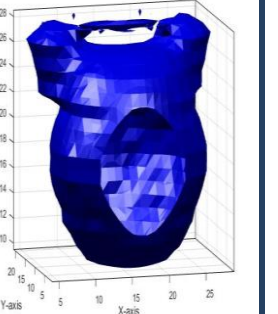
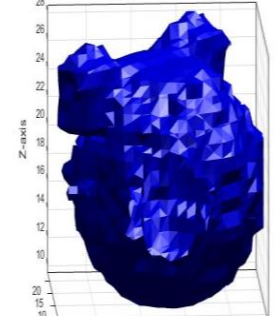
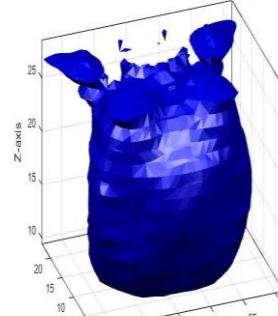
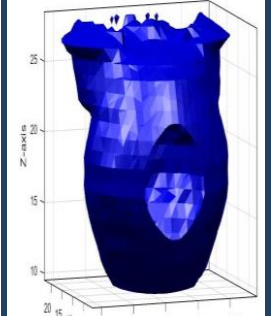
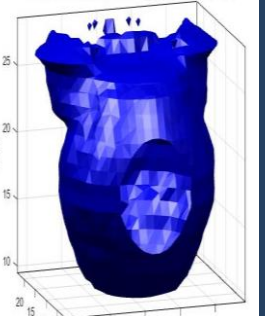
In spite of that, the FST (with or without interpolation process) gives the best results, but regarding the object shape, it is deformed badly after angular difference beyond 15°, the table (4-12) shows the change of the shape of the retrieved object by the FST with the increase of the angular interval.

Table 4-12 The change of the shape of the retrieved object by the FST method with the increase of the angular interval.

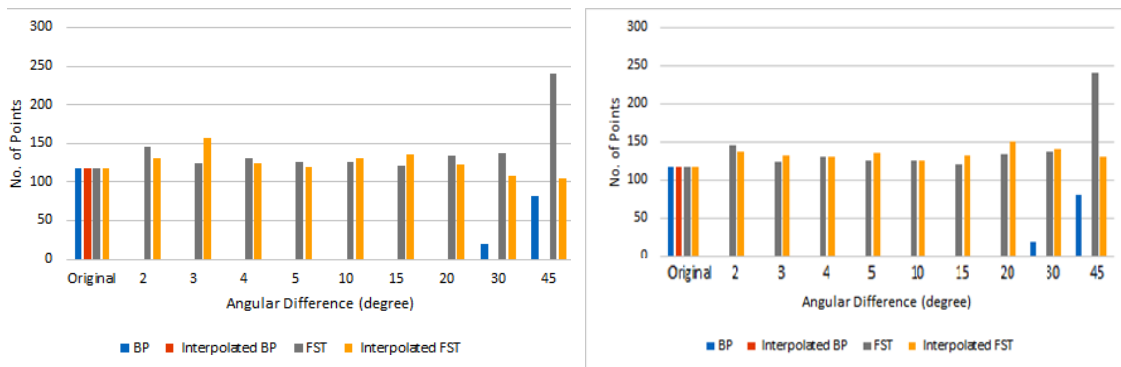
<i>Delta</i>	<i>WithOut Interpolation</i>	<i>Nearest Neighbor interpolation</i>	<i>Linear interpolation</i>	<i>Non-Linear interpolation</i>
2				
15				
30				
45				

While the results obtained from the BP reconstruction method (with or without interpolation process) maintain the basic object shape even after 15°, see table (4-13).

Table 4-13 The change of the shape of the retrieved object by the BP method with the increase of the angular interval.

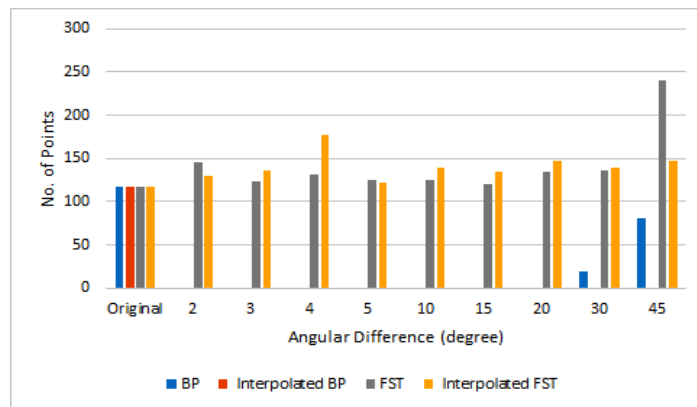
<i>Delta</i>	<i>WithOut Interpolation</i>	<i>Nearest Neighbor interpolation</i>	<i>Linear interpolation</i>	<i>Non-Linear interpolation</i>
2				
15				
30				
45				

The BP reconstruction method couldn't recognize the internal hollow sphere inside the object due to the blurring artifact, see figure (4-46). In contrast to the FST reconstructions method, it recognizes it due to the filtering process which removes the blurring artifact, where the linear interpolation process gave the best results. The values calculated for the internal hollow sphere after angular difference greater than 20° using the BP reconstruction method are due mainly to the deformation in the object shape.



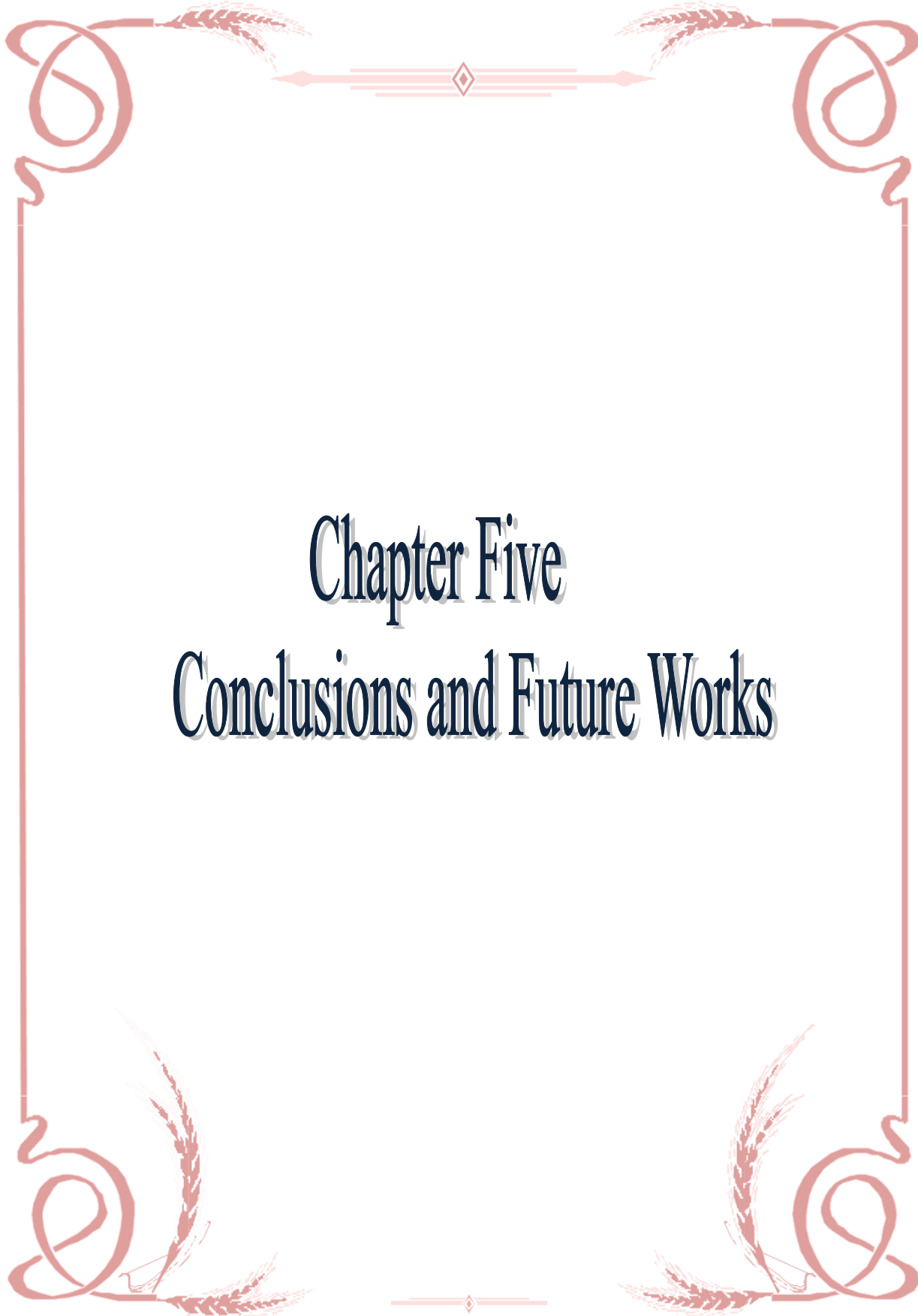
(a) Nearest Neighbor interpolation

(b) Linear interpolation



(c) Non-Linear interpolation

Figure 4-46 Number of points that belong to the hollow sphere.



Chapter Five
Conclusions and Future Works

Chapter Five

Conclusions and Future Works

5.1 Conclusions

Depending on the results in the chapter four, the following conclusions can be derived:

1. When the Standard Back Projection method applied to reconstruct the 3D object on the three forward projections method; first (Slicing reconstruction method), second (Direct reconstruction from 3D Projections) and third (Reconstruction from X-ray transform (4D projections)) methods of reconstructing 3D object, they failed to restore internal points of the object, due to the participation of external points which do not belong to the internal object in the linear integration calculation to restore the internal object this causes the blurring artifact and disappearance of the internal object.
2. The retrieved object was significantly improved when using the Ramp Filter in the frequency domain on the object produced by the Back-Projection method as filtering for the points resulting from the blurring effect that the Back-Projection method could not be removed.
3. The internal object has been retrieved in the solid big sphere by Back-Projection method after Ramp Filter in the frequency domain application in the first method (slicing), while the internal object could not be retrieve in the head of Mickey Mouse after application

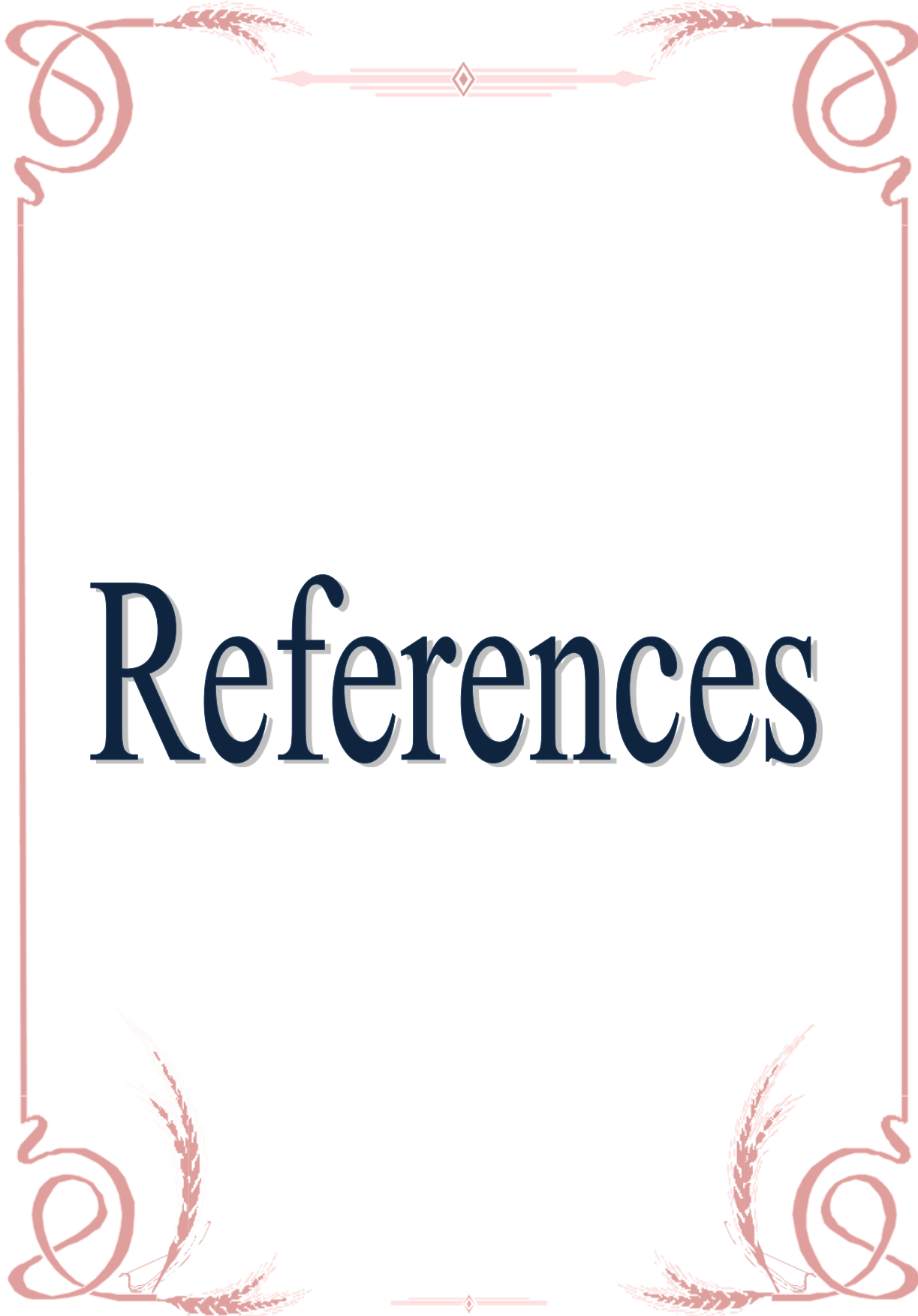
the Ramp Filter in the frequency domain, but the internal object has been retrieved in the head of Mickey Mouse after applying the threshold value on the produced after applying the ramp filter, the internal object begins to appear when the threshold value equal to 0.5. When the threshold is increased, the inner object is more prominent, but this is accompanied by a distortion in the external structure of Mickey Mouse. While in the second and third method the internal object has not been retrieved in both objects after the application of the Ramp Filter in the frequency domain and threshold value.

4. The Fourier slice theorem method that using in the first method (slicing reconstructing) to reconstruct the object, succeeded to restore the external structure and internal points of the object, because only the points that belong to the internal object be shared in the restoration of the internal object. The retrieved object was significantly improved when applying the threshold value on the produced object by the Fourier Slice Theorem method as filtering the points resulting from the blurring effect that the Fourier Slice Theorem method could not be removed.
5. The interpolation methods were applied to find the approximate value of missing data in projection space. The reconstructed object from the interpolated projections by linear interpolation is somewhat improved by both methods of reconstruction (Back-Projection and Fourier slice theorem). the Fourier method excelled more than the back-projection method in restoring the internal body in all interpolation methods but failed when the angular difference in taking the projections was greater than 20 degrees.

6. When calculating the amount of distortion in the retrieved object at the threshold value between 0.5 and 0.65, the object retrieved by the back projection method retains its external features even when the angular difference in the taking of the projections greater than 15 degrees, while the object retrieved by the Fourier slice theorem began deformation when the angular difference greater than 15 degrees.

5.2 *Future Works*

1. Study the 3D Fourier slice theorem to reconstruct 3D object.
2. Apply the X-ray transform to the X-ray profiles to produce 3D representation of the internal structure.
3. Study more effective filters that give better results with the 3D Tomography.
4. Suggest using this study in the industrial field, for example, the structure of the material.
5. Replace the terahertz ray (THz) instead of X-ray, which has a great possibility for using in the medical field better than other medical imaging technologies. It is safe, non-ionizing ray and does not cause damage to organisms.
6. Apply this study on the X-ray medical images for patients.



References



References

- [1] A. C. Kak and M. Slaney, Principles of Computerized Tomographic Imaging, 2nd ed., New York: SIAM, 2001.
- [2] Y. Cheng, "3-dimensional reconstruction from 2-dimensional images and applications to cell cytoskeleton", Ph.D. Thesis, Department of Mechanical Engineering, Massachusetts Institute of Technology, 2001.
- [3] S. Umbaugh, Digital Image Processing and Analysis Human and Computer Vision Applications with CVIP tools, 2nd ed., U.S.A: CRC Press, 2010.
- [4] D. Prakash, Nuclear Medicine: A Guide for Healthcare Professionals and Patients, 1st ed., India: Springer, 2014.
- [5] P. Grangeat, Tomography, 1st ed., Britain: ISTE Ltd & WILEY, 2009.
- [6] A. Markoe, Analytic Tomography, 1st ed., U.S.A.: Cambridge University Press, 2006.
- [7] J. Hsieh, Computed tomography: principles, design, artifacts, and recent advances, 2nd ed., USA: SPIE, 2009.
- [8] W. H. Oldendorf, "Isolated flying spot detection of radio density discontinuities: displaying the internal structural pattern of a complex object," IEEE, vol. 8, no. 1, pp. 68–72, 1961.
- [9] D. E. Kuhl and R. Q. Edwards, "Reorganizing data from transverse section scans of the brain using digital processing," Radiology, vol. 91, no. 5, pp. 975–983, 1968.
- [10] S. Webb, "A brief history of tomography and CT", Proceedings 7th Asian & Oceanian Congress of Radiology, 1995.

References

- [11] Y. Haemisch and C. K. Hannes, *Image Fusion in Preclinical Applications*, 1st ed., USA: Springer, 2019.
- [12] F. Natterer and F. Wubbeling, *Mathematical Methods in Image Reconstruction*, 1st ed., Philadelphia: SIAM, 2001.
- [13] Z. Mu, B. Hong, S. Li and Y.-H. Liu, "A novel three-dimensional image reconstruction method for near-field coded aperture single photon emission computerized tomography," *medicine physics*, vol. 36, no. 5, pp. 1533–1542, 2009.
- [14] P. F. Fulgham and B. R. Gilbert, *Practical Urological Ultrasound*, 2nd ed., Switzerland: Humana Press, 2017.
- [15] A. G. Filler, "The History, Development and Impact of Computed Imaging in Neurological Diagnosis and Neurosurgery: CT, MRI, and DTI," *Nature Precedings*, vol. 7, no. 1, pp. 1-85, 2009.
- [16] L. E. Romans, *Computed tomography for technologists: a comprehensive text*, 1st ed., Wolters Kluwer Health/Lippincott Williams & Wilkins, 2011.
- [17] M. N. Asl and A. Sadremomtaz, "Analytical image reconstruction methods in emission tomography," *J. Biomedical Science and Engineering*, vol. 6, no. 1, pp. 100-107, 2013.
- [18] S. Tong, A. M. Alessio and P. E. Kinahan, "Image reconstruction for PET/CT scanners: past achievements and future challenges," *Imaging in medicine*, vol. 2, no. 5, pp. 529-545, 2010.
- [19] P. P. Bruyant, "Analytic and iterative reconstruction algorithms in SPECT," *Journal of Nuclear Medicine*, vol. 43, no. 10, pp. 1343-1358, 2002.
- [20] R. Cierniak, *X-Ray Computed Tomography in Biomedical Engineering*, 1st ed., London: Springer Science & Business Media, 2011.

References

- [21] R. C. Gonzalez and R. E. Woods, *Digital Image Processing*, 2nd ed., New Jersey: Prentice Hall, 2008.
- [22] S. N. SRIHARI, "Representation of Three-Dimensional Digital Images," *ACM Computing Surveys (CSUR)*, vol. 13, no. 4, pp. 399-424, 1981.
- [23] G. T. Herman, *Image reconstruction from projections: Fundamentals of Computerized Tomography*, second edition., New York: Springer Science & Business Media, 2009.
- [24] R. M. Zain, A. M. Razali, K. A. Salleh and R. Yahya, "Image Reconstruction of X-ray Tomography by Using Image J Platform," *AIP Conference Proceedings*, vol. 1799, no. 1, pp. 050010(1-6), 2017.
- [25] H. M. Abdul Jabar, "Image reconstruction from its 2D Projections," M.Sc. Thesis, Physics Department, College of Education for Pure Science Ibn Al-Hatham, University of Bagdad., 2002.
- [26] F. R. Verdun, D. Racine, J. G. Ott , M. J. Tapiovaara, P. Toroi , F. O. Bochud, W. J. Veldkamp , A. Schegerer, R. W. Bouwman, I. H. Giron and N. W. Marshal, "Image quality in CT: From physical measurements to model observers," *European Journal of Medical Physics* , vol. 31, no. 8, pp. 823-843, 2015.
- [27] W. C. Scarfe and C. Angelopoulos, *Maxillofacial Cone Beam Computed Tomography Principles, Techniques and Clinical Applications*, 1st ed., Switzerland: Springer, 2018.
- [28] A. Staude and J. Goebbels, "Determining the Spatial Resolution in Computed Tomography – Comparison of MTF and Line-Pair Structures," Berlin, 2011.
- [29] P. Sprawls, *Physical Principles of Medical Imaging*, 2nd ed., U.S.A.: Medical Physics Publishing Corporation, 1995.

References

- [30] W. M. Haschek, C. G. Rousseaux and M. A. Wallig, Haschek and Rousseaux's Handbook of Toxicologic Pathology, 3rd ed., London: Academic Press Elsevier Inc., 2013.
- [31] P. E. Christian and K. M. Waterstram-Rich, Nuclear Medicine and PET/CT Technology and Techniques, 7th ed., U.S.: Elsevier Health Sciences, 2013.
- [32] A. M. A. Yousif, "Quality Control of Some CT scanners in Khartoum State," M.Sc. Thesis, Medical Physics Department, Sudan Academy of Sciences (SAS), 2013.
- [33] F. E. Boas and D. Fleischmann, "CT artifacts: causes and reduction techniques," *Imaging in Medicine*, vol. 4, no. 2, pp. 229–240, 2012.
- [34] D. Zhang and E. Angel, "Single Energy Metal Artifact Reduction A Reliable Metal Management Tool in CT," Toshiba America Medical Systems, INC., 2017.
- [35] K. Kalisz, J. Buethe, S. S. Saboo, S. Abbara, S. Halliburton and P. Rajiah, "Artifacts at Cardiac CT: Physics and Solutions," *RadioGraphics*, vol. 36, no. 7, pp. 2064–2083, 2016.
- [36] S. Lanzavecchia, P. L. Bellon and M. Radermacher, "Fast and Accurate Three-Dimensional Reconstruction from Projections with Random Orientations via Radon Transforms," *Journal of Structural Biology*, vol. 128, no. 2, pp. 152–164, 1999.
- [37] G. L. Zeng, "Image reconstruction - a tutorial," *Computerized Medical Imaging and Graphics*, vol. 25, no. 2001, pp. 97-103, 2000.
- [38] D. Zosso, M. B. Cuadra and J.-P. Thiran, "Direct Fourier Tomographic Reconstruction Image-To-Image Filter," *The Insight Journal*, 2007.
- [39] K. Rajendran and Karthikeyan B. R., "Radon Transform based Local Tomography Algorithm for 3D Reconstruction," *International*

References

- Journal of Biology and Biomedical Engineering, vol. 6, no. 1, pp. 1-8, 2012.
- [40] S. S. M. Sobani, S. A. Daud and N. H. Mahmood, "3D Model Reconstruction from Multi-views of 2D Images using Radon Transform," *Jurnal Teknologi (Sciences & Engineering)*, vol. 74, no. 6, pp. 21–26, 2015.
- [41] Q. Tang, "3D Alignment of Projections in Electron Tomography," M.Sc. Thesis, Signal Processing Department, College of Computing and Electrical Engineering, Tampere University of Technology, 2015.
- [42] X. Yang, "Precise and Automated Tomographic Reconstruction with a Limited Number of Projections," PhD Thesis, Department of Electrical Engineering and Information Technology, Karlsruhe Institute of Technology, 2016.
- [43] M. Vassholz, B. Koberstein-Schwarz, A. Ruhlandt, M. Krenkel and T. Salditt, "New X-Ray Tomography Method Based on the 3D Radon Transform Compatible with Anisotropic Sources," *American Physical Society*, vol. 166, no. 8, pp. 088101(1-5), 2016.
- [44] L. Godon, "3D Imaging by Cone Beam Computed Tomography: Experimental Characterization of CT-system and Applications," M.Sc. Thesis, Department of Electrical Engineering and computer science, - College of Applied Sciences- University of Liège, 2018.
- [45] G. Kim, C. Park, D. Lee, H. Cho, C. Seo, S. Park, K. Kim, H. Lim, H. Lee, S. Kang, J. Park, D. Jeon, W. Kim and Y. Lim, "Analytic Computed Tomography Reconstruction in Sparse-Angular Sampling Using a Sinogram-Normalization Interpolation Method," *Journal of the Korean Physical Society*, vol. 73, no. 3, pp. 361- 367, 2018.

References

- [46] F. Kharfi, *Imaging and Radio Analytical Techniques in Interdisciplinary Research: Fundamentals and Cutting Edge Applications*, 1st ed., Croatia: InTech, 2013.
- [47] P. A. Penczek, "Fundamentals of three-dimensional reconstruction from projections.," *Methods in enzymology*, vol. 482, no. 1, pp. 1-33, 2010.
- [48] K. Erlandsson, "Positron Emission Tomography with Three-dimensional reconstruction," PhD. Thesis, Radiation Physics Department, Institute of the Jubileum, University of Lund, 1996.
- [49] C. Hoiland, "The Radon Transform," Aalborg University, VGIS, 07gr721, 2007.
- [50] J. Beatty, "The Radon Transform and the Mathematics of Medical Imaging," *Digital Commons*, pp. 646, 2012.
- [51] G. Zeng, *Medical Image Reconstruction: A Conceptual Tutorial*, 1st ed., Salt Lake: Springer Science & Business Media, 2010.
- [52] J. Fessler, "Analytical Tomographic Image Reconstruction Methods," in Ch. 3, 19 November 2009.
- [53] W. Cong, A. Momose and G. Wang, "Fourier transform-based iterative method for differential phase-contrast computed tomography," *Optical Society of America*, vol. 37, no. 11, pp. 1784-1786, 2012.
- [54] S. R. Zhaoa, D. Jiang, K. Yang and K. Yanga, "Generalized Fourier slice theorem for cone-beam image reconstruction.," *Journal of X-Ray Science and Technology*, vol. 23, no. 2, pp. 157-188, 2015.
- [55] C. C. Shaw, *Cone Beam Computed Tomography Imaging in Medical Diagnosis and Therapy*, 1st ed., U.S.A.: CRC, 2014.
- [56] H. J. Scudder, "Introduction to computer aided tomography," *IEEE*, vol. 66, no. 6, pp. 328-337, 1978.

References

- [57] P. G. Challenor, P. Cipollini and D. Cromwell, "Use of the 3D Radon transform to examine the properties of oceanic Rossby waves," *Journal of Atmospheric and Oceanic Technology*, vol. 19, no. 5, pp. 1558-1566, 2002.
- [58] A. Averbuch and Y. Shkolnisky, "3D Fourier based discrete Radon transform," *Applied and Computational Harmonic Analysis*, vol. 15, no. 1, pp. 33-69, 2003.
- [59] C. Axelsson, "Direct Fourier Methods in 3D-reconstruction from Cone-beam Data," PhD. Thesis, Image Processing Laboratory, Electrical Engineering Department, University of Linköping, 1994.
- [60] M. Wernick and J. N. Aarsvold, *Emission Tomography: The Fundamentals of PET and SPECT*, 1st ed., China: Elsevier, 2004.
- [61] M. E. Lyra and A. Ploussi, "Filtering in SPECT image reconstruction," *International Journal of Biomedical Imaging*, vol. 2011, no. 693795, pp. 1-14, 2011.
- [62] G. A. Wigunaa and G. B. Suparta, "interpolation method in simple computed tomography scanner," Singapore, 2015.
- [63] H. K. Homood, "Lagrange Interpolation for Mobile Agent Connection Encryption," *Ibn Al-Haitham Journal for Pure and Applied Science*, vol. 25, no. 1, pp. 1-12, 2011.
- [64] E.-J. Lee and K.-C. Jin, "Comparative Analysis of Sinogram Interpolation Methods for Computer Tomographic Images," Madrid, Spain, 2015.
- [65] H. M. Abdul Jabar, "Fusion Techniques for Globalizing the Features of Satellite Images," Ph.D. Thesis, Physics Department, College of Education for Pure Science Ibn Al-Haitham, University of Bagdad, 2006.

References

- [66] S. Zhang, J. Zhang, X. Huang and D. Liu, "Image interpolation used in three-dimensional range data compression," *Optical Society of America, Applied Optics*, vol. 55, no. 15, pp. 4123-4131, 2016.
- [67] P. S. Parsania and P. V. Virparia, "A Review: Image Interpolation Techniques for Image Scaling," *International Journal of Innovative Research in Computer and Communication Engineering*, vol. 2, no. 12, pp. 7409 - 7414, 2014.
- [68] S. P. Jaiswal, V. Jakhetiya, A. Kumar and A. K. Ti, "A low complex context adaptive image interpolation algorithm for real time applications," *IEEE Trans. Circuits Syst. Video Technol*, pp. 969-972, May 2012.
- [69] S. H. Mahajan and V. K. Harpale, "Adaptive and Non-Adaptive Image Interpolation," Pune, India, 2015.
- [70] A. Tripathi, P. K. Khatri, G. L. Baheti and K. C. Songara, "Interpolation Technique in Computed Tomography Image Visualisation," *Defence Science Journal*, vol. 52, no. 3, pp. 317-324, 2002.
- [71] A. K. Jain, *Fundamentals of Digital Image Processing*, 1st ed., U.S.A: Prentice Hall, 1989.
- [72] H. H. Chyad, "Speeding-Up Fractal Gray Level Image Compression Using Moments Features," M.Sc. Thesis, Physics Department, College of Education for Girls, University of Kufa, 2014.
- [73] Y. Q. Shi and H. Sun, *Image and video compression for multimedia engineering fundamentals, algorithms and standards*, 2nd ed., U.S.A.: CRC Press, 2008.
- [74] K. H. Thung and P. Raveendran, "A Survey of Image Quality Measures," Kuala Lumpur, Malaysia, 2009.

References

- [75] S. E. Umbaugh, *Computer Vision and Image Processing: A Practical Approach Using CVIP Tools*, 1st ed., U.S.A: Prentice Hall PTR, 1998.
- [76] Z. Wang, "Objective Image/ Video Quality Measurement," A Literature Survey, Electrical and Computer Engineering Department, Multidimensional Digital Signal Processing, University of Texas at Austin, 1998.

الخلاصة

تم فتح افق جديد للباحثين في مجال تقانة التصوير المقطعي المحوسب Computed Tomography (CT) نظرا لامكانية هذه التقانة على انتاج صور ثلاثية الابعاد للبنية الداخلية للجسم دون الحاجة الى اتلاف الجسم

يركز هذا العمل على دراسة نماذج لإعادة بناء الصور ثلاثية الأبعاد من إسقاطاتها لجسمين؛ متناظر وغير متناظر باستعمال ثلاث طرق.

تستعمل الطريقة الأولى (طريقة اعادة اعمار الشرائح) تحويل رادون ثنائي الابعاد لإنشاء مساقط ثنائية الأبعاد لكل شريحة من الجسم ثلاثي الأبعاد على ارتفاعات مختلفة. تستعمل طريقة الإسقاط العكسي ثنائي الأبعاد و طريقة نظرية شريحة فورير (FST) لإعادة بناء كل شريحة إسقاط ثنائية الأبعاد للجسم ثلاثي الأبعاد. في الطريقة الثانية (اعادة الاعمار المباشرة من المساقط ثلاثية الابعاد) تم استعمال تحويل رادون ثلاثي الأبعاد لإنشاء مساقط ثلاثية الابعاد للجسم ثلاثي الأبعاد. تم استعمال الاسقاط العكسي ثلاثي لاعادة بناء الجسم ثلاثي الابعاد. الطريقة الثالثة تمت باستعمال تحويل الاشعة السينية لخلق مساقط رباعية الابعاد ثم استعادة الجسم من هذه المساقط رباعية الابعاد باستعمال طريقتين وهما طريقة التحويل المركزي وطريقة الاسقاط العكسي ثلاثي الابعاد. تم استعمال مرشح رامب وقيمة حد العتبة لتحسين الجسم الذي تمت استعادته.

في هذه العمل تم اقتراح ثلاثة اساليب من الاستيفاء لتقليل جرعة الإشعاع للمريض ووقت إعادة بناء الجسم هي (الاستيفاء بأقرب جار ، الاستيفاء الخطي ، والاستيفاء الغير خطي) يتم تطبيق هذه الاساليب على المساقط ثنائية الأبعاد المأخوذة عند الفارق الزاوي أكبر من درجة واحدة. تم تبني طريقتين لإعادة الإعمار في هذه الدراسة ، هما طريقة الإسقاط العكسي وطريقة نظرية شريحة فوريه. تم تطبيق قيمة العتبة لإزالة النقاط الزائدة ، الناتجة تأثير الضبابية ثم تم حساب حجم الاجسام المستعادة.

أظهرت نتائج الطريقة الاولى (طريقة اعادة اعمار الشرائح) قدرة طريقة نظرية فورير على إعادة بناء الهيكل الخارجي للجسم والبنية الداخلية له لكنها لم تستطع إزالة كل نقاط

الضبابية ، لذلك ، اقترح هذا العمل تطبيق حد العتبة لإزالة النقاط الزائدة بسبب الضبابية ، في حين طريقة الإسقاط العكسي ، اظهرت قدرتها على إعادة بناء الهيكل الخارجي للجسم و عدم قدرتها على إعادة بناء الهيكل الداخلي للجسم بسبب تأثير الضبابية ، لذلك ، اقترح في هذا العمل ، مرشح رامب في المجال الترددي الذي اثبت جدارته في ازالة الضبابية واسترداد البنية الداخلية للجسم.

بينما أظهرت نتائج الطريقة الثانية (إعادة الأعمار المباشرة من المساقط ثلاثية الأبعاد) حيث من النتائج لاحظنا ان هذه الطريقة لها القدرة على إعادة بناء الهيكل الخارجي للجسم وعدم قدرتها على إعادة بناء الهيكل الداخلي له بسبب تأثير الضبابية ، لذلك ، اقترح في هذا العمل استخدام مرشح رامب في الفضاء الترددي لازالة تأثير الضبابية ولكن تبين من النتائج انه اخفق في إزالة تأثير الضبابية بالطريقة التي تمكنه من استرداد البنية الداخلية للجسم ثلاثي الأبعاد.

وأظهرت نتائج الطريقة الثالثة (إعادة الإعمار من تحويل الأشعة السينية) (الإسقاطات رباعية الأبعاد)) تبين من النتائج ان طريقة التحويل المركزي اخفقت في استعادة الجسم بسبب ضعف امكانياتها في رص المساقط الرباعية عند تحويلها الى مساقط ثلاثي الأبعاد. بينما طريقة الإسقاط العكسي تمكنت من استعادة الجسم ثلاثي الأبعاد لكنها فشلت في استعادة البنية الداخلية له وبعد تطبيق مرشح رامب في الفضاء الترددي لاحظنا انه اخفق ايضا في استعادة البنية الداخلية للجسم ثلاثي الأبعاد.

من خلال تطبيق أساليب الاستيفاء في هذا العمل اظهرت إن أفضل قيمة عتبة لفصل النقاط التي تنتمي إلى الجسم تتراوح بين 0.50-0.65. حيث إعادة بناء الجسم بطريقة FST مع عملية الاستيفاء أفضل النتائج للتفاصيل الداخلية عن طريقة BP ، في حين فشلت طريقة FST في استرداد شكل الجسم الأساسي بشكل صحيح لفارق زاوي أكبر من 20° . بينما إعادة البناء بطريقة BP تحافظ على شكل الجسم الأساسي حتى بعد الفارق الزاوي أكبر من 15° . بشكل عام ، أعطى الاستيفاء الخطي أفضل النتائج.



جمهورية العراق
وزارة التعليم العالي والبحث العلمي
جامعة بغداد
كلية التربية للعلوم الصرفة / ابن الهيثم
قسم الفيزياء

محاكاة التصوير المقطعي للصور ثلاثية الابعاد

اطروحة مقدمة الى
كلية التربية للعلوم الصرفة / ابن الهيثم / جامعة بغداد
وهي جزء من متطلبات نيل شهادة الدكتوراه في علوم الفيزياء

من قبل

حوراء هادي چياد

(بكالوريوس علوم في الفيزياء - قسم الفيزياء - كلية التربية - جامعة القادسية - 2011)

(ماجستير علوم في الفيزياء - قسم الفيزياء - كلية التربية للبنات - جامعة الكوفة - 2015)

بإشراف

أ.م.د . حميد مجيد عبد الجبار

2019 م

1441 هـ